

Gas Chromatographic Instrumentation for Gas Analysis of the Martian Atmosphere

FINAL REPORT

Volume II

Overall Program Summary

25 September 1962

Contract No. 950326

GPO PRICE \$ _____

OTS PRICE(S) \$ _____

Hard copy (HC) 5.00

Microfiche (MF) 1.00

Submitted to

JET PROPULSION LABORATORIES
Pasadena, California

MELPAR INC

A SUBSIDIARY OF WESTINGHOUSE AIR BRAKE COMPANY

3000 ARLINGTON BOULEVARD

FALLS CHURCH, VIRGINIA

FACILITY FORM 602

N 65 12616

(ACCESSION NUMBER)

162

(PAGES)

CR-59773

(NASA CR OR TMX OR AD NUMBER)

(THRU)

1

(CODE)

(CATEGORY)

RC # 62-632

GAS CHROMATOGRAPHIC INSTRUMENTATION
FOR
GAS ANALYSIS OF THE MARTIAN ATMOSPHERE

Final Report
Volume II
Overall Program Summary

25 September 1962

Contract No. 950326

Submitted to
Jet Propulsion Laboratories
Pasadena, California

Submitted by
Melpar, Incorporated
3000 Arlington Boulevard
Falls Church, Virginia

TABLE OF CONTENTS

	<u>Page</u>
1. INTRODUCTION	8
2. CONFIGURATION OF OVERALL SYSTEM	9
3. OVERALL SYSTEM PERFORMANCE	15
4. DETAILED DISCUSSION OF COMPONENT PARTS	46
4.1 Columns	46
4.2 Detectors	50
4.3 Gas Chromatographic Oven	57
4.4 Sampling and Injection Valve	73
4.5 Critical Orifice and Venturi Pump	79
4.6 Reference Gas Injection	80
4.7 Transit Sealing	81
4.8 Carrier Gas Reservoir and Controls	82
4.9 Packaging for Demonstration	84
4.10 Electronic Components	86
5. SUMMARY	125
APPENDIX -- Laboratory Model Design Drawings	130

LIST OF ILLUSTRATIONS

<u>Figure</u>		<u>Page</u>
1	Overall System Drawing	10
2	System Lay-Out	11
3	Photograph of Laboratory Model	12
4	Photograph of Laboratory Model	14
5	Chromatograms with Detectors 1 and 2	16
6	Chromatograms with Detectors 3 and 4	17
7	Response Curve for N ₂ (Syringe Injection)	19
8	Response Curve for H ₂ O (Syringe Injection)	20
9	Response Curve for CH ₄ (Syringe Injection)	21
10	Response Curve for Ne (Syringe Injection)	22
11	Response Curve for NH ₃ (Syringe Injection)	23
12	Response Curve for O ₂ (Syringe Injection)	24
13	Response Curve for A (Syringe Injection)	25
14	Response Curve for CO ₂ (Syringe Injection)	26
15	Response Curve for C ₂ H ₆ (Syringe Injection)	27
16	Response Curve for N ₂ O (Syringe Injection)	28
17	Response Curve for CO (Syringe Injection)	29
18	(a) Response Curve for Kr (Syringe Injection) and (b) Response Curve for H ₂ (Syringe Injection)	30
19	New Martian Atmosphere Simulator	32
20	Response Curve for Xe	34
21	Response Curve for Ethane	35
22	Response Curve for N ₂ O	36

LIST OF ILLUSTRATIONS (Continued)

<u>Figure</u>		<u>Page</u>
23	Response Curve for Argon	37
24	Response Curve for Kr	38
25	Response Curve for CH ₄	39
26	Response Curve for CO ₂	40
27	Response Curve for CO	41
28	Response Curve for H ₂ (Stream Splitter)	43
29	Response Curve for O ₂ (Stream Splitter)	44
30	Response Curve for N ₂	45
31	Melpar Cross Section Ionization Detector	54
32	Effect of Voltage on Base Line Current	55
33	Photograph of Oven	58
34	Cross Section of a Chemical Heater Cartridge	63
35	Firing Sequence for Chemical Heaters	66
36	Schematic of Firing Control Circuit for Oven	67
37	Photograph of Control Assembly	68
38	Photograph of Control Assembly	69
39	Temperature Characteristics of Simulated Oven Heated with Chemical Heaters	72
40	Slide Injection Valve (Side View)	75
41	Slide Injection Valve (Top View)	76
42	Squib-Actuated, Two-Way Valve	83
43	Mock-up Board	85

LIST OF ILLUSTRATIONS (Continued)

<u>Figure</u>		<u>Page</u>
44	Simplified Operational Amplifier Connection	88
45	Infinite Impedance Input Equivalent Circuit	90
46	High Input Impedance D.C. Amplifier	92
47	Equivalent of Input Signal Sampling Amplifier	94
48	Input Impedance Multiplication by Sampling	95
49	Functional Block Diagram of Sampling D.C. Amplifier	97
50	Schematic Diagram of P-2 Operational Amplifier	100
51	Customary Laboratory Buckout Network	101
52	Servo-Type Automatic Zeroing System	102
53	Switched Electronic Automatic Zeroing System	104
54	Functional Block Diagram of Self-Zeroing Electrometer Amplifier	106
55	Frequency Response of Electrometer	109
56	Block Diagram of the Logarithmic Amplifier	112
57	Response of Logarithmic Amplifier to a Triangular Waveform	114
58	Response Function of Logarithmic Amplifier	115
59	Logarithmic Modification of Detected Gas Sample	116
60	Low-Voltage Power Supply	117
61	Typical Series Voltage Regulator	119

LIST OF ILLUSTRATIONS (Continued)

<u>Figure</u>		<u>Page</u>
62	Functional Block Diagram of Gas Chromatograph Amplifier	121
A 1	Injector Valve	131
A 1.D1	Squib Retaining Plate	132
A 1.D2	Squib Retaining Block	133
A 1.D8	Squib Housing No. 2 Rocker Arm	134
A 1.D9	Plate	135
A 1.D10	Base Plate	136
A 1.D11	Pressure Plate	137
A 1.D12	Plate Spacer	138
A 1.D13	Pressure Spring Plate	139
A 1.D14	Side Plate, Selector Valve	140
A 1.D15		
16	Cage End Plate and Pin	141
A 1.D17	Retaining Plate	142
A 1.D18	Selector Valve	143
A 1.D19	Spring	144
A 2	Pump Nozzle Restrictor	145
A 3	Pump Body	146
A 4	Reference Gas Chamber	147
A 5	Squib-Actuated, Two-Way Valve	148
A 5.D1	Squib Retained	149

LIST OF ILLUSTRATIONS (Continued)

<u>Figure</u>		<u>Page</u>
A 5.D2	Squib Housing No. 1	150
A 5.D3	Squib Seal	151
A 5.D4 D5	Spacers	152
A 5.D6	Glass Diaphragm	153
A 5.D7	Plunger	154
A 5.D8	Squib Housing No. 2	155
A 5.D9	Squib Housing No. 3	156
A 5.D10	Seal	157
A 6	Electronic Chassis	158
A 7	Cover for Electronic Chassis	159
A 8	Design Drawing for Gas Chromatography Oven	160
A 9	Design Drawing for Cross Section Ionization Detector	161

1. INTRODUCTION

This volume of the final report is an overall summary of Melpar's efforts under JPL Contract No. 950326. Included are (1) the configurational lay-out of the laboratory model, (2) performance data, (3) a somewhat detailed consideration of the various components and their characteristics and behavior, and (4) design drawings.

It has not been considered appropriate to repeat in this volume detailed results from the three monthly reports, particularly when such results do not directly pertain to the finalized laboratory model. Reference will be made from time to time to the monthly reports in supplementing certain aspects of the presentation in this volume.

As a whole, the functional laboratory model meets the specifications delineated by Jet Propulsion Laboratories. These specifications in some instances are exceeded. By the same token, in a few instances, certain specifications are approached but not completely realized.

Design drawings for the most part are given in the appendix.

2. CONFIGURATION OF OVERALL SYSTEM

The final system as developed in this project, shown schematically in figure 1, is believed to approach closely the optimum compromise between the numerous configurations possible. The schematic, although not to scale, indicates the column and detector configuration. This system will provide the desired separation and sensitivity for nearly all the possible components projected to last in the Martian atmosphere. Reliability was the major factor considered in the design of the system. Dynamic range, sensitivity, separation, power requirements, and weight were other major considerations. Figures 2 and 3 are photographs of the laboratory model on a mock-up board.

The system, as shown in figure 1, is designed to operate at 300°K with a flow rate of 175 ml He/min. STP. The absolute inlet pressure is 80 psi, while the exit pressure is 20 psi. The helium used in this system is common tank gas purified only by a molecular sieve trap. The injection valve is a sliding plate type operated by squibs.

All detectors are microcross section detectors. Output from the first two detectors is sent to amplifier 1, while detectors 3 and 4 are connected to amplifier 2.

The first column is designed to elute NH_3 shortly after air and to elute water within 5 to 6 minutes. Column 2A is an empty tube, designed to delay the passage of air into

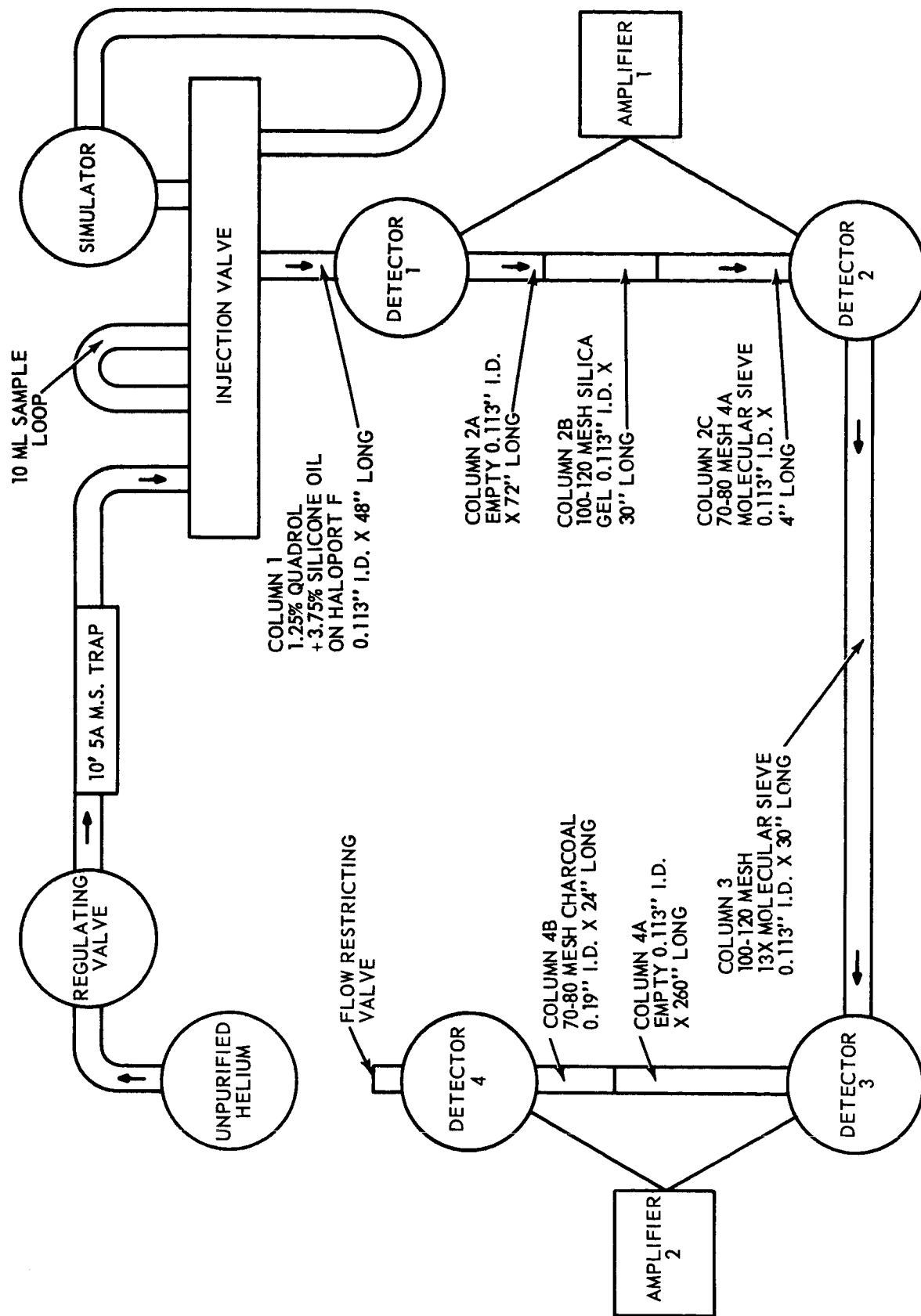


Figure 1. Overall System Drawing

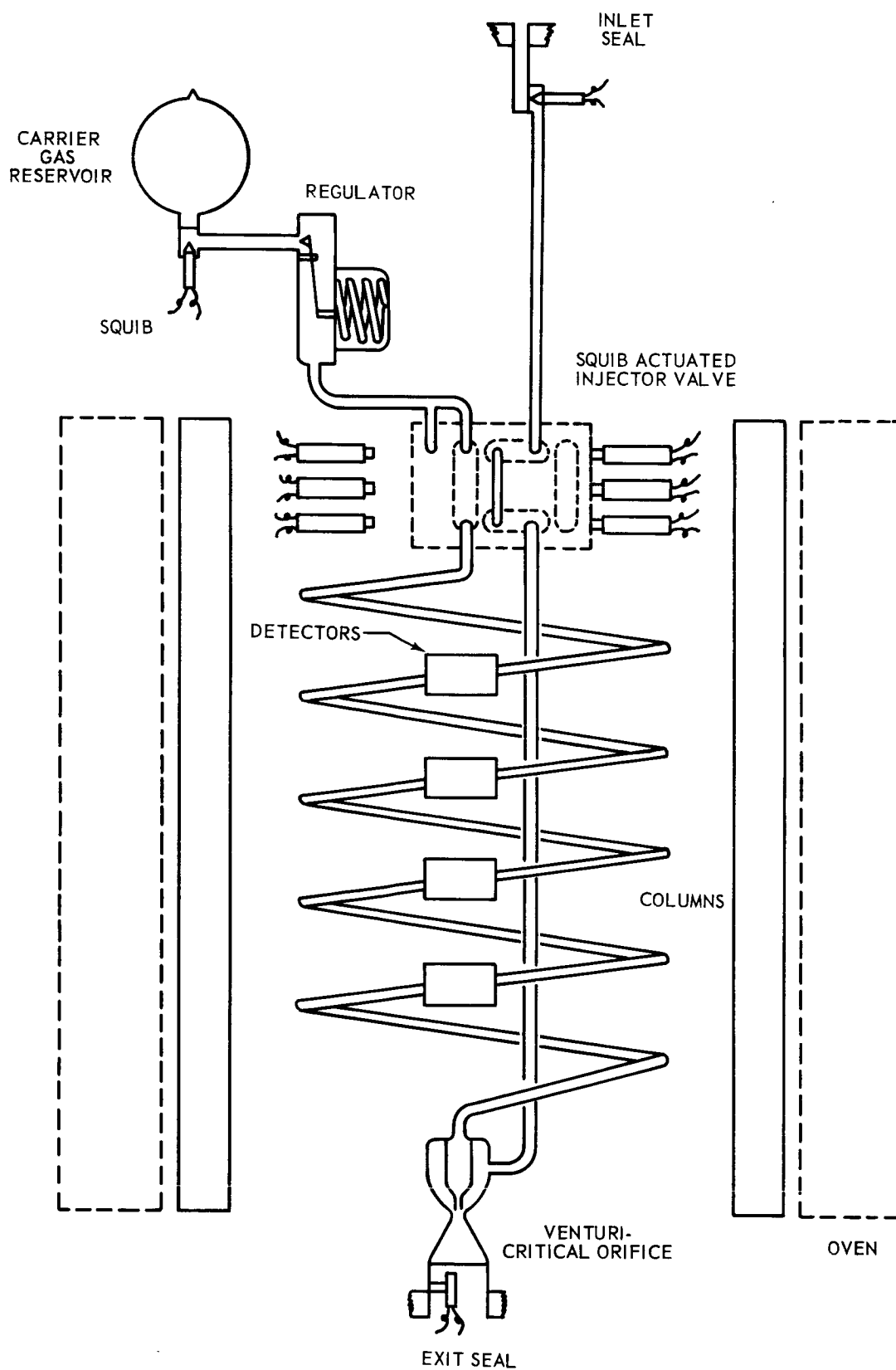
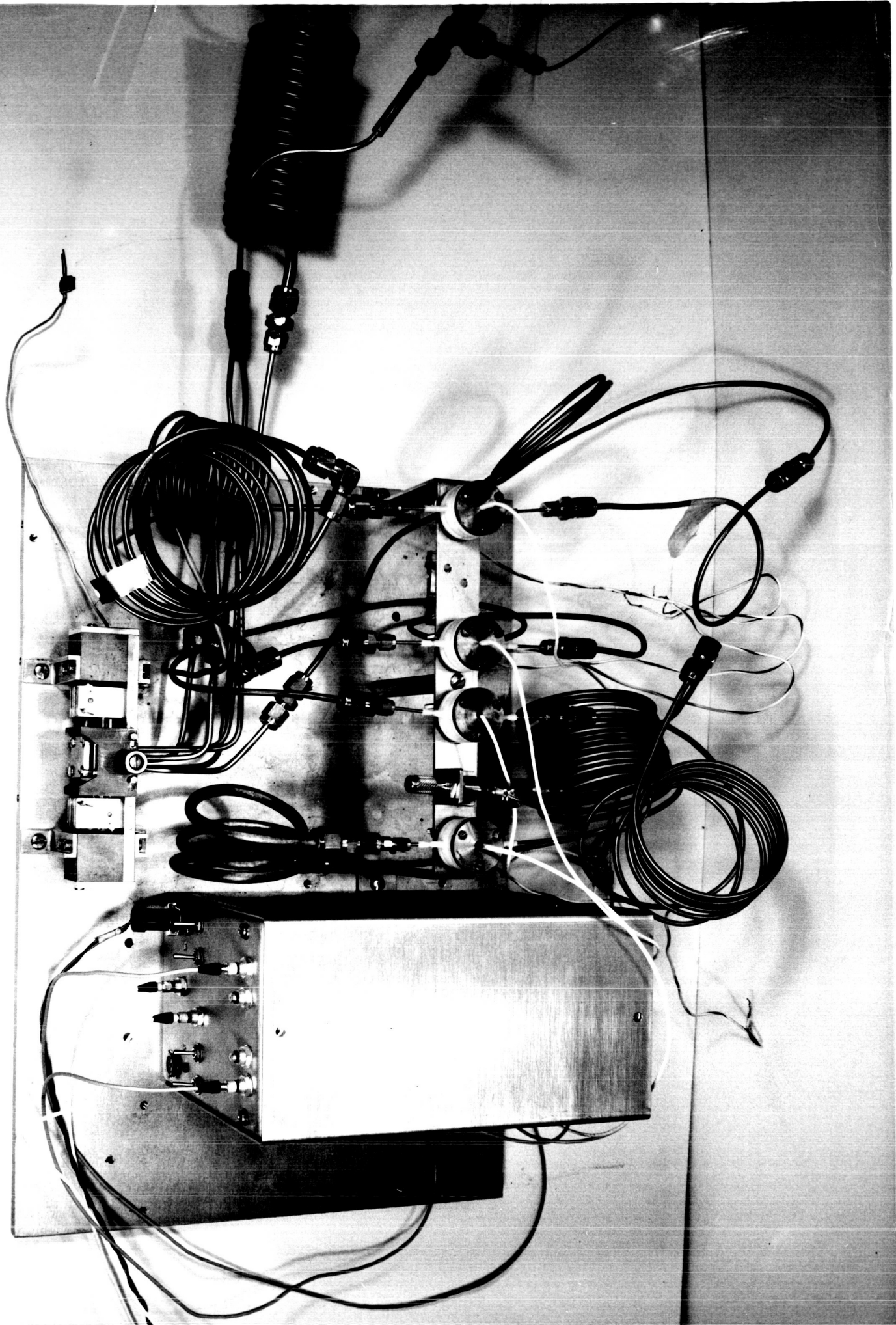


Figure 2. System Lay-out



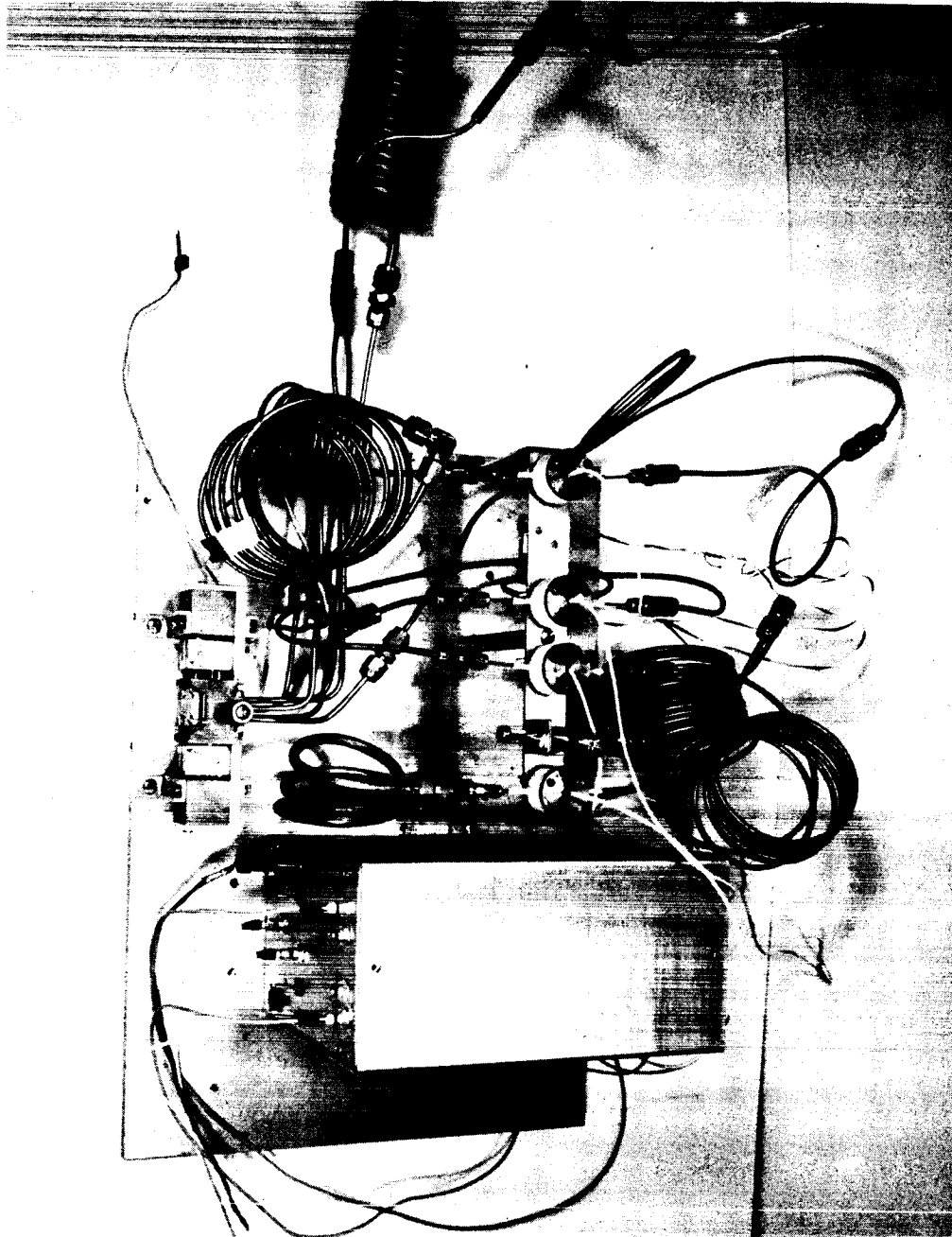
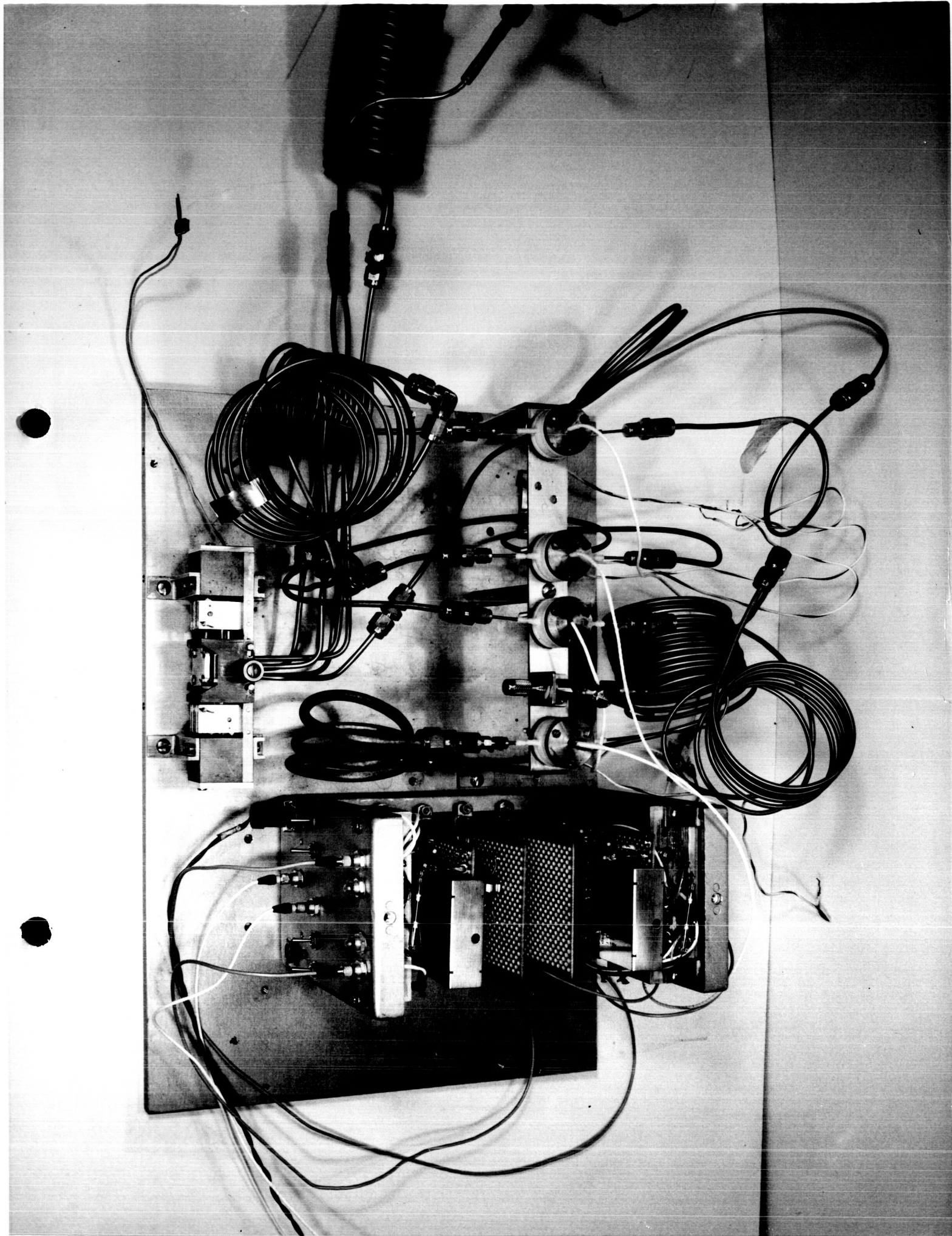


Figure 3. Photograph of Laboratory Model

detector 2 until after NH_3 has been eluted from column 1. Column 2B is a short silica gel column used to separate Kr, Xe, C_2H_5 , and CO_2 . Column 2C, a short molecular sieve column, permits the otherwise impossible separation of N_2O from CO_2 . Column 3 is a conventional molecular sieve column serving to separate H_2 -Ne, A- O_2 , N_2 , CH_4 , CO, and Xe. Column 4B is a highly activated charcoal column which adsorbs O_2 , thus allowing A to appear as a separate peak. Column 4A is designed to delay the elution of compounds into detector 4 to prevent interference with detector 3 peaks. A number of compounds appear more than once. Kr and Xe are detected by both detector 2 and 3. H_2 and N_2 are seen by detectors 3 and 4. This repetition is highly desirable since it acts as an internal check on the performance of both the columns and detectors.

In figure 4, the general schematic of the mechanical layout for the system is shown. Of particular interest here are the Venturi used for pumping a sample through the sample loop, the critical orifice for regulating helium flow through the system, a squib actuated injector valve, and the in-transit sealing provision.



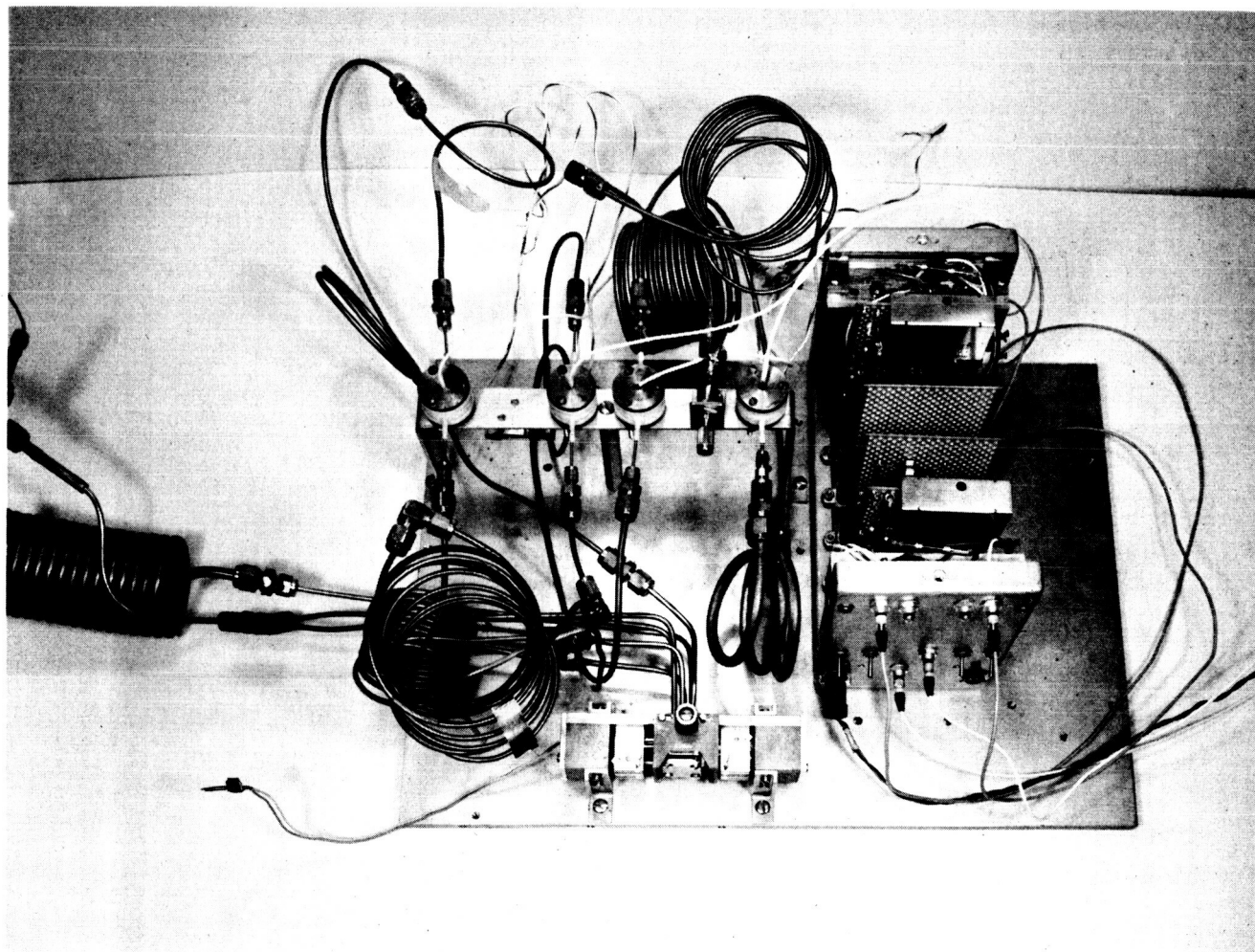


Figure 4. Photograph of Laboratory Model

3. OVERALL SYSTEM PERFORMANCE

Typical chromatograms as seen by amplifiers 1 and 2 are shown in figures 5 and 6, respectively. As seen in figure 5, the composite air peak seen by detector 1 is the first to appear, followed shortly thereafter by the NH_3 peak. The composite air peak then appears in detector 2 and is followed by the krypton peak. Xenon appears by itself, followed by C_2H_6 , N_2O and CO_2 in detector 2. Some peak overlapping of N_2O and C_2H_6 exists, but the present separation would be adequate for any situation except where ethane was present in very large quantities and N_2O was present in very low concentration or vice versa. This is highly unlikely. H_2S is not separated within the present 5-minute analysis period. Such separation, could be realized within an analysis time of the converter. NO and NO_2 are irreversibly adsorbed by the columns.

Figure 6 shows the chromatogram of the remaining possible atmospheric compounds as seen by amplifier 2. H_2 , O_2 , and N_2 appear in the normal molecular sieve fashion. Argon, if present, is eluted with the O_2 peak. Kr, which had been previously separated in column 2 and seen by detector 2, is eluted shortly after N_2 . CH_4 is separated on column 3 and seen by detector 3. H_2 again appears at detector 4. This is followed by CO at detector 3. Argon alone and N_2 are eluted into detector 4. This enables differentiation between

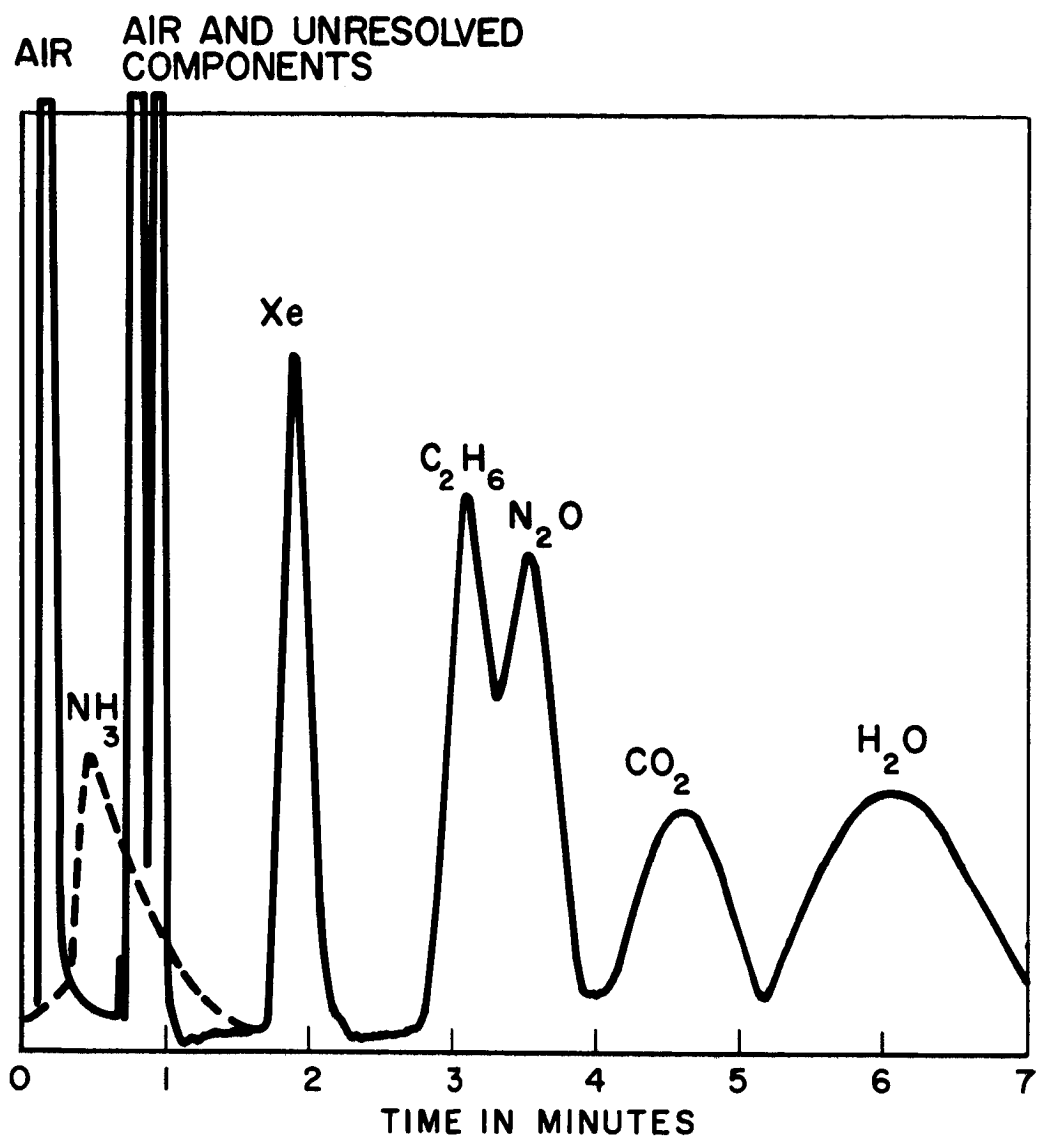


Figure 5. Chromatograms with Detectors 1 and 2

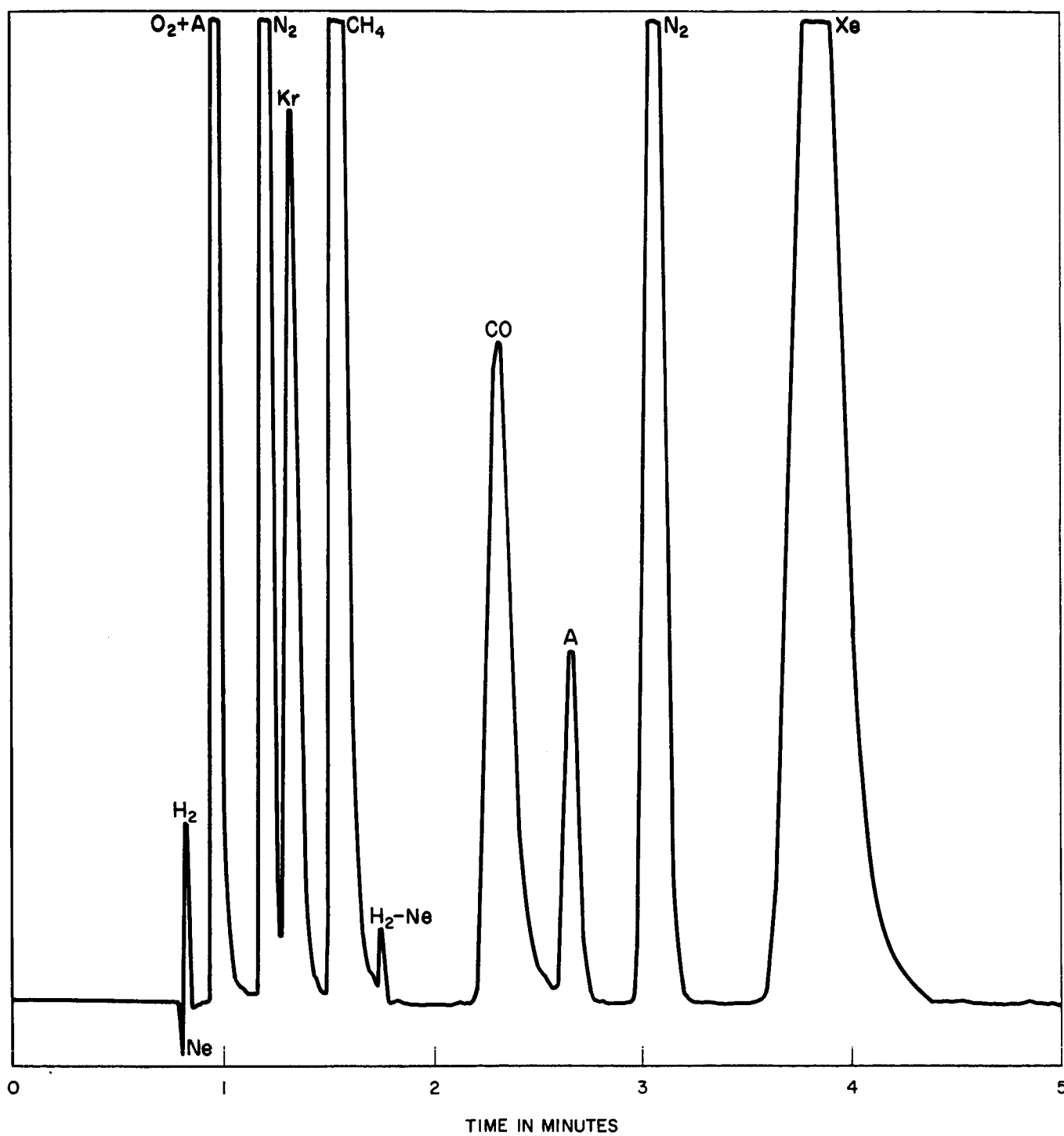


Figure 6. Chromatograms with Detectors 3 and 4

A and O_2 to be made. Xe then appears again at detector 3. Thus, a separation of all the major components has been achieved. Since several of these are seen twice, as an internal check exists for the system most of the minor components also have been separated. N_2O is a highly desirable component; its separation has been achieved through the use of a short molecular sieve column. The detection of N_2O in the Martian atmosphere would indicate the probable presence of other nitrogen oxides since they tend to form equilibrium mixtures.

The type of microcross section detectors previously investigated were used in this system. Initial calibration studies were made with gas-tight syringes and a rubber septum. The test gases were either used directly or as 1% mixtures in helium. Calibration curves for the various compounds are shown in figures 7-18. Because of sampling errors and impurities present in the gases, the estimated error for any one point on the curves may be 1% too high or 10% too low. Since the total noise and drift at amplifier 1 is 3×10^{-12} amperes and that at amplifier 2 is 2×10^{-12} amperes, less than 0.01 μl of most of the compounds could readily have been detected. The sensitivity to NH_3 is poor. This is no doubt due to column adsorption. Neon and hydrogen are not resolved. The sensitivity to neon is Ca. 1%. This low sensitivity can be considered advantageous in that neon would

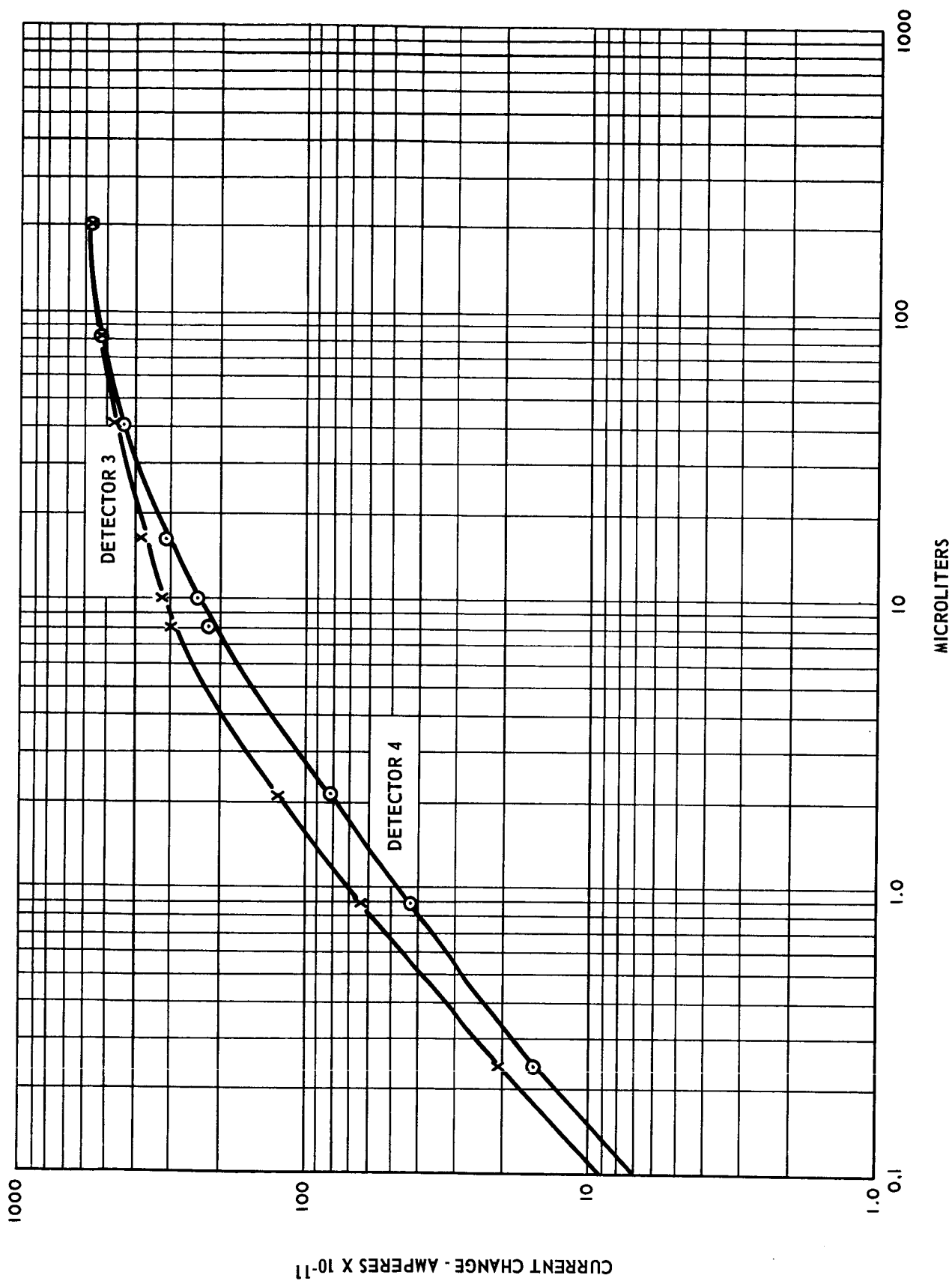


Figure 7. Response Curve for N_2 (Syringe Injection)

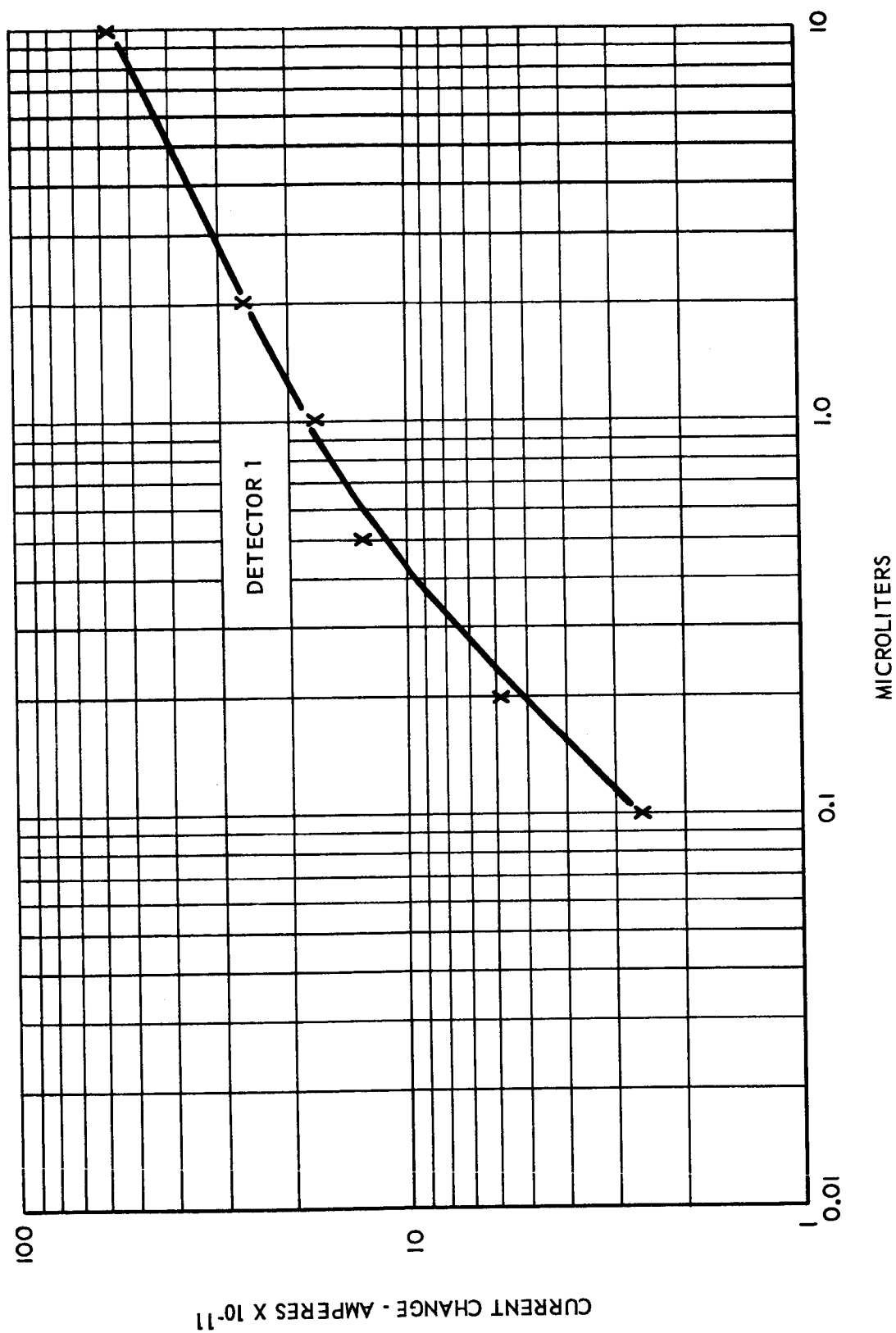


Figure 8. Response Curve for H₂O (Syringe Injection)

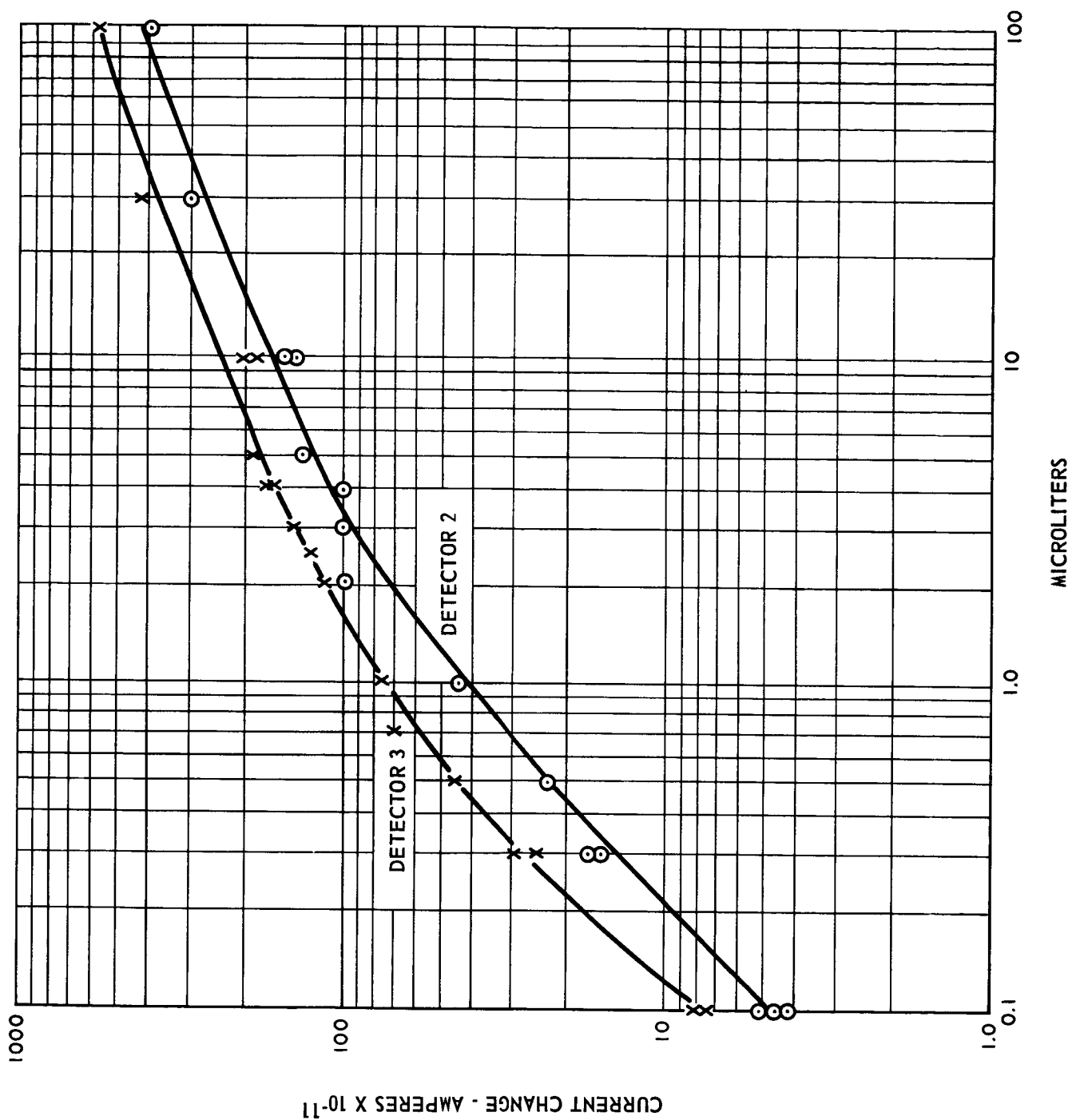


Figure 9. Response Curve for CH_4 (Syringe Injection)

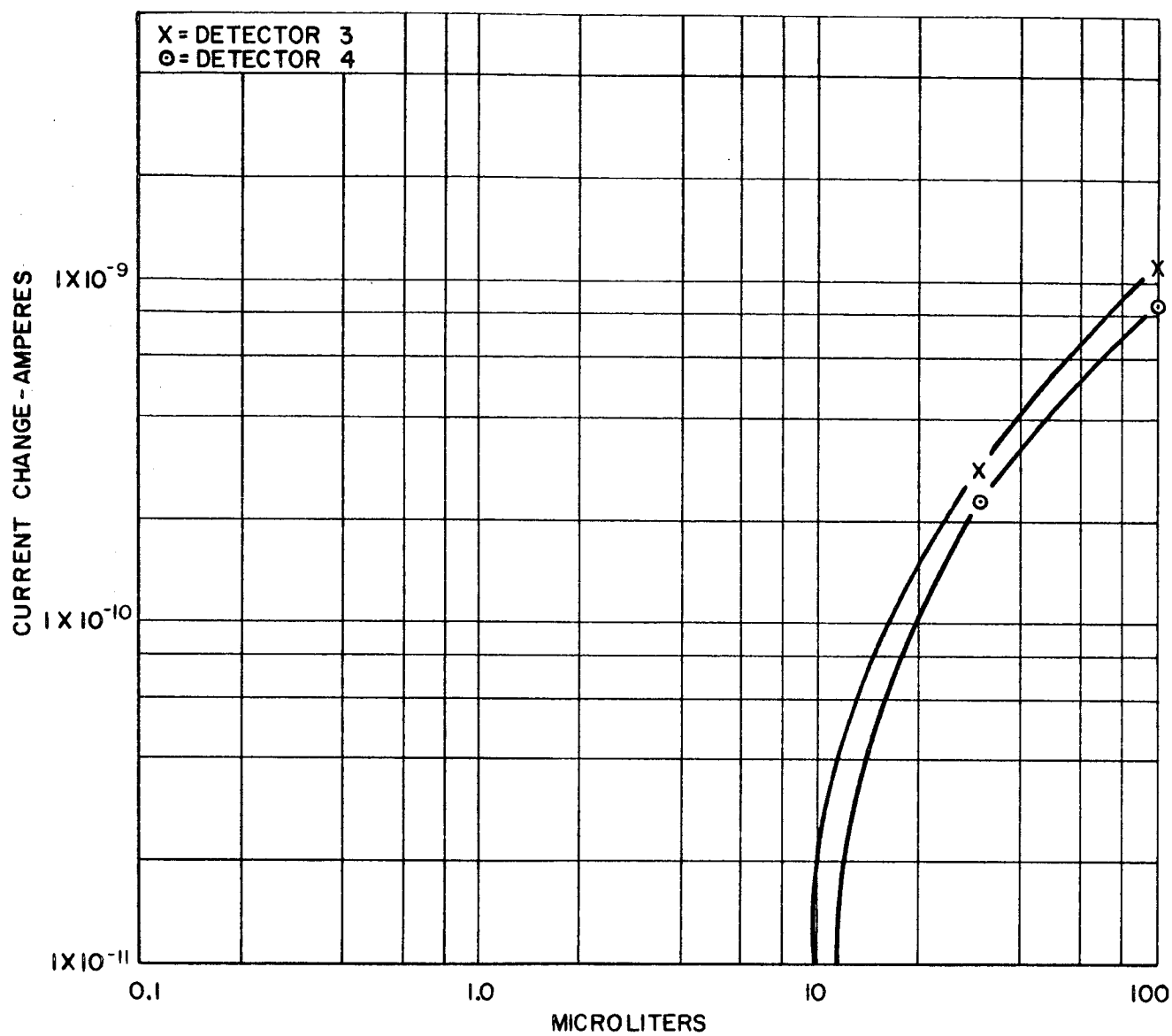


Figure 10. Response Curve for Ne (Syringe Injection)

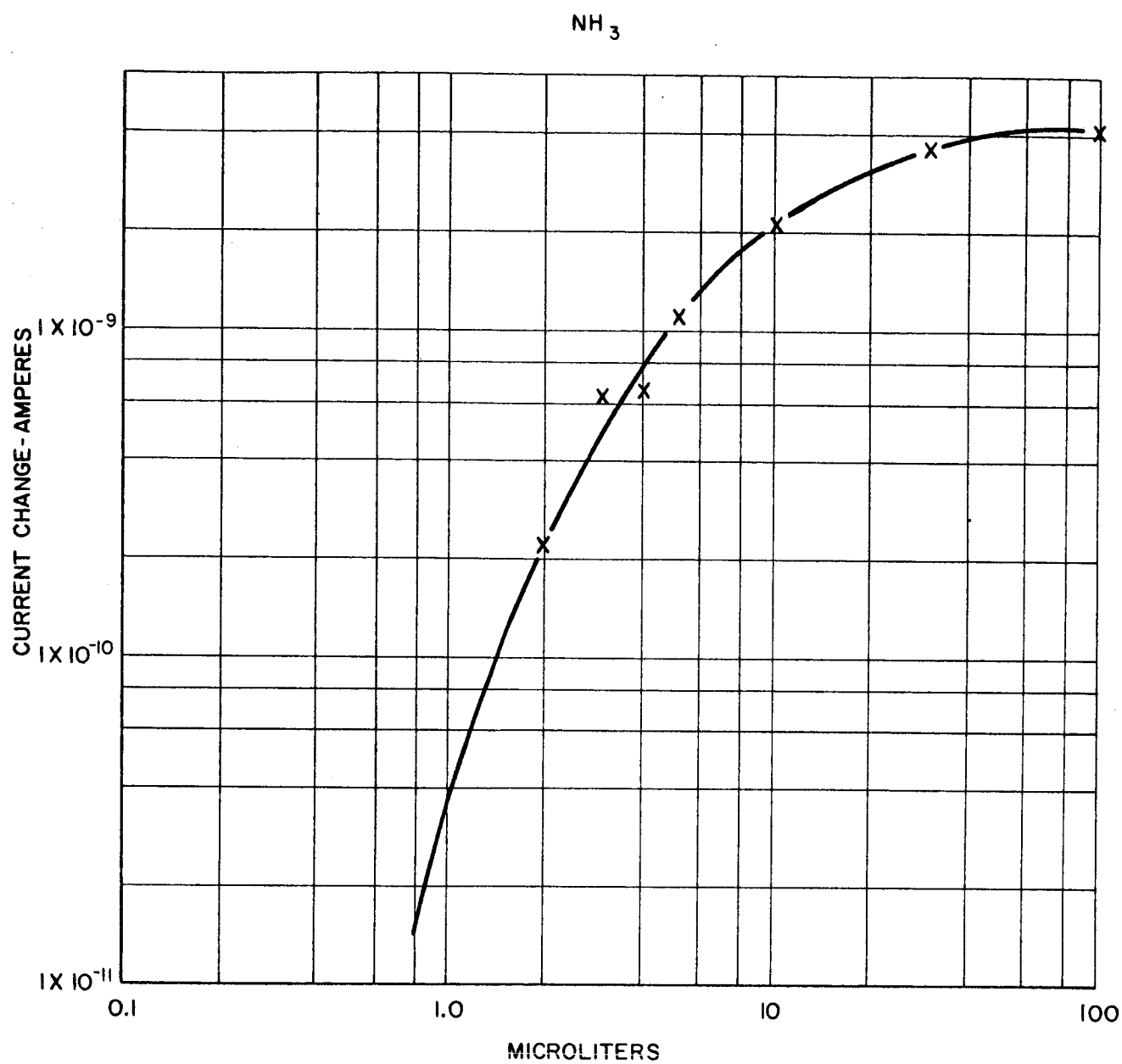


Figure 11. Response Curve for NH_3 (Syringe Injection)

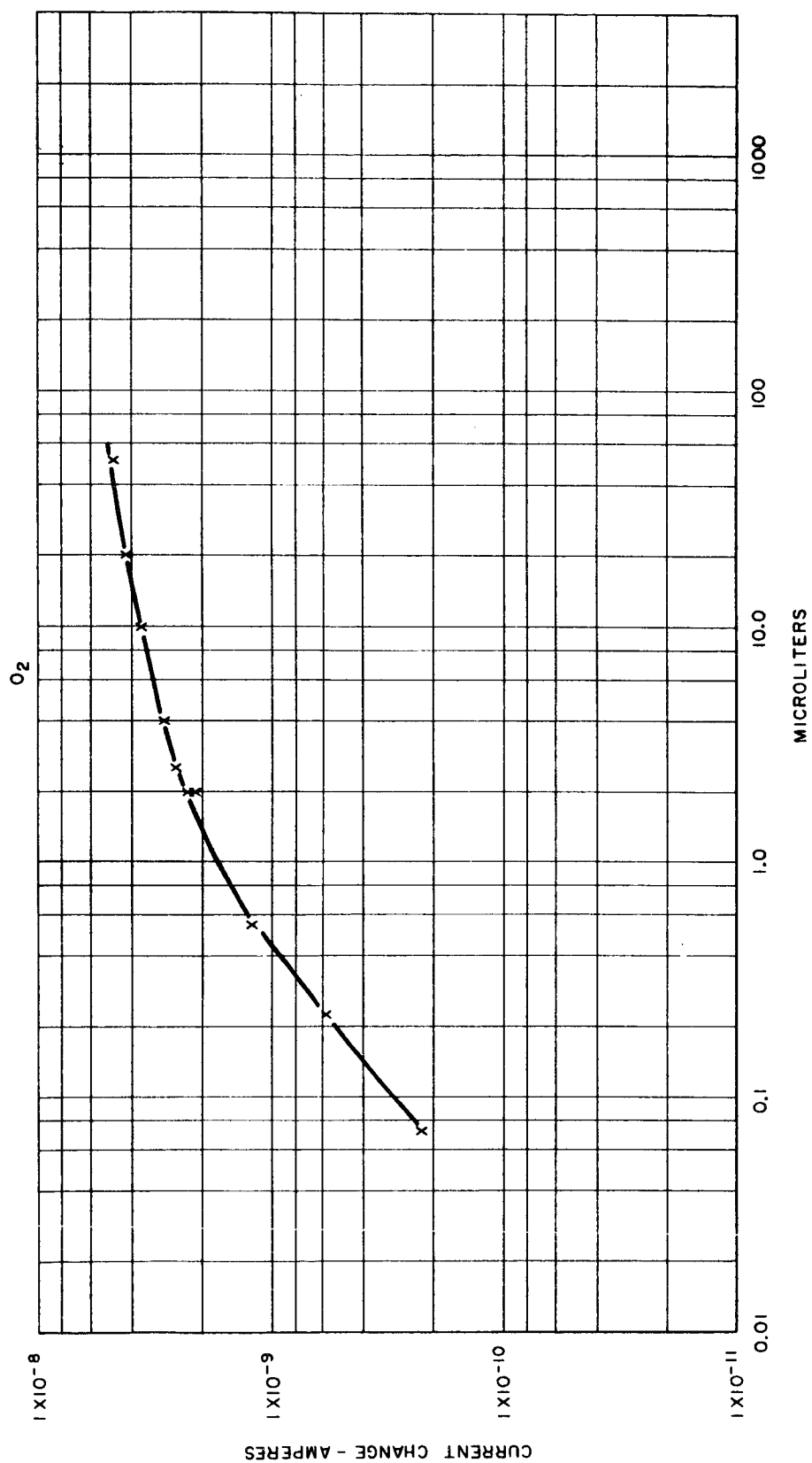


Figure 12. Response Curve for O_2 (Syringe Injection)

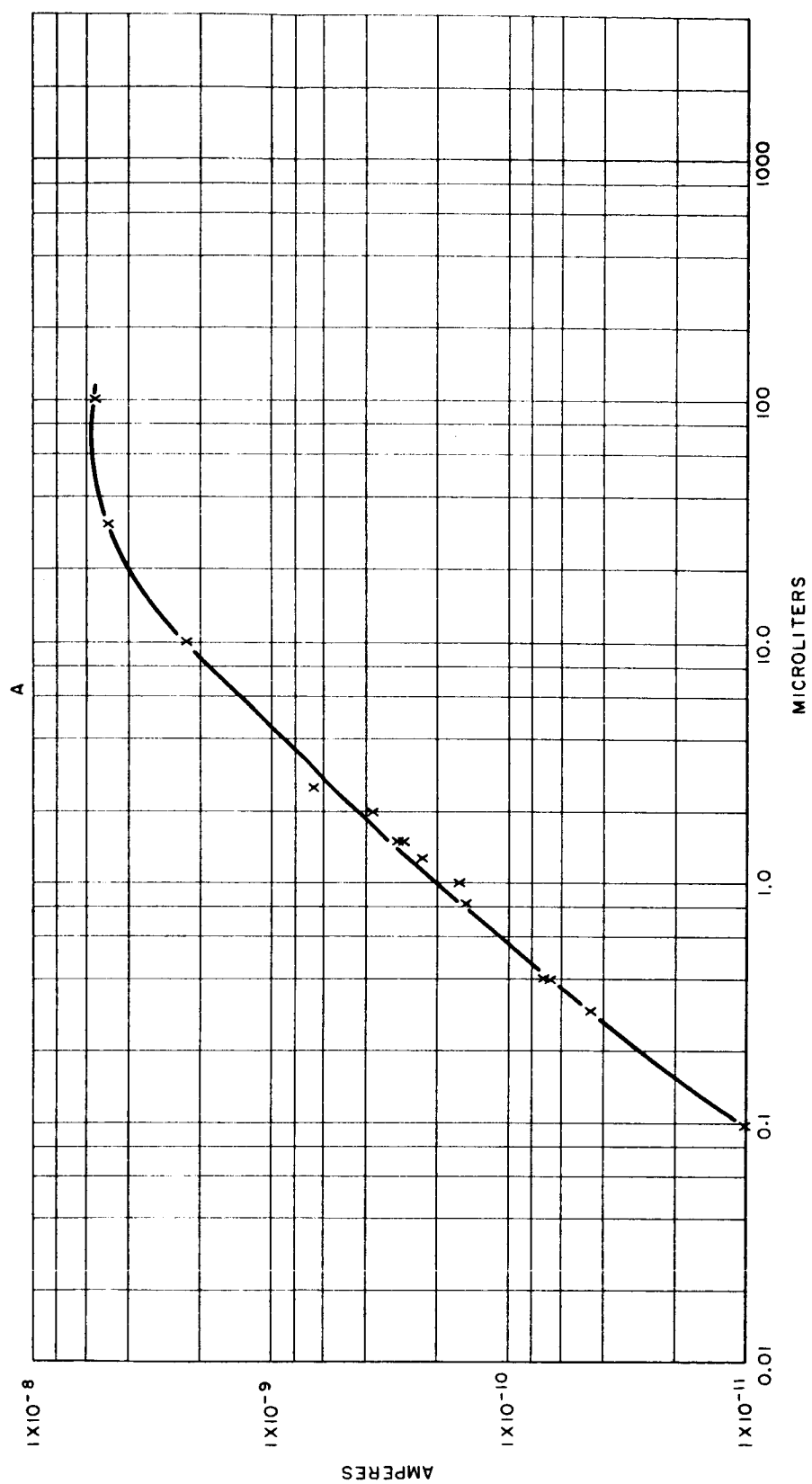


Figure 13. Response Curve for A (Syringe Injection)

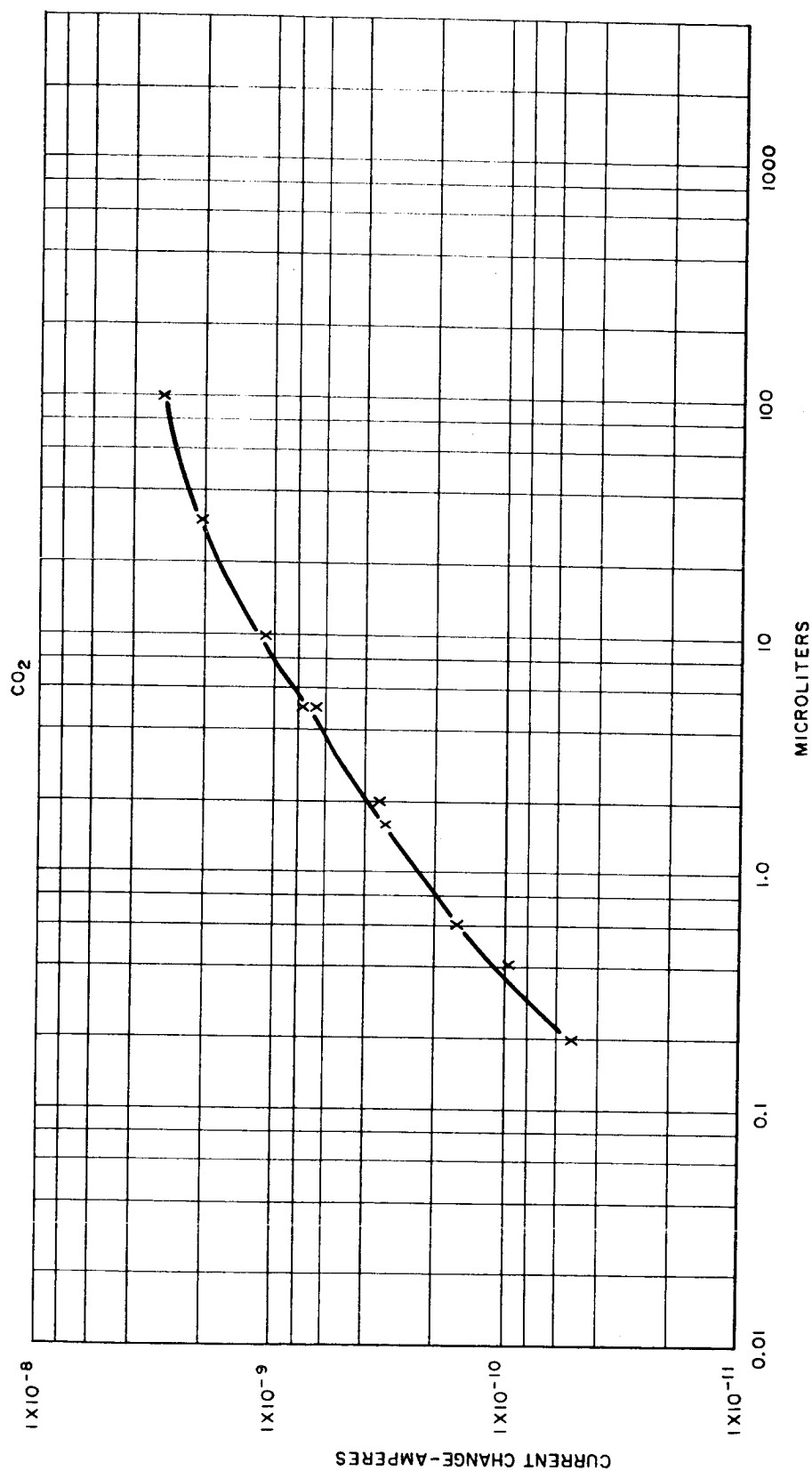
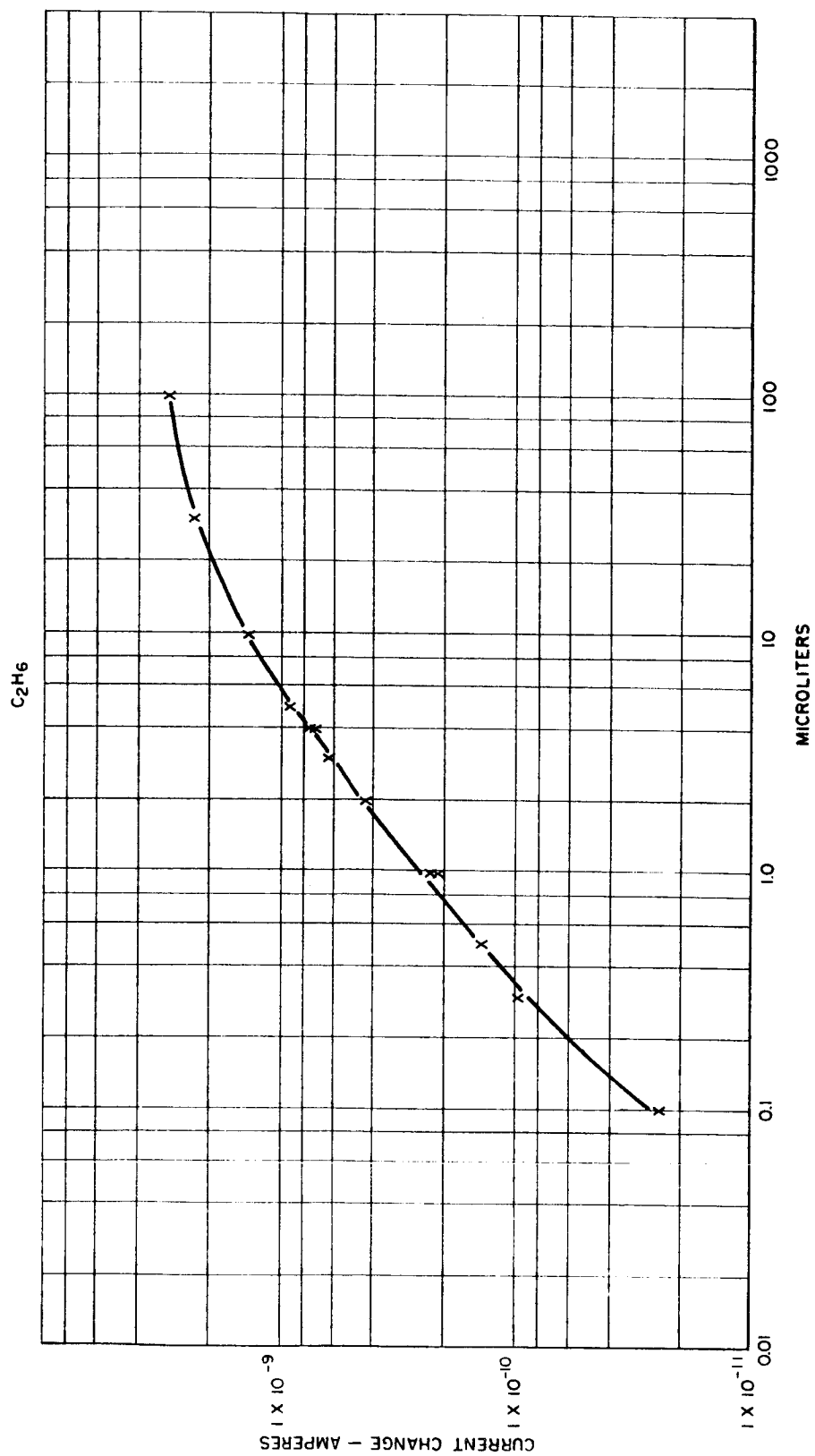


Figure 14. Response Curve for CO₂ (Syringe Injection)

Figure 15. Response Curve for C_2H_6 (Syringe Injection)

R4388

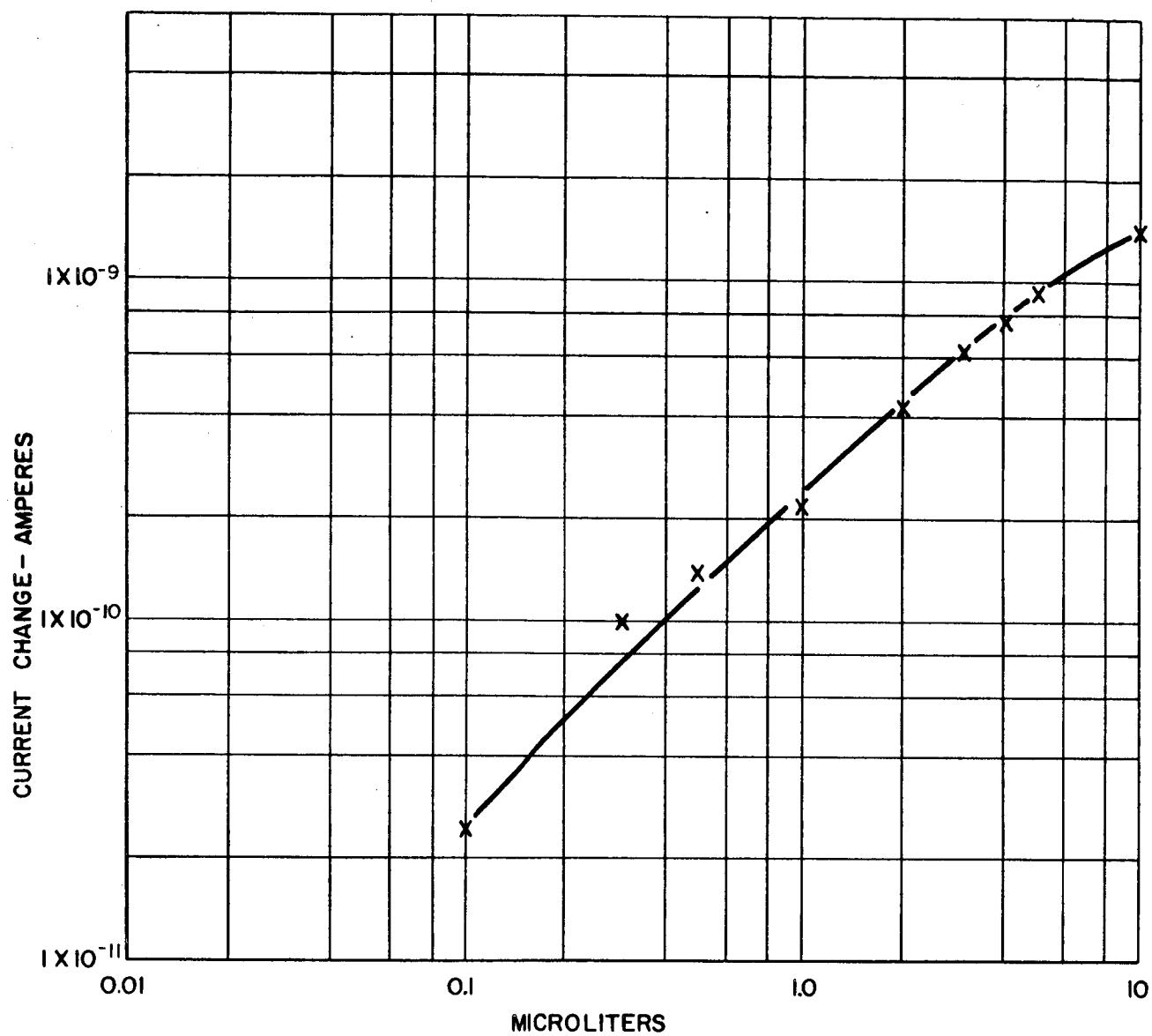
 N_2O 

Figure 16. Response Curve for N_2O (Syringe Injection)

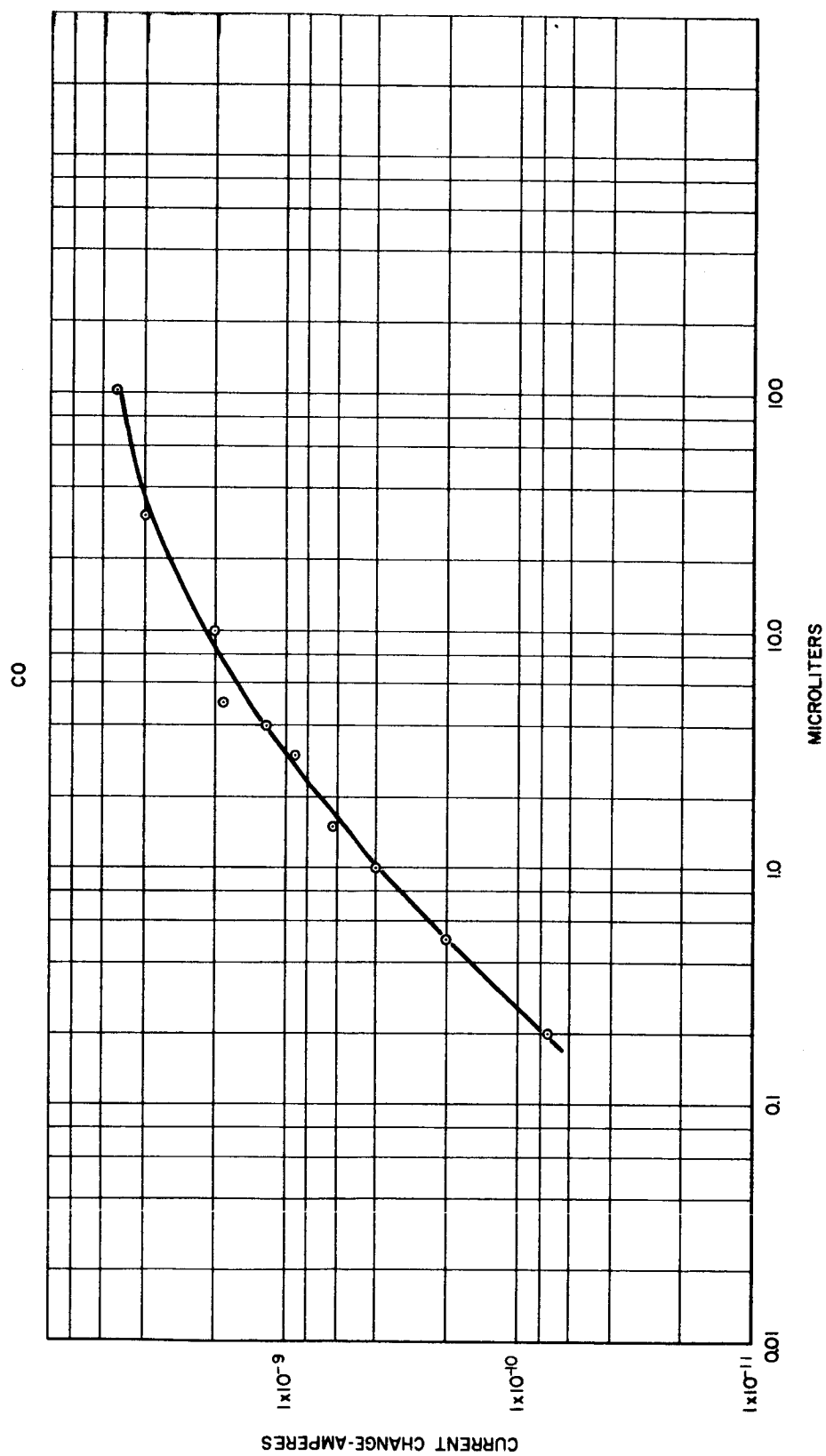


Figure 17. Response Curve for CO (Syringe Injection)

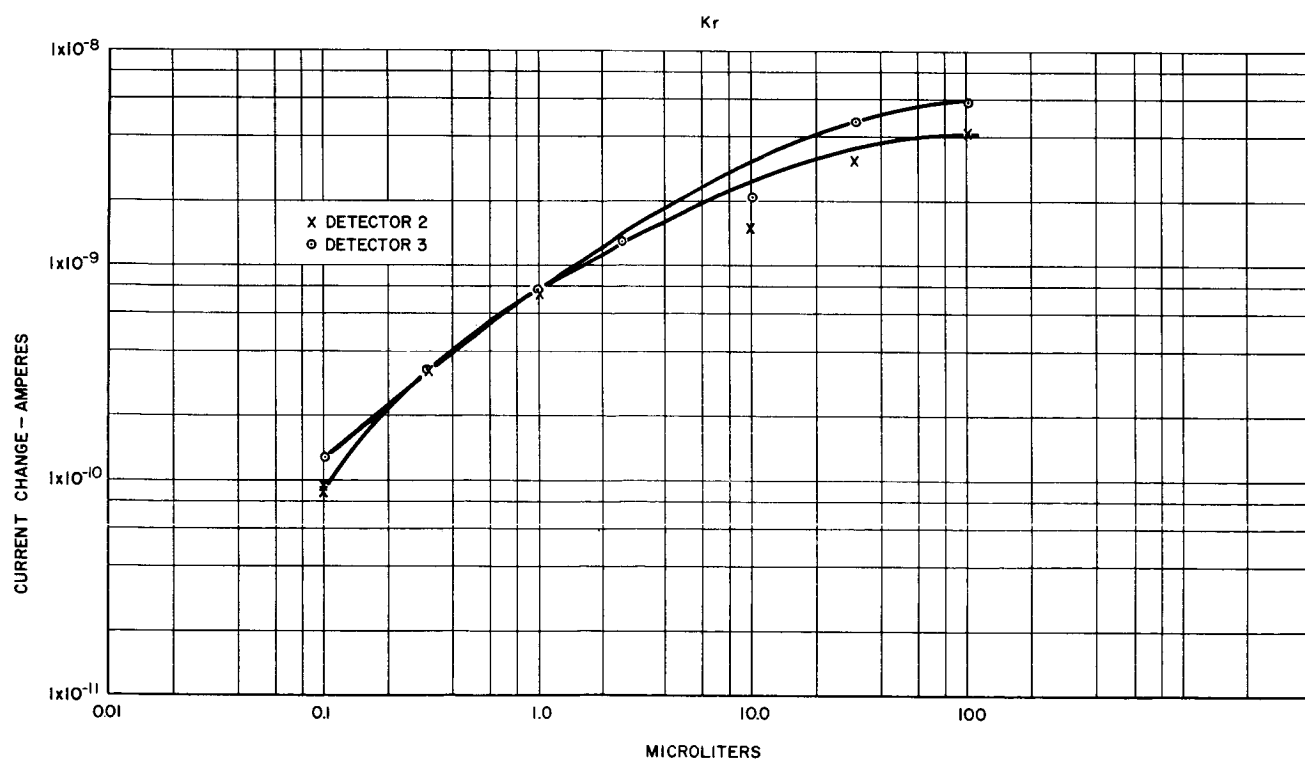
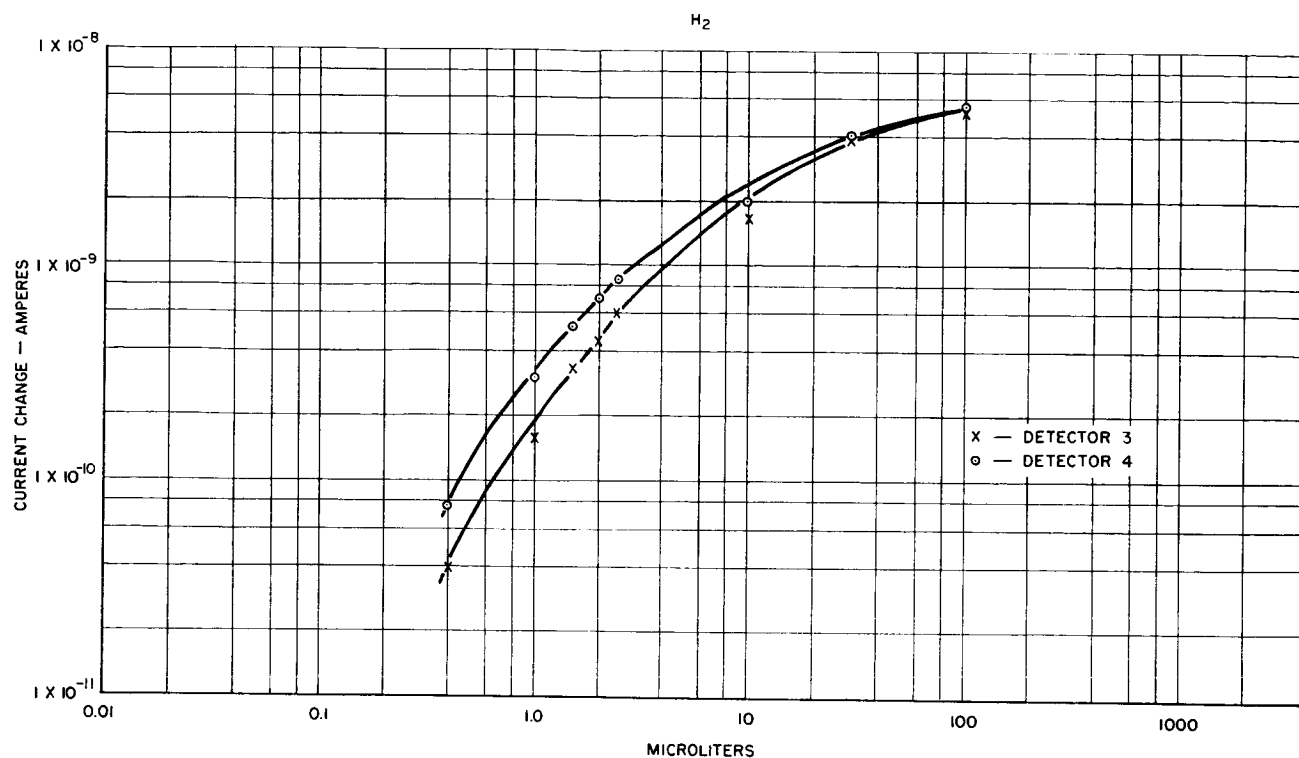


Figure 18. a. Response Curve for Kr (Syringe Injection) and
b. Response Curve for H_2 (Syringe Injection)

otherwise interfere with the hydrogen analysis. Neon is not expected to be present in concentrations greater than 1%.

Considerable difficulties were experienced in obtaining calibration curves with the injection valve and Martian simulator. Extraneous peaks corresponding to 5, 6 and 7 carbon hydrocarbons appeared with strong intensities. After approximately eight hours of operation, response to all compounds would be tremendously reduced due to a leak in the injection valve. Inspection of the valve showed that foreign particles had ground ridges in the valve. This dirt is believed to have originated from either the vacuum pump or sealant used to seal the simulator. Consequently, a new simulator system was built and used for all further calibration studies. This is shown in figure 19. The sequence of operational events with this simulator was as follows: (1) Open vacuum pump valve, (2) Open helium flushing gas valve, (3) Close helium flushing gas valve, (4) Close vacuum pump valve, (5) Insert sample with syringe, (6) Admit small amount of helium, (7) Allow 30 minutes equilibration time, (8) Operate injection valve. This procedure allowed reproducible results to be obtained. It was found to be impossible to calibrate for H_2O , O_2 , or N_2 by this method because of the large amounts of these compounds always present. H_2 could not be analyzed with this apparatus because of diffusion through the rubber components. Calibration curves

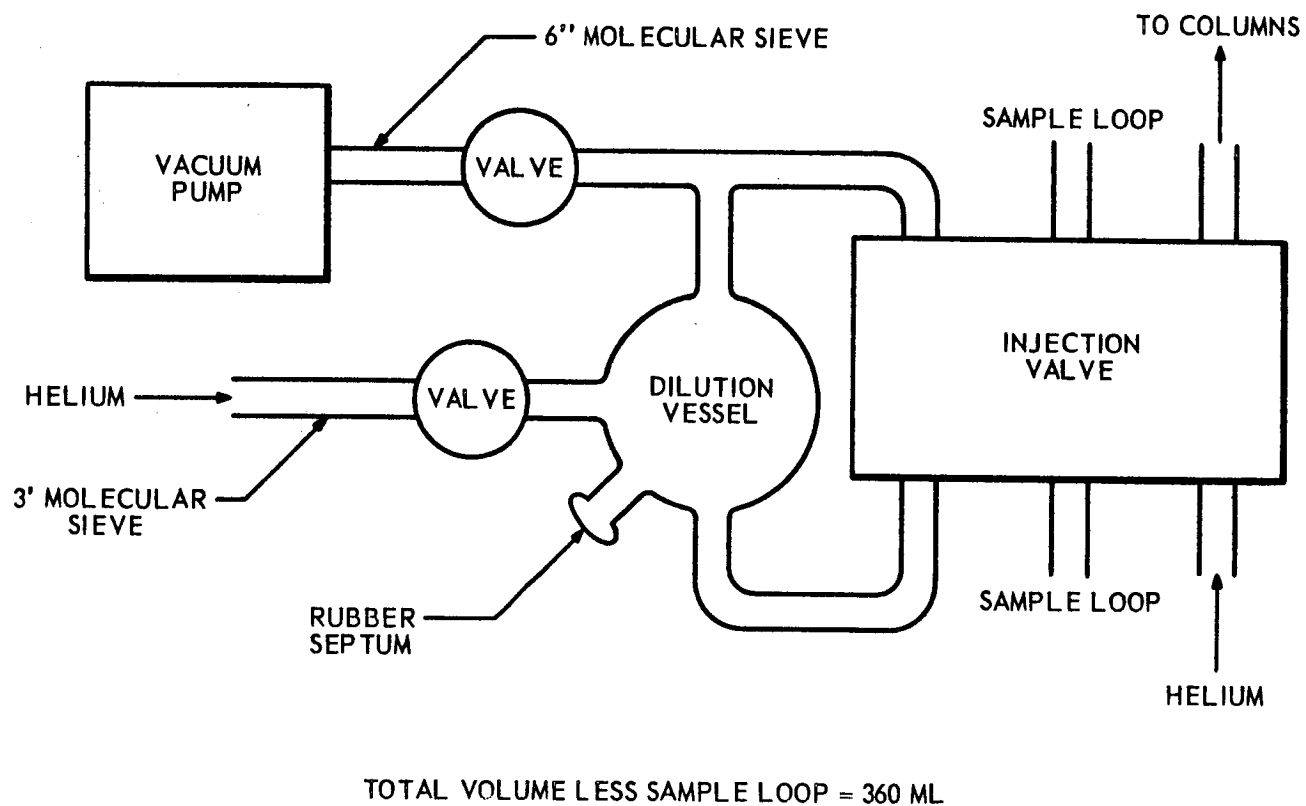


Figure 19. New Martian Atmosphere Simulator

for the compounds other than H_2O , O_2 , N_2 and H_2 are shown in figures 20-27. These curves were obtained with a 15cc sample loop. It may be seen that less than 10 ppm of all these compounds could easily be detected. Values for some of the compounds at the 13% concentration level were extrapolated from their peak shapes because the limit of detectability with the present amplifiers is 6×10^{-9} amperes. Peaks larger than this value are, therefore, squared off at this value. This limitation could be easily corrected by attenuation of the amplifier input (the extreme sensitivity capabilities of the amplifiers is not needed) or by the use of logarithmic amplifiers. The detectors, however, show no signs of saturation since the response is still increasing at the 13% level. Thus, a dynamic range of 10^4 has been proven, and the true dynamic range of the detectors is probably close to 10^6 . The required dynamic range is 10^5 for N_2 but only 10^4 for the other components.

In addition to calibration problems previously mentioned with this technique, it is still doubtful that the calibration mixtures were completely equilibrated. Since the mixtures were injected at the furthest point from the sample loop, any nonequilibration would lead to lower response values. The sensitivities implied by these calibration curves may, therefore, be too conservative. Even though any error is on

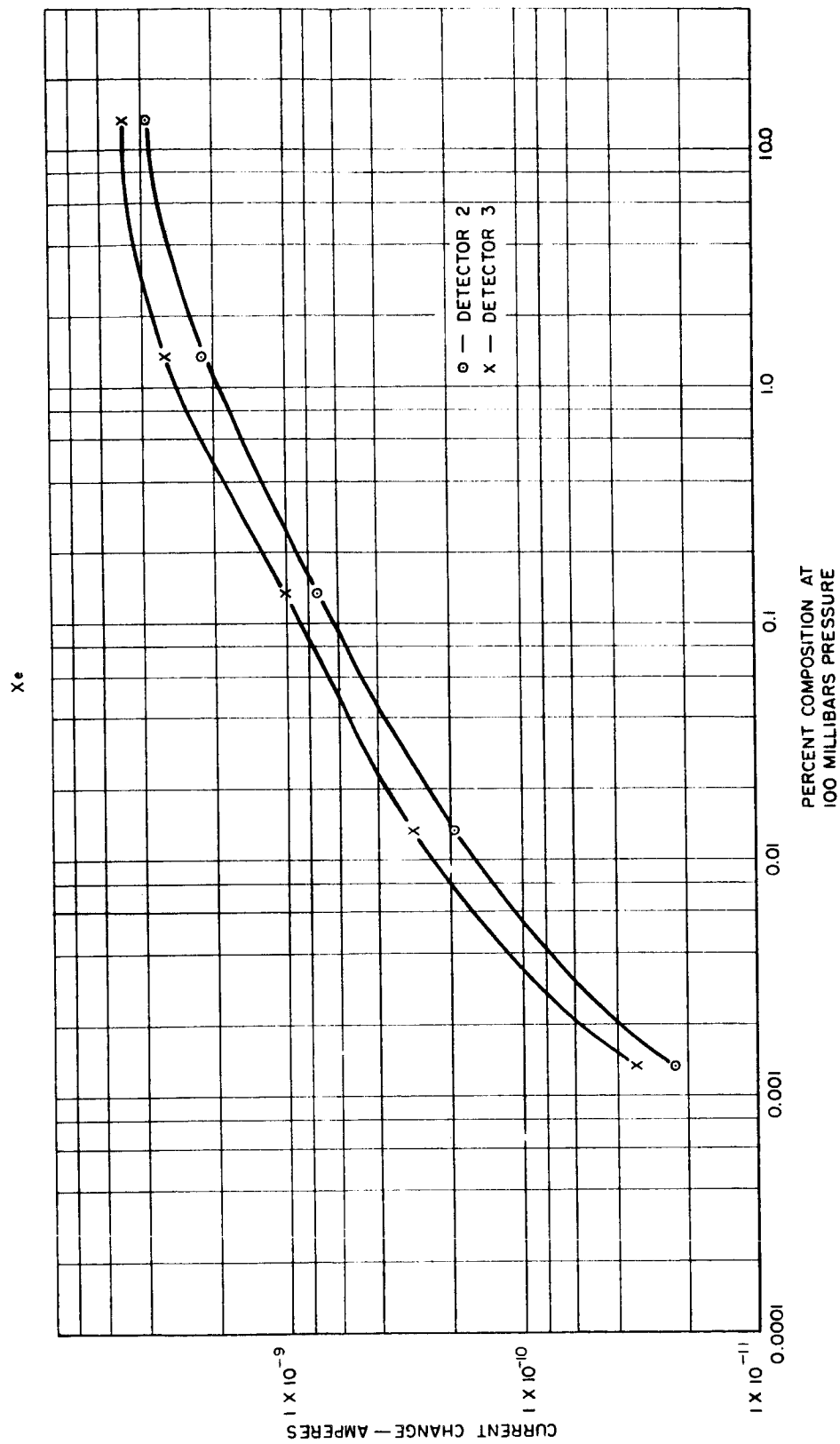


Figure 20. Response Curve for Xe

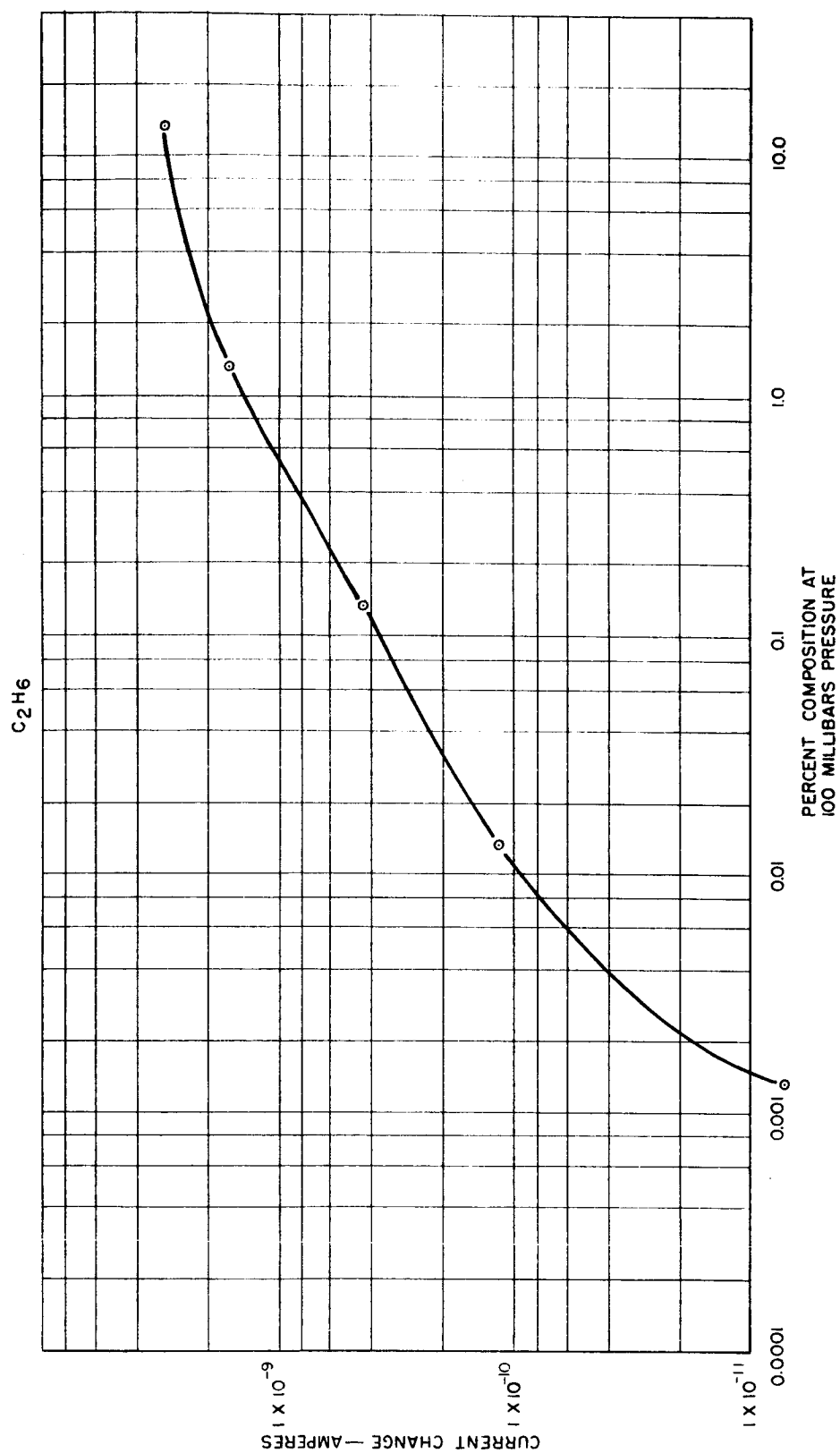
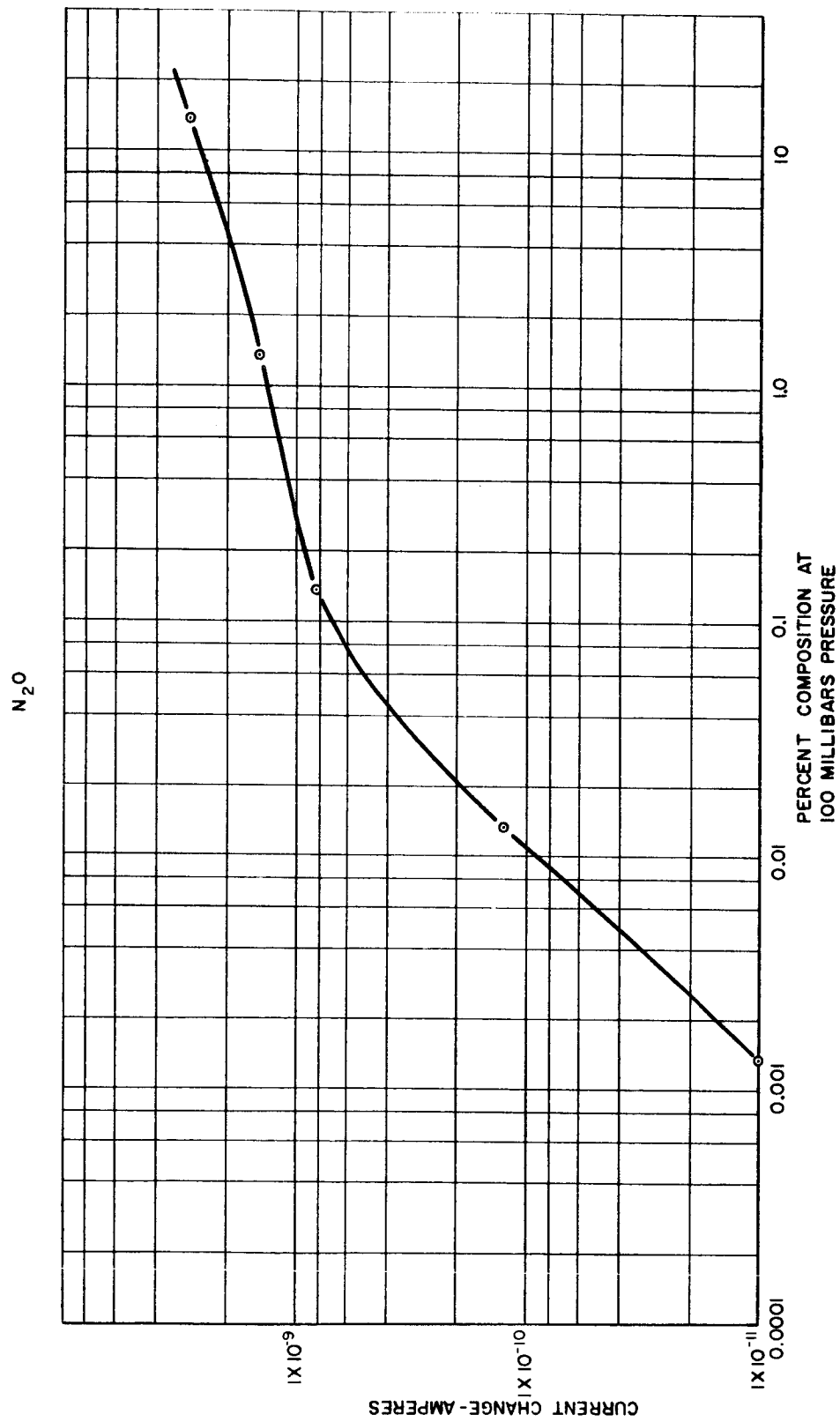


Figure 21. Response Curve for Ethane

Figure 22. Response Curve for N_2O

R4394

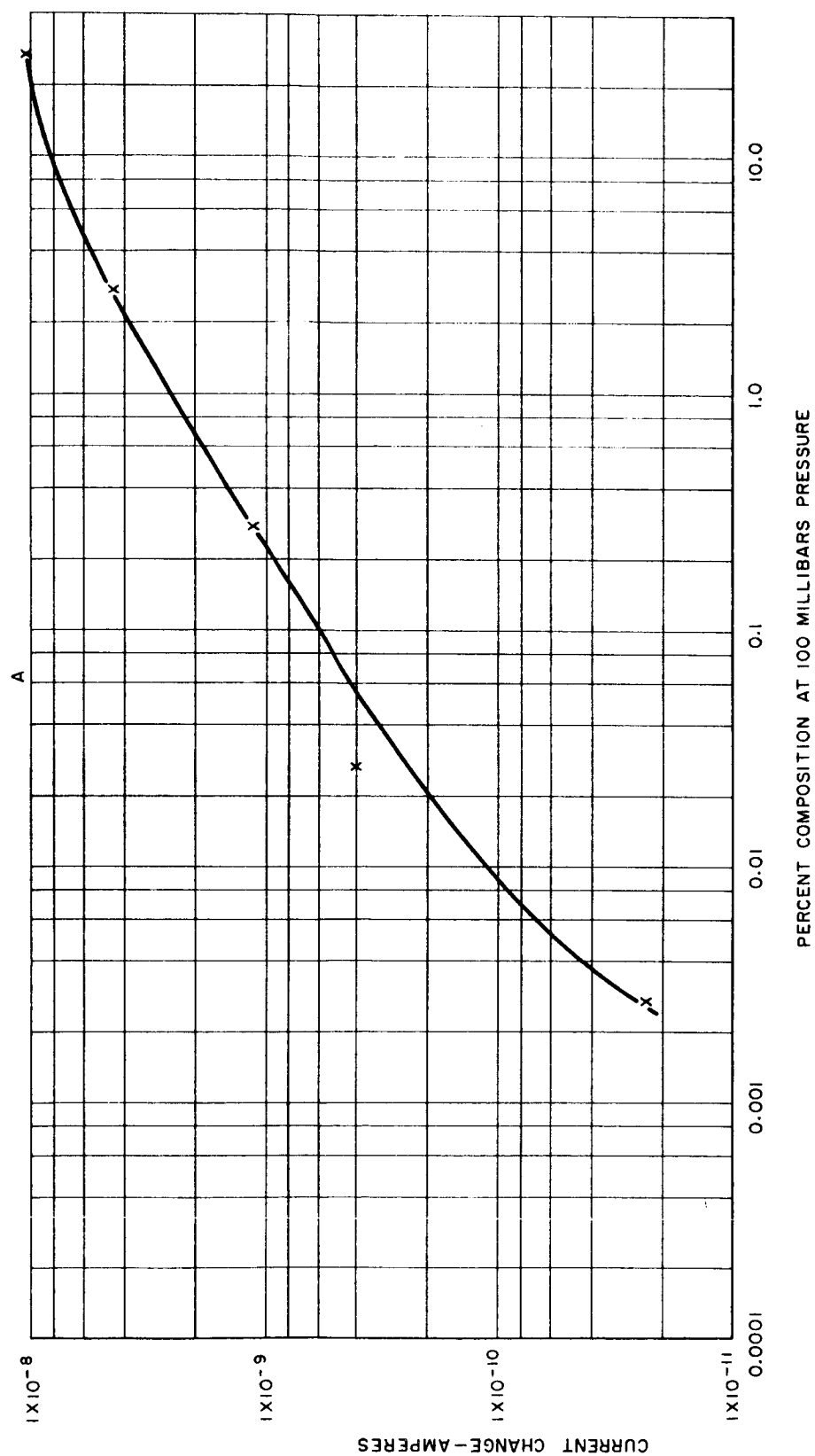


Figure 23. Response Curve for Argon

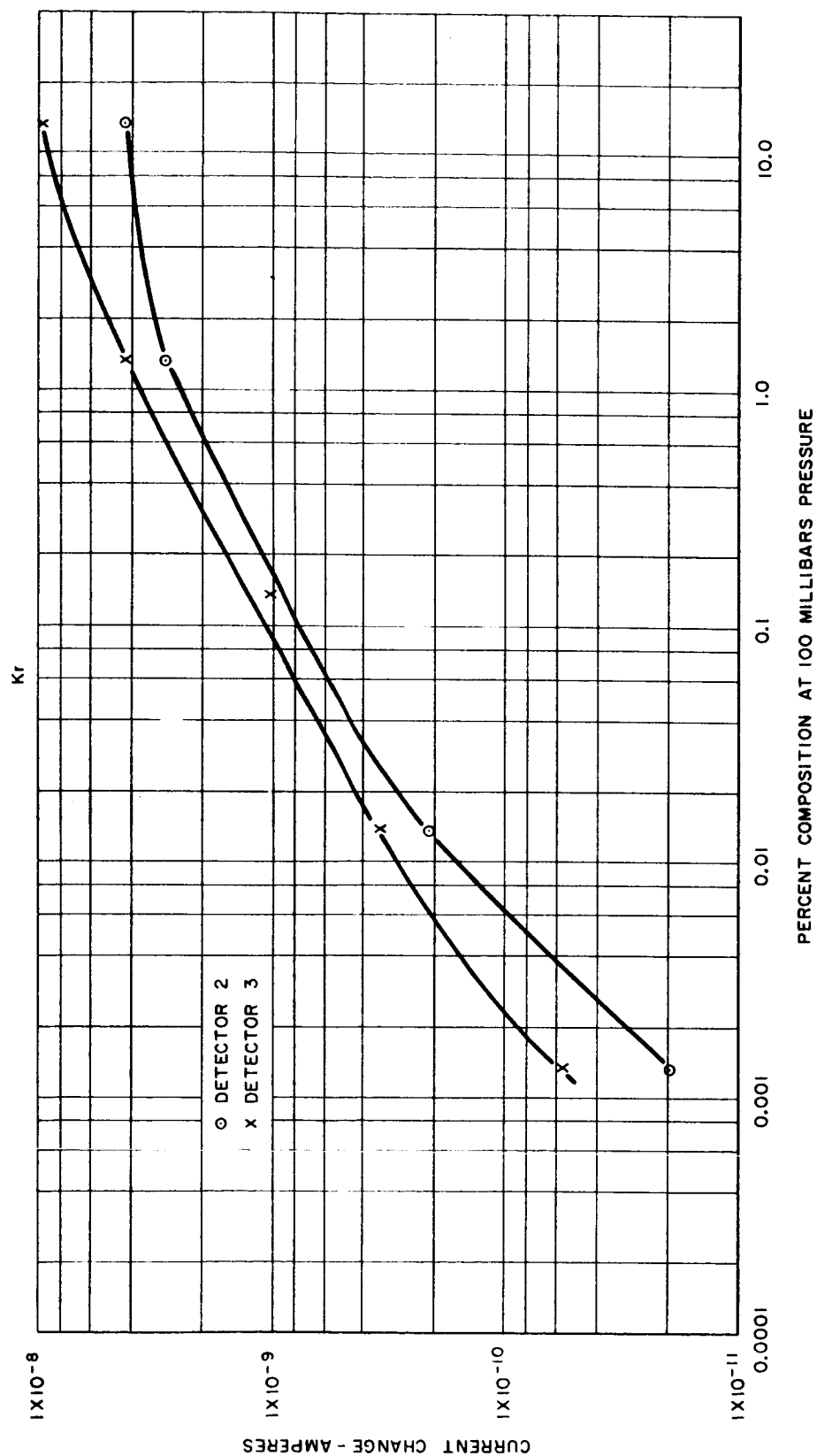


Figure 24. Response Curve for Kr

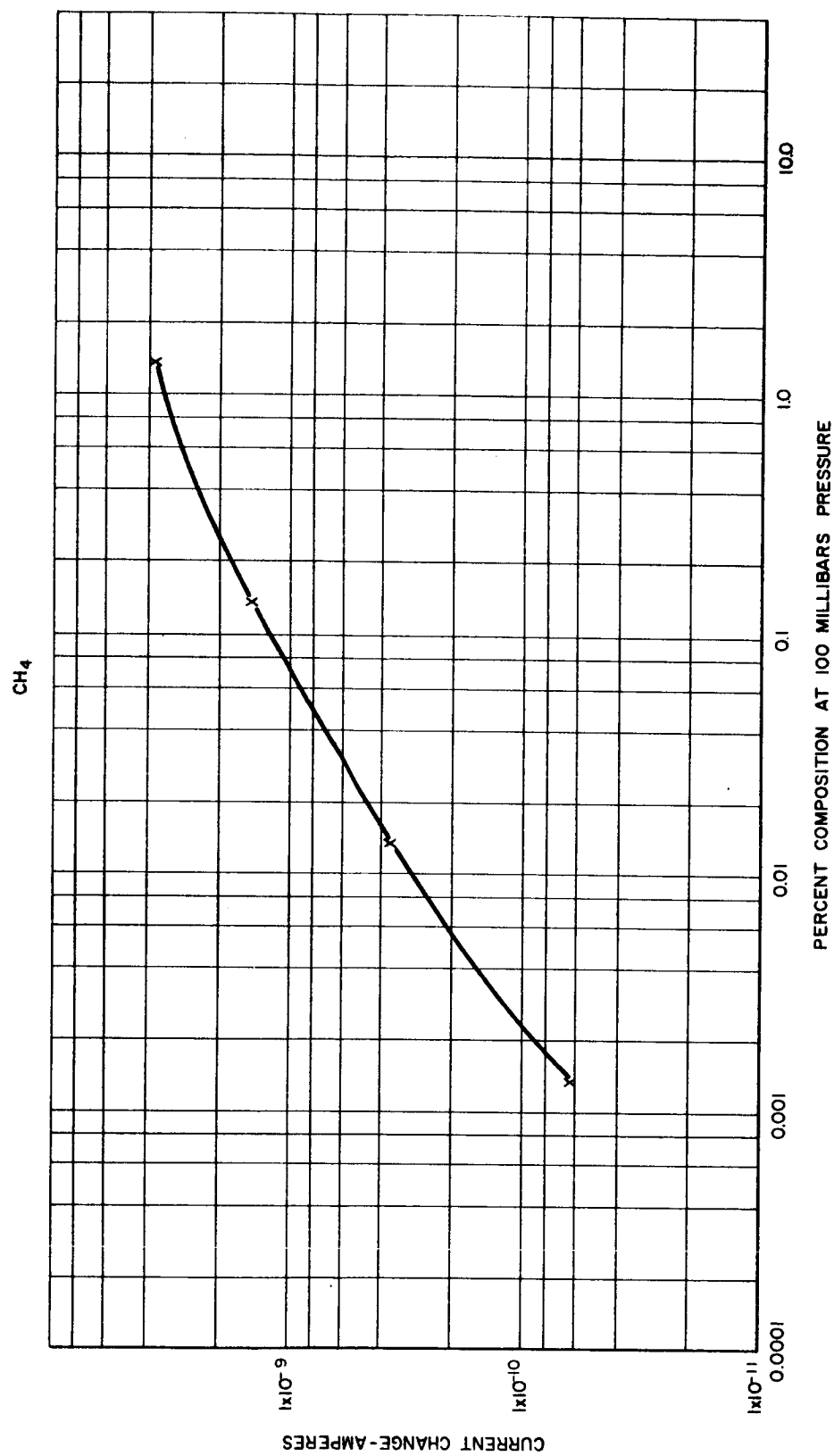


Figure 25. Response Curve for CH₄

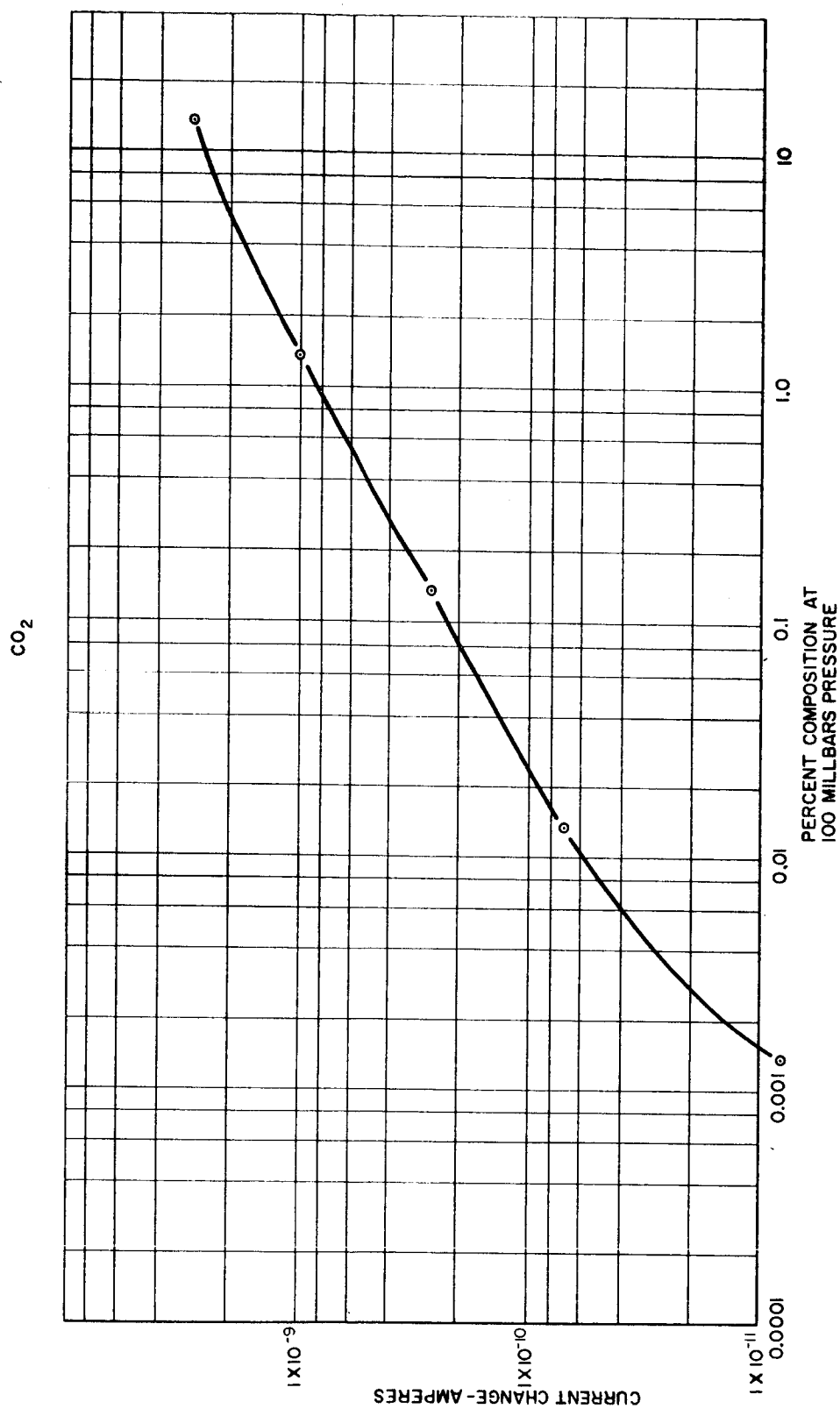


Figure 26. Response Curve for CO_2

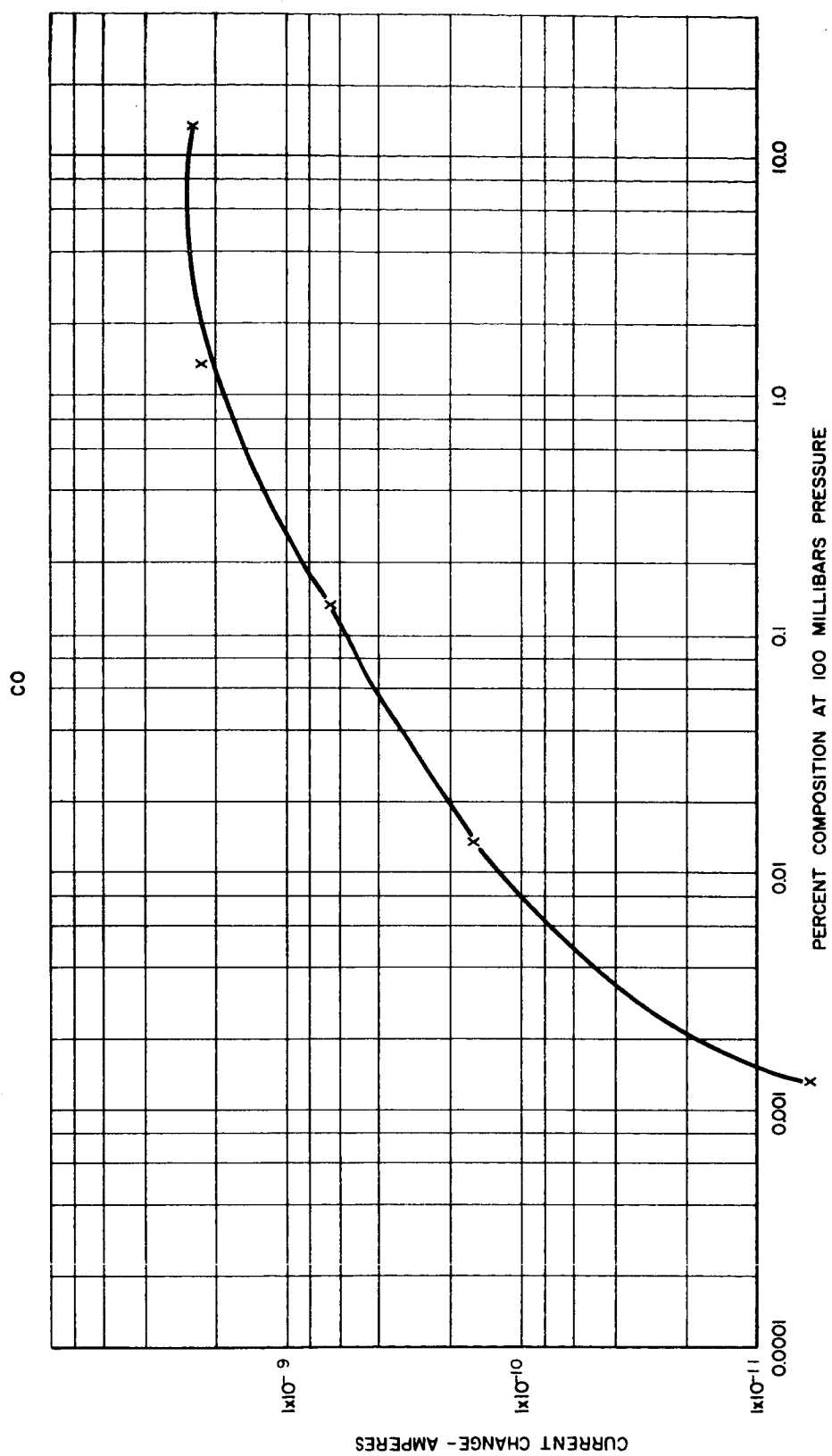


Figure 27. Response Curve for CO

the safe side, a much more elaborate simulator will be built for the next phase of this program; and very reliable response curves for the breadboard unit will be obtained.

In view of the difficulties experienced in obtaining calibration curves for H_2 , O_2 , and N_2 , a single stage helium stream splitter was used with these gases. Calibration curves obtained with this splitter are shown in figures 28-30. These data are subject to the usual stream splitter errors plus the error incurred by operating the sample loop at over 1000 mb pressure. This pressure would tend to greatly increase the injection time and broaden the peaks. Even so, it may be seen that a sensitivity of 10 ppm could be easily attained. The upper concentration tested (65%) although not strictly applicable because of the effects of peak broadening in this case, does show that large samples can easily be handled by these detectors.

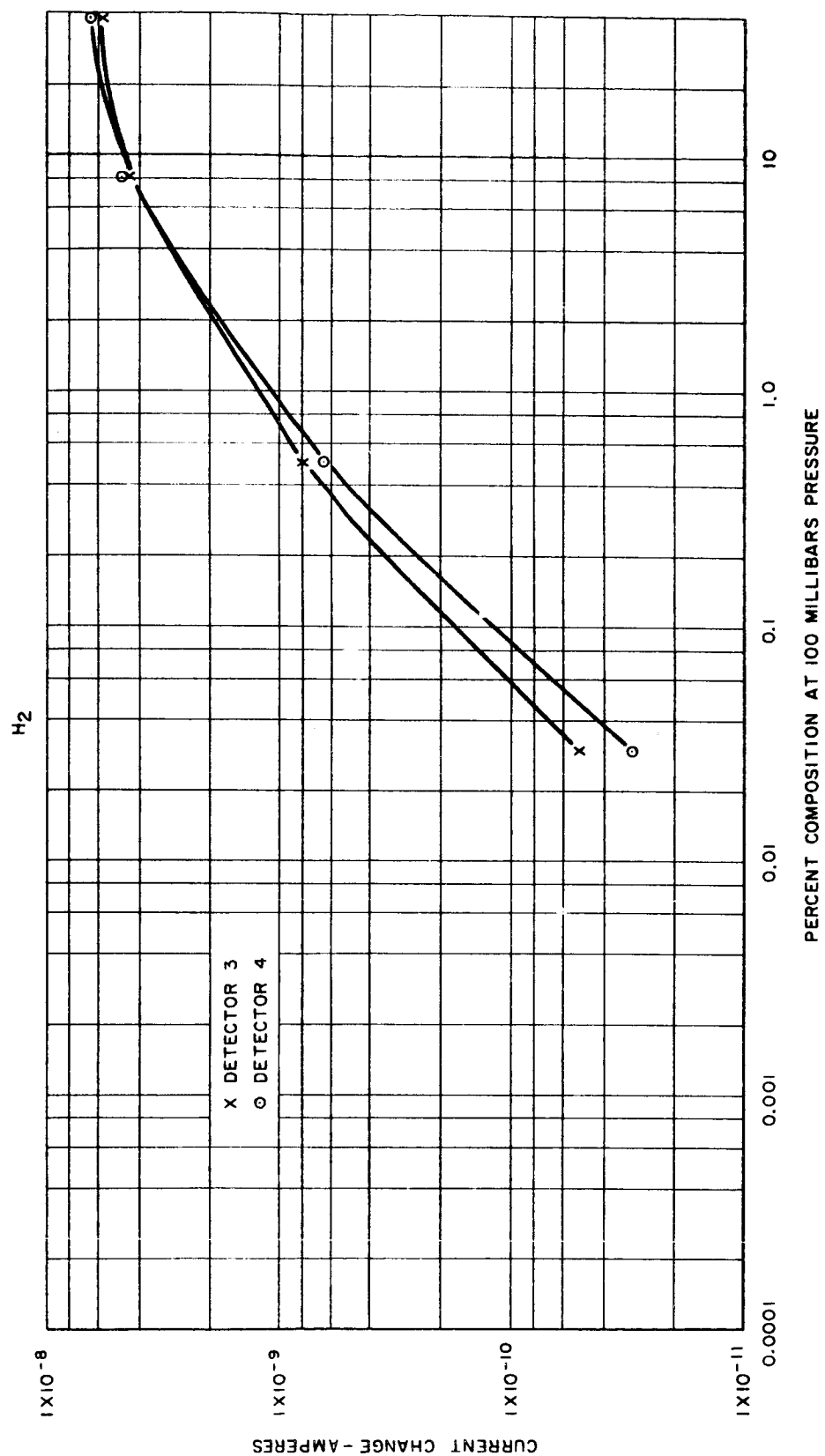


Figure 28. Response Curve for H_2 (Stream Splitter)

R4409

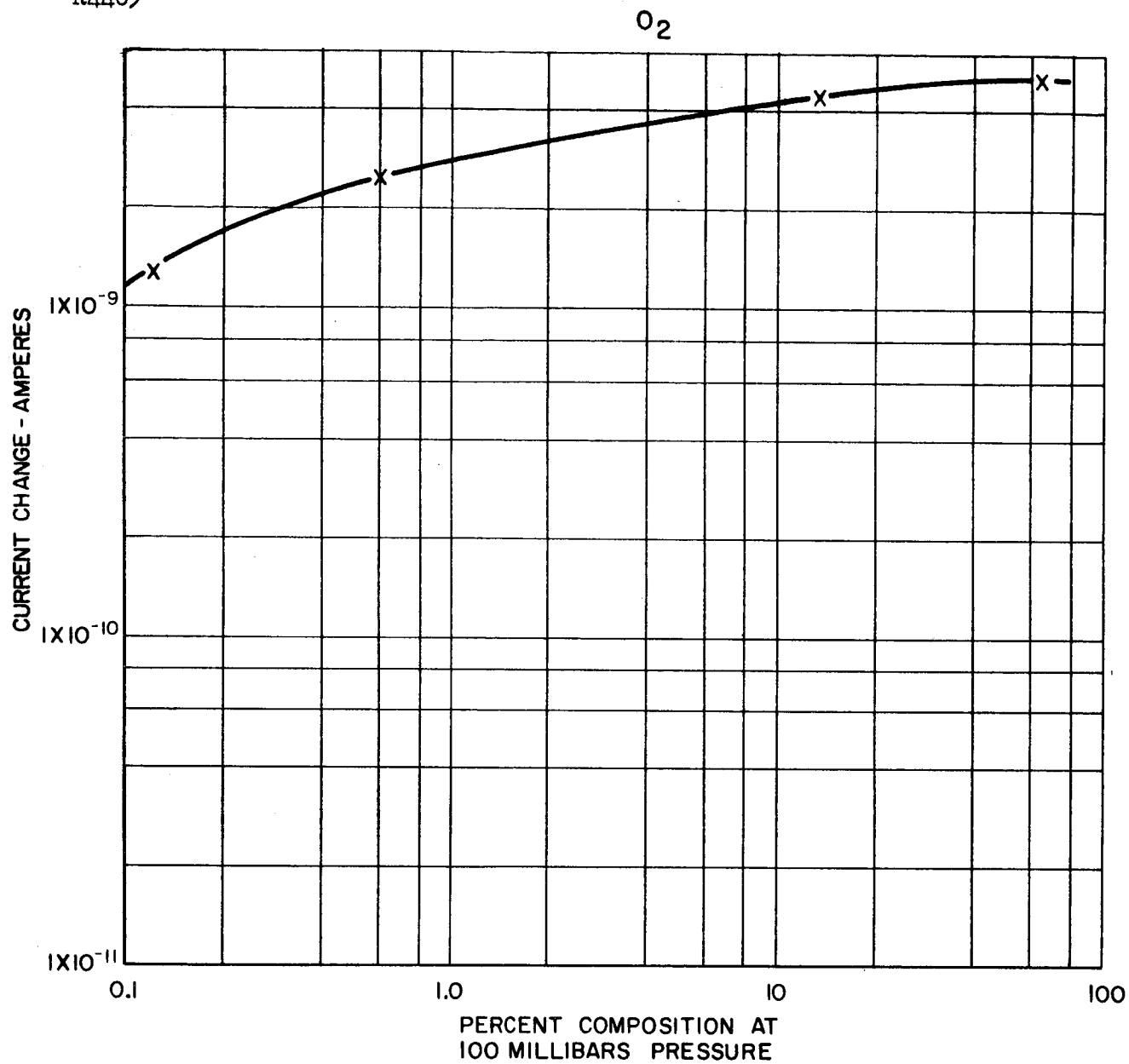
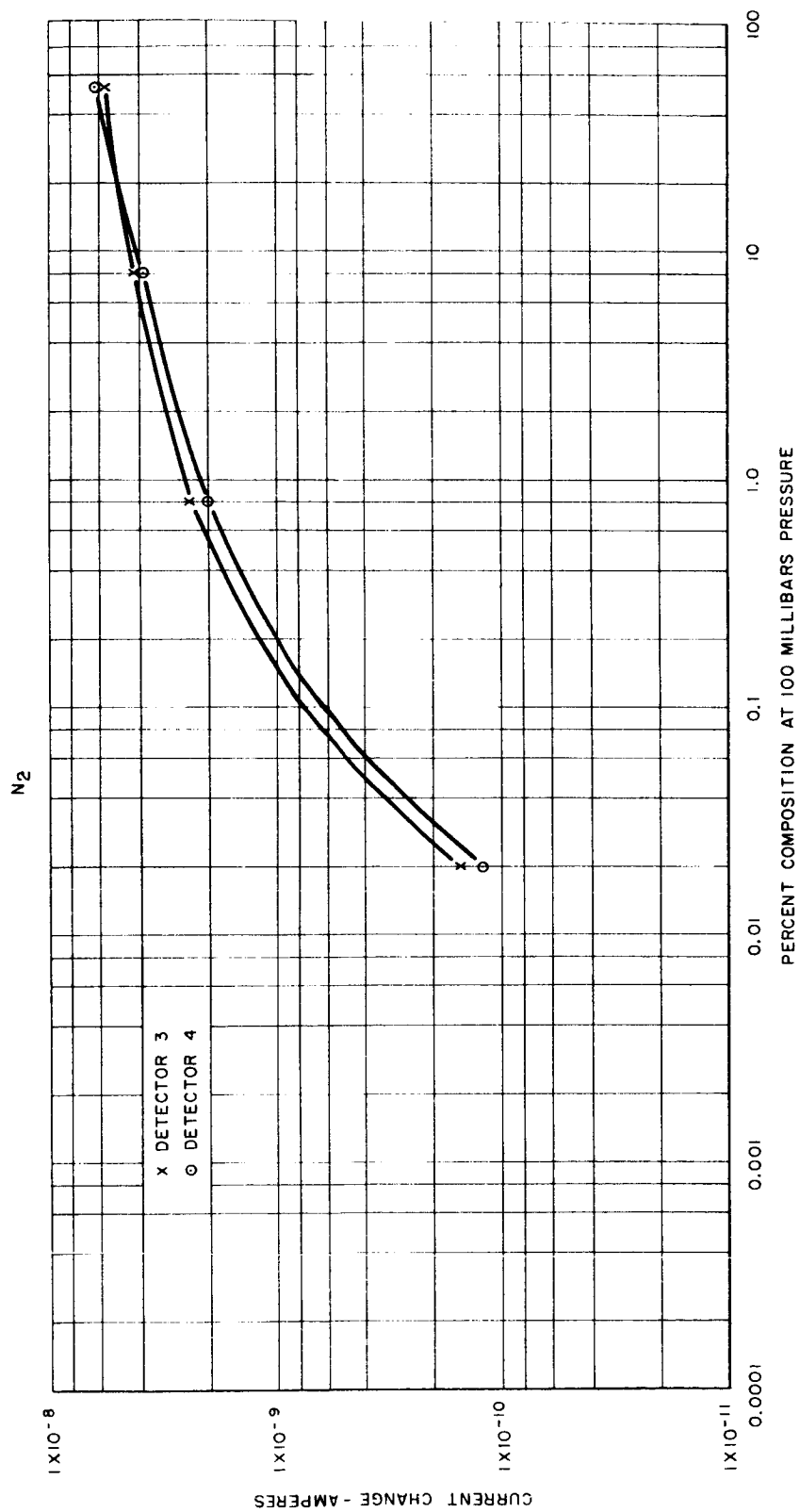


Figure 29. Response Curve for O_2 (Stream Splitter)

Figure 30. Response Curve for N_2

4. DETAILED DISCUSSION OF COMPONENT PARTS

4.1 Columns

A large number of columns were tested before the present system was evolved. Original consideration was given to a liquid partitioning column capable of separating NH_3 , H_2S , ethane, CO_2 and H_2O . It was found necessary to use Teflon particles as the solid support media in these columns to prevent undesirable adsorptive tendencies. It also was found necessary to use an alkaline liquid phase in order to retard the CO_2 sufficiently to obtain complete separation. Although this system worked quite well with freshly prepared columns, storage of the columns for more than a month caused them to lose much of their alkaline properties, thus reducing the relative retention time of CO_2 . Since a drastic change in retention time would make positive peak identification impossible, this type of column was abandoned.

It was then decided to use a silica gel column for the CO_2 separation. This did not entail any extra columns since a silica gel column was needed in any case for the N_2/Kr separation.

With this system, it would be desirable to elute with the liquid NH_3 shortly after air, and water in five to six minutes. Three different methods of accomplishing this were tested. A CaC_2 tube was used to convert water to acetylene, and the acetylene was separated on the silica gel column.

This method had a big disadvantage in that acetylene was retained twice as long as CO_2 , thus necessitating a very short, and consequently inefficient, column in order to elute acetylene within five minutes. The CaC_2 was then placed in the middle of the liquid phase column system (that is, the liquid column was split into two parts) so that H_2O would be retained for five minutes, be converted to acetylene, and immediately analyzed by the first detector. This approach did not prove satisfactory because the efficiency of the CaC_2 converter was greatly impaired by the bleeding from the liquid column. The third approach, which was the one actually adopted, was to use a relatively non-polar column that was only slightly basic. Quadrol was chosen as the slightly alkaline polar portion of the column and D-C silicone oil 550 as the non-polar portion because of their good efficiency and stability characteristics. This column does elute NH_3 and H_2O at the desired times. Due to its low polarity and plasticity, efficiency and adsorptive tendencies are less than desired. This may be improved with a more alkaline liquid phase.

Column 2A, the delay column, delays the passage of air into detector 2 until after NH_3 is seen by detector 1. Only a relatively short length of empty tubing is needed for this purpose since the flow rate at this point is only about 40 ml/min. Column 2B is a short silica gel column used

to separate Kr, Xe, N_2O , C_2H_6 and CO_2 . By itself, this silica gel column would not adequately separate N_2O and CO_2 from ethane, nor N_2O from CO_2 . Column 2C, the short molecular sieve column, slightly retards N_2O , and it greatly retards CO_2 . As a consequence, adequate separation between all three compounds is achieved with 2B and 2C.

Column 3 is a typical molecular sieve column which elutes H_2 -Ne, O_2 -A, N_2 , Kr, CH_4 , CO, and Xe. No separation is achieved between the H_2 -Ne pair nor the O_2 -A pair. The interference of Ne with H_2 is not expected to be a major problem because the sensitivity of the detectors to Ne is extremely low, 1%. The differentiation between A and O_2 is made with the charcoal column.

Earlier work aimed at the A- O_2 differentiation centered around the use of an electron capture detector at the exit of the main molecular sieve detector. This detector would detect O_2 but not A. An evaluation of the electron capture detector for this system showed that it possessed a number of disadvantages: (1) it required a different voltage supply, (2) it didn't have adequate sensitivity, and (3) its current level was highly dependent on the voltage supplied to it.

Another consideration, made in connection with this problem, was the actual separation of A, O_2 , and N_2 by means of a charcoal column. It was found that A and O_2 were

eluted together in the typical molecular sieve fashion without separation when the charcoal was conditioned at 200°C or less. At conditioning temperatures of 300°C or more, charcoal columns eluted this trio in the order A, N₂, and O₂. The O₂ peak was very broad and could not be detected at all until massive amounts were injected.

In the system finally used the adsorptive characteristics of charcoal are used to advantage, in that O₂ is completely adsorbed while A is passed in obtaining the A-O₂ differentiation. (Oxygen is then determined by subtracting the A contribution from the A-O₂ peak.) Since adsorptive efficiency is always improved by slower flow rates, the diameter of this column was increased in order to decrease the gas velocity. The charcoal column was activated at 500°C for six hours with over 100 ml He/min, flowing through it.

Since the gas velocity in this system normally increases as it reaches the exit end, the larger tubing used for the charcoal column does not prevent interference between peaks associated with detectors 3 and 4. An empty delay column was therefore placed ahead of the charcoal column so that the H₂, A, and N₂ peaks eluted from the charcoal column would not interfere with peaks associated with detector 3. CF₃Cl with a retention time of 1.5 minutes approves suitable as a standard.

4.2 Detectors

Two fundamental detector designs were investigated. These were parallel plate and concentric detectors. All detectors, when used with helium, gave an increasing amount of current with increasing voltage at low voltages; increasing voltage at mid-voltage regions produced no current increase; and increasing voltage in the higher voltage regions produced increasing current. This response corresponds to the usual ionization curve. The low-voltage, voltage-dependent region is the electron capture region where electronegative compounds reduce the standing current. This model was found to be too insensitive for most of the compounds of interest. The medium voltage, voltage-independent region is the cross-section mode where all compounds produce an increase in current. This cross-section region was extensively studied. The high-voltage, voltage-dependent region produced either a decrease (quenching) or increase (ionization) in base current with compound elution. The direction of change is dependent on helium purity, sample size, and detector configuration. The quenching type mode was found to have too short a dynamic range to be useful.

Concentric detectors were found to be most suitable for operation in the ionization mode. The helium ionization detector was found to have extremely high sensitivity. It also had a number of highly undesirable characteristics.

Samples larger than approximately 1% of the chamber volume produce inverted peaks. This necessitates the use of an extremely small sample loop if components concentrations of 10% or more are to be measured in the Martian atmosphere. This small sample loop, in turn, would allow compounds at the 10 ppm level to be detected only under optimum conditions. A much greater problem found with this detector was its instability. The helium ionization detector base current was found to be highly dependent on the operating voltage. Minor shut-downs were found to require over 60 minutes helium flushing before baseline current and response characteristics were restored.

Different cell dimensions, capping of the center electrode tip, purified helium and recessing of the center electrode were some of the methods used in an attempt to improve stability. None of these methods caused any significant response change or stability improvement. Operation at elevated pressures produced a slight response and stability improvement.

It was concluded from the helium ionization detector studies that the only advantage offered by this type of detector is its high sensitivity. However, since the sensitivity of other more stable detectors such as the cross-section detector is adequate at the 10 ppm level in atmospheres as dense as the Martian atmosphere, effort in

this direction was discontinued. This detector would be used however for the measurement of atmospheric composition where the atmosphere is considerably less dense (1 m.b. or less). Actually some work will be carried out on an independent program with this detector for the application.

Both parallel plate and concentric detectors were operated in the cross-section mode. Parallel plate detectors had a much longer and less critical current plateau and were used in all further work. (See figures 3 and 4 of first monthly report). This current level was directly proportional to the activity of the radioactive foil. Voltage required to reach the current plateau level was found to be inversely proportional to the square of the electrode distance. Sensitivity, expressed as amount of sample required to give the same percentage current change, was not affected by electrode area or spacing but was increased with larger cell volumes. This was possibly due to longer residence time within the chamber.

The cross-section detector is less sensitive than the ionization detector, but is superior in every other respect. Baseline current and sensitivity are not affected by large changes in voltages. Thus, voltage regulation is much less critical than with the ionization detector which operates in a rising portion of the ionization curve. With suitable electrode spacing, the cross-section detector can be operated

directly from the Martian ship's power supply. Reliability, however, is the primary feature of the cross-section detector. Even after opening the system to the atmosphere, it is ready for operation after five minutes. It is not drastically affected by helium impurities, and requires absolutely no maintenance to obtain proper and reproducible operation.

The cross-section detectors used in the breadboard unit have the general configuration shown in figure 31. A design drawing of the detector is given in figure A9 in the Appendix. Detector 1 has an internal diameter of 0.40 inches and an electrode separation of 1/16 inch. Detectors 2, 3 and 4 have internal dimensions of 0.40 inches diameter and 1/8 inch electrode spacings. Detectors 1 and 3 use electrodes made of 1C/in² tritium foil while detectors 2 and 4 use electrodes made of 4C/in² tritium foil. Contrary to previous results, no significant current increase was obtained with the 4C/in² tritium foil. This was found to be due to the fact that the tritium was imbedded much more deeply in the 4C/in² foil.

The voltage-current curves for each of these detectors are shown in figure 32. It may be seen that the voltage is not critical over a wide range. This chart also shows that higher pressures require higher voltages (comparison of 2, 3, and 4) and that a smaller electrode spacing greatly reduces the voltage requirement (comparison of 1 and 2). In

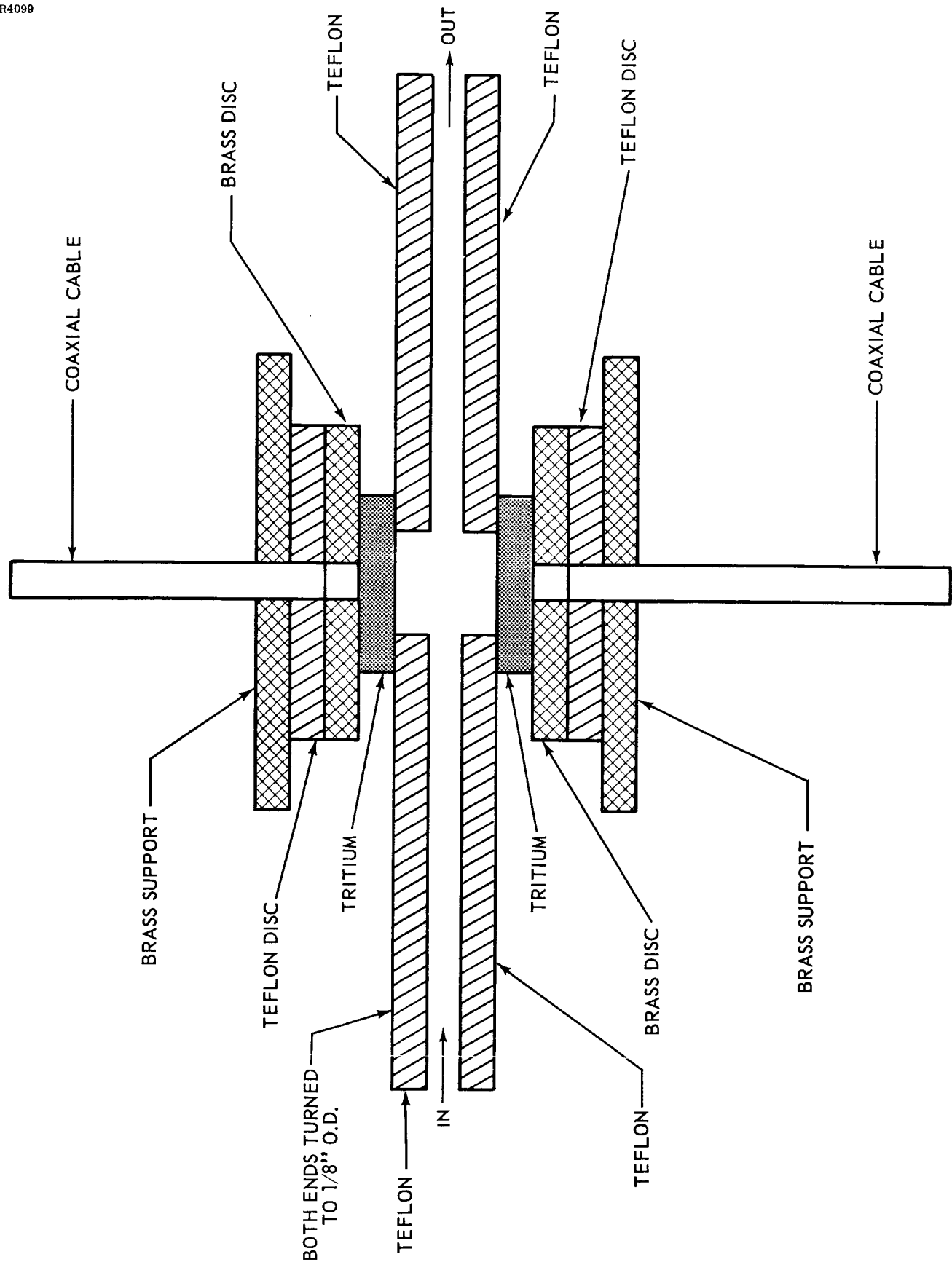


Figure 31. Melpar Cross Section Ionization Detector

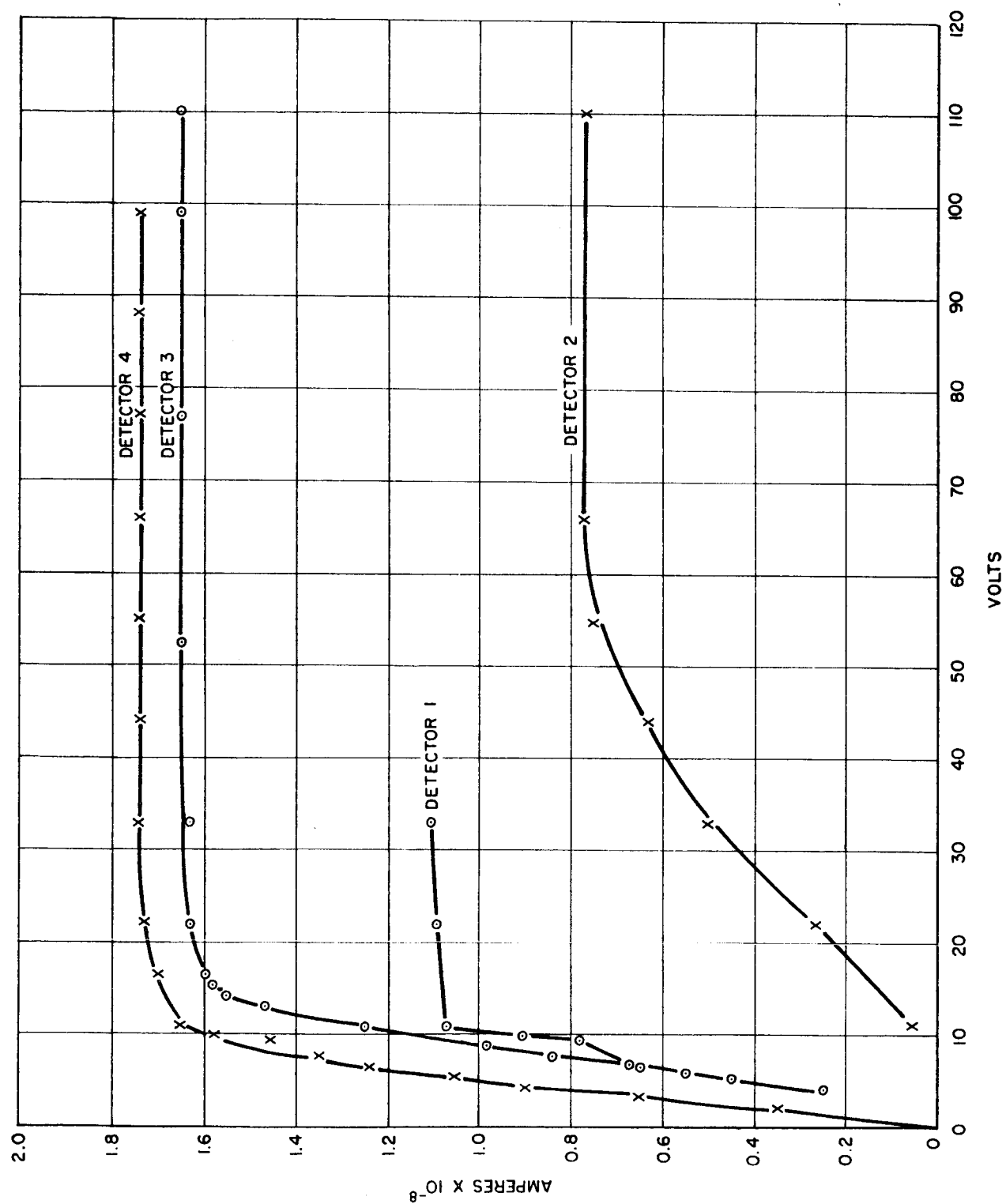


Figure 32. Effect of Voltage on Base Line Current

order to reduce the voltage requirements and make all detectors comparable, the electrode spacing in detectors 2 and 3 would be reduced. This reduction would have made it possible to operate directly from the Mariner battery. With the detectors as they now exist in the laboratory model the detectors all could be operated satisfactorily at a potential of 65 volts or greater.

As shown in the previous section, the sensitivity of this detector is more than adequate at the 10 ppm level for H_2 , O_2 , A, N_2 , Kr, CH_4 , CO, Xe, C_2H_6 , and CO_2 . Sensitivity to H_2O is approximately 11 ppm. Sensitivity to NH_3 is poor at the moment but this is undoubtedly due to column adsorption rather than to detector sensitivity. Detection sensitivity of Ne is Ca. 1%. This insensitivity to wear, however, is an advantage since H_2 and Ne are not separated; and H_2 is an important component.

The shape of all the calibration curves is essentially linear at the lower concentration levels. A linear slope improves accuracy at the low concentration levels while a logarithmic slope improves accuracy at the high concentration levels. The shape of these calibration curves could be drastically altered by amplifiers and readout circuit adjustments. In view of the extremely large dynamic range of these detectors, the shape of the response curves in the flyable unit will be governed primarily by the type of readout

circuit used. This, in turn, will be governed by whether or not absolute or proportional accuracy is desired.

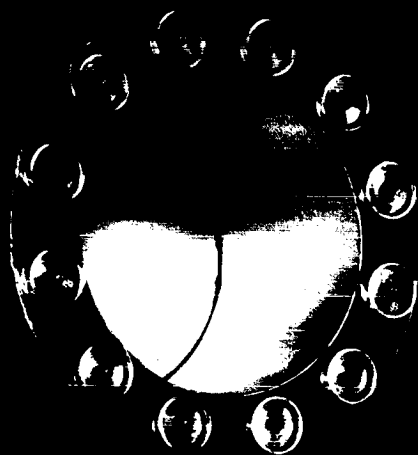
4.3 Gas Chromatographic Oven

The gas chromatographic oven constructed for the laboratory model is shown in figure 33. This oven in essence consists of a three-inch diameter well three inches deep surrounded by a bank of chemical heater cartridges and then an effective insulation sheath. The diameter of the entire oven assembly is six inches. Figure A8 in the Appendix shows the design drawing for the oven.

4.3.1 Insulation Sheath

The establishment of an oven temperature of 310°K for an outside ambient temperature as low as 140°K in the Martian atmosphere meant that an effective insulation sheath had to be found. (The 310°K temperature was initially selected. However, a temperature of 300°K used in column work could be just as easily realized in the oven.) The insulation sheath had to fulfill two main criteria: (1) it obviously had to have a relatively low thermal conductivity, and (2) it was not subject to failure from shock and/or vibration. For the laboratory model a low density foam was selected for the insulation. A sheath involving vacuum insulation could not be conveniently used.

Initial experiments were conducted using a chamber surrounded with a 3/8-inch insulation sheath. The oven was



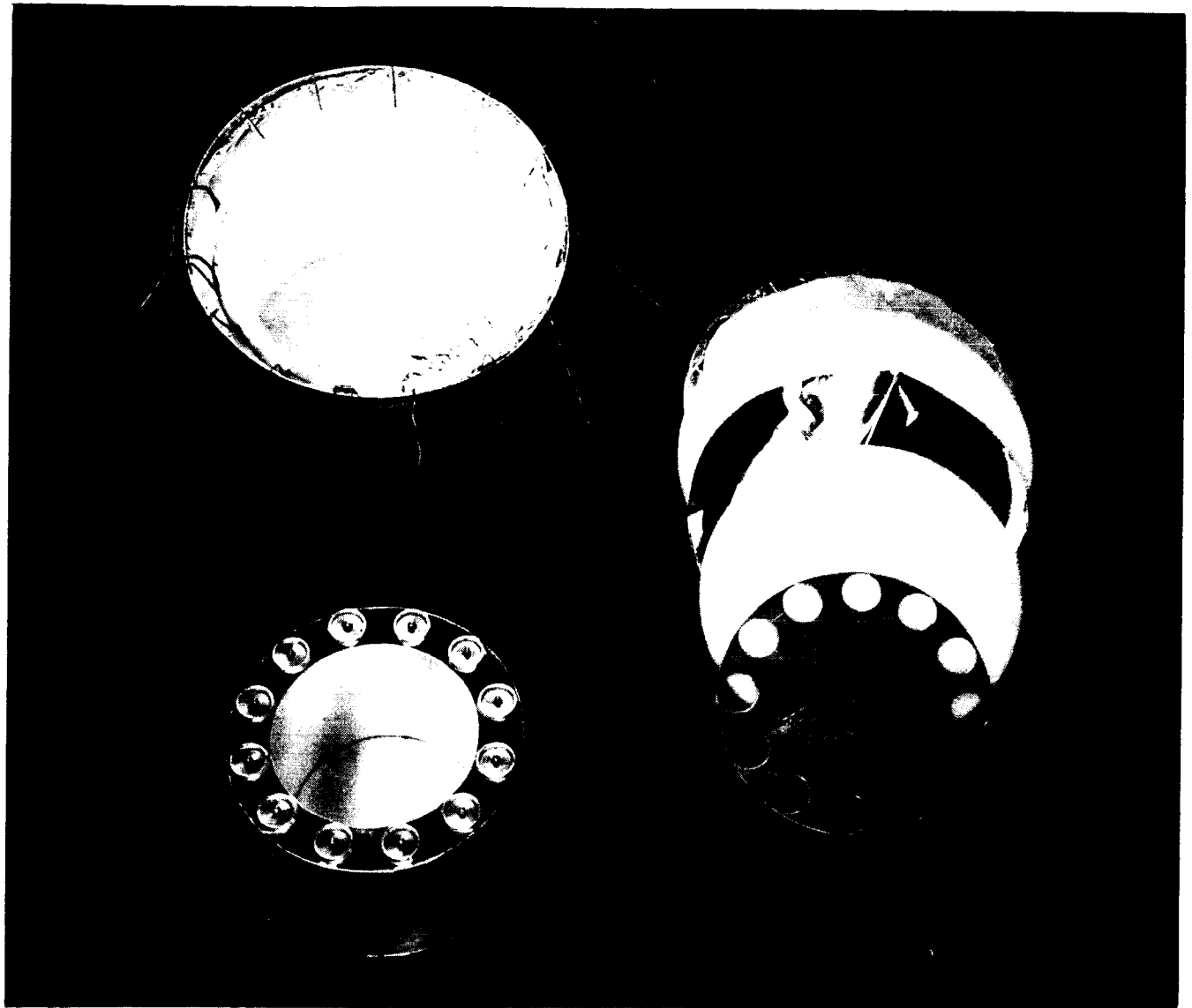


Figure 33. Photograph of Oven

heated electrically from dry ice temperatures (-70°C) to room temperature in obtaining the necessary performance data of the oven. The results agreed well with expectations. As a result Melpar was able to design later chambers with a high degree of confidence.

The present laboratory oven contains $3/4$ inch of foam insulation. The insulation sheath is divided into two layers of $3/8$ inch each in thickness by a sheet of aluminum foil. The foil acts as a radiation shield in reflecting heat back into the oven. The cover for the assembly is soldered in place and a hermetic seal is obtained on the entire unit.

4.3.2 Chemical Heating

Once the necessary insulation design had been established, Melpar was confronted with the actual mechanics of heating the chamber. The heating of the final unit was necessarily to be accomplished by chemical heating. This meant that the heat would be supplied in short-term pulses of high enthalphy. Here again, Melpar utilized electrical heaters to simulate the process. It was necessary to run test after test with the chambers at 200°K , to determine the effects of the quantity of heat in a given pulse, duration of the pulse, and time between pulses. Test run at 77°K verified the 200°K data.

After these factors had been resolved, and the optimum

method of heating established, it soon became apparent that the material rate of cooling resulting from the total heat leak of the unit was excessive, moreover, the gradients within the chamber were unsatisfactory. This meant that there had to be some means incorporated into the unit to release thermal energy into the system at a constant rate slower than the heat leak, while at the same time helping to distribute the energy uniformly throughout the chamber.

The desirability of an isothermal chamber or heating process suggested the phenomenon utilized in a Bunsen-type ice calorimeter; in this case, the heat of fusion of ice in equilibrium with water at the freezing point provides a convenient means of thermal transfer without changing the temperature of the ice-water equilibrium. Melpar pursued this technique and investigated the various salts available that possessed the desired property of a high heat fusion, with a melting point near room temperature. For the purposes of the laboratory unit, Melpar selected $\text{Na}_2\text{HPO}_4 \cdot 12\text{H}_2\text{O}$ with a heat of fusion of 66.8 cal/gram and a melting point of 36.1°C . This proved very satisfactory. Slightly over 100 grams of the salt allows the total heat available from one chemical heater to be stored and released gradually as the chamber cools due to the natural heat leak. It should be noted that the operational range of this unit can be changed simply by the substitution of a different salt with a melting

point corresponding to the desired temperature.

The problem of providing a given operational temperature regardless of the ambient environment over an extremely large temperature range was also simplified through the incorporation of the fusion process of a salt. The ability of this system to prevent a serious temperature overshoot permits the use of a single thermostat set for the lower limit of operational temperature to establish the control function.

The initial efforts towards the use of a chemical heating system for bringing the oven to 310°K from an ambient temperature possibly as low as 140°K involved an experimental consideration of thermitic heating. The thermitic reaction is quite exothermic and unfortunately quite rapid and at times violent. Melpar spent considerable effort in connection with the aluminum-iron oxide thermitic mixture which gave approximately a heat reaction of 800 calories/gram of reaction mixture. It was found possible to adjust the parameters of this system in such a way that the mixture could be fired anywhere from liquid nitrogen temperatures to 310°K . However, one of the major problems encountered in the investigations of the thermites and in particular the $\text{Al-Fe}_2\text{O}_3$ system was that of containment. In this connection the reaction rate was so rapid that the local temperatures were sufficient to melt the aluminum container and/or produce blow-out through holes drilled for the electrical connections to the electrical

ignitor.

In attempting to reduce the rate of the thermitic reaction the particle size of the aluminum and iron oxide are reduced and the packing density within the aluminum cartridge was varied. With this approach Melpar was able to package the thermite in an aluminum cartridge 1/8 inch in thickness and lined with a ceramic layer that did contain the reaction. However, the reliability of the system was not too good. For instance, one cartridge out of 20 approximately failed when fired. For the same size container it was possible to inhibit through a variation of the parameters the reaction to the point where the reaction could be contained reliably at room temperature; but under these conditions a firing at -70°C was not possible. It was felt that the extra weight of container required for containing the reaction to the extent that the thermitic units could be used at all temperatures was not warranted. A slightly less energetic chemical heating system was considered. (The reader is referred to pp 34-55 of the first monthly report for more details on the initial thermitic heating approach).

In figure 34 a sketch is shown of the cartridge finally adapted for the demonstration of the feasibility of the approach for the laboratory model. This cartridge consisted of a 1/18 in. aluminum shell and 3/8 in. diameter a delay line charge

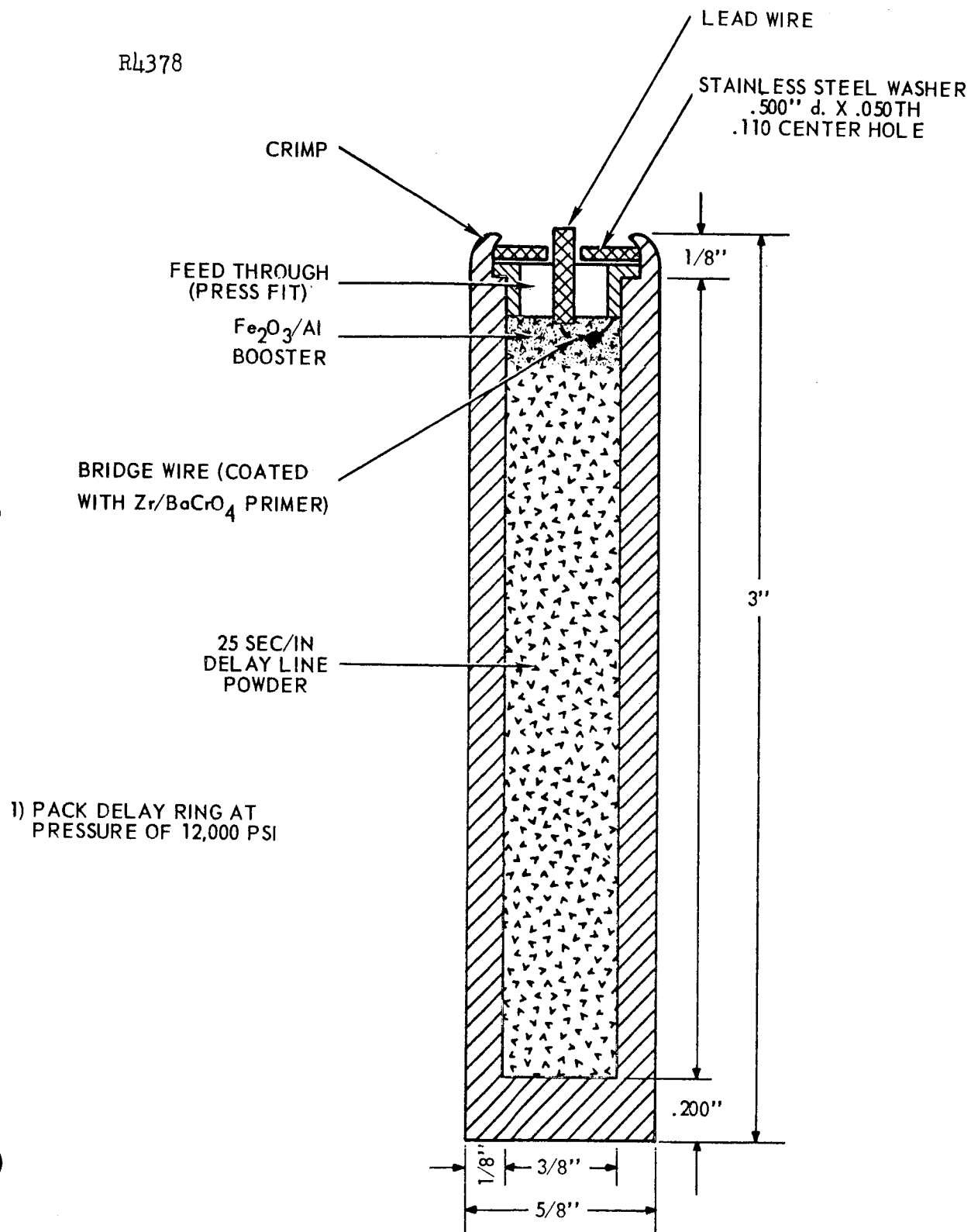


Figure 34. Cross Section of a Chemical Heater Cartridge

obtained from the Atlas Chemical Company. A primer on the bridge wire (Zr/BaCrO_4) is followed by a finally divided mixture of $\text{Al-Fe}_2\text{O}_3$ booster and then by the main charge. The main charge after ignition burns at the rate of one inch per six seconds for the $3/8$ in. cross-section used in the laboratory model. These units each produce 6,000 calories and are adequate for the required heating cycle. The weight of the cartridge with charge is approximately 40 grams, and the charge in this cartridge amounted to approximately 13.5 grams. (The heat of the reaction is approximately 500 calories per gram).

For this same configuration and weight, it was not possible to contain in the preliminary studies the $\text{Al-Fe}_2\text{O}_3$ thermitic reaction with reliability.

As mentioned previously the temperature stability of the oven was improved immensely by partially filling the dead space in the chamber with 250 grams of $\text{Na}_2\text{HPO}_4 \cdot 12 \text{H}_2\text{O}$. The heat of fusion of this salt provides an ideal heat sink; it (1) minimizes temperature overshoot as the oven is brought up to temperature, and (2) it feeds heat into the oven with solidification and thus imparts temperature stability to it in maintaining a temperature of 310°K . Aluminum shavings were mixed with the salt in improving heat transfer.

The firing sequence used in the firing of the chemical heater cartridges in the subsequent effective tests to be

discussed below is indicated in figure 35.

4.3.3 Firing Control System

In figure 36 is shown the schematic of the firing control circuit used for the oven. Figures 37 and 38 are photographs of this system. Sequence firing is necessary for this application to provide the necessary flexibility in temperature control. The system must be operational in the range of 140 to 310°K. Since the initial starting temperature can range from 140 to 250°K, sequence firing must be used in enabling the system to approach thermal equilibrium after each shot if an appreciable overshooting of the final temperature is to be avoided. Also the use of a control circuit avoids the significant local heating that could otherwise develop and that could produce detrimental effects on the various and sundry components within the oven.

The firing element in each cartridge may be fired at 3 volts and a current drain of 0.5 amperes. The power requirement of 1.5 watts is thus well within the specifications.

The operation of the control system or programmer may be seen from figure 35. Each of the twelve heaters mounted around the oven periphery is wired to one of the individual contacts on the printed circuit commutator boards. The wiper of this commutator board is connected to the power supply used for firing; and it is driven by a small motor geared down to drive the wiper at the rate of 1/16 rpm.

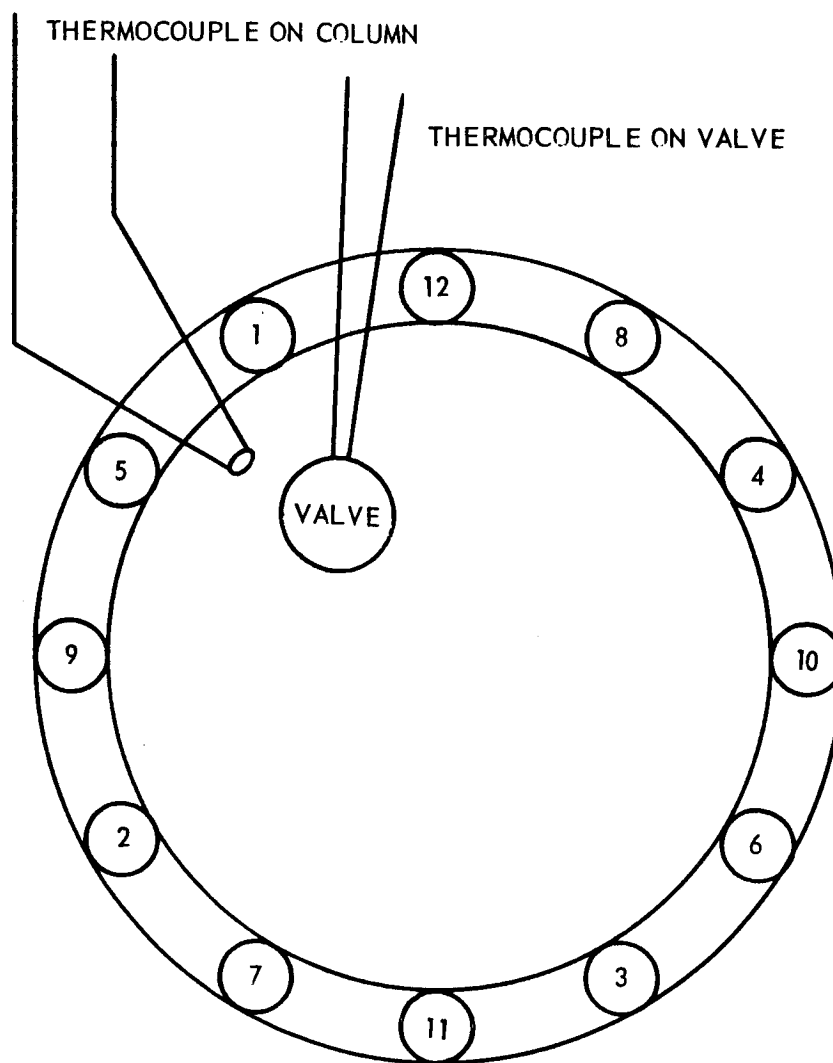


Figure 35. Firing Sequence for Chemical Heaters

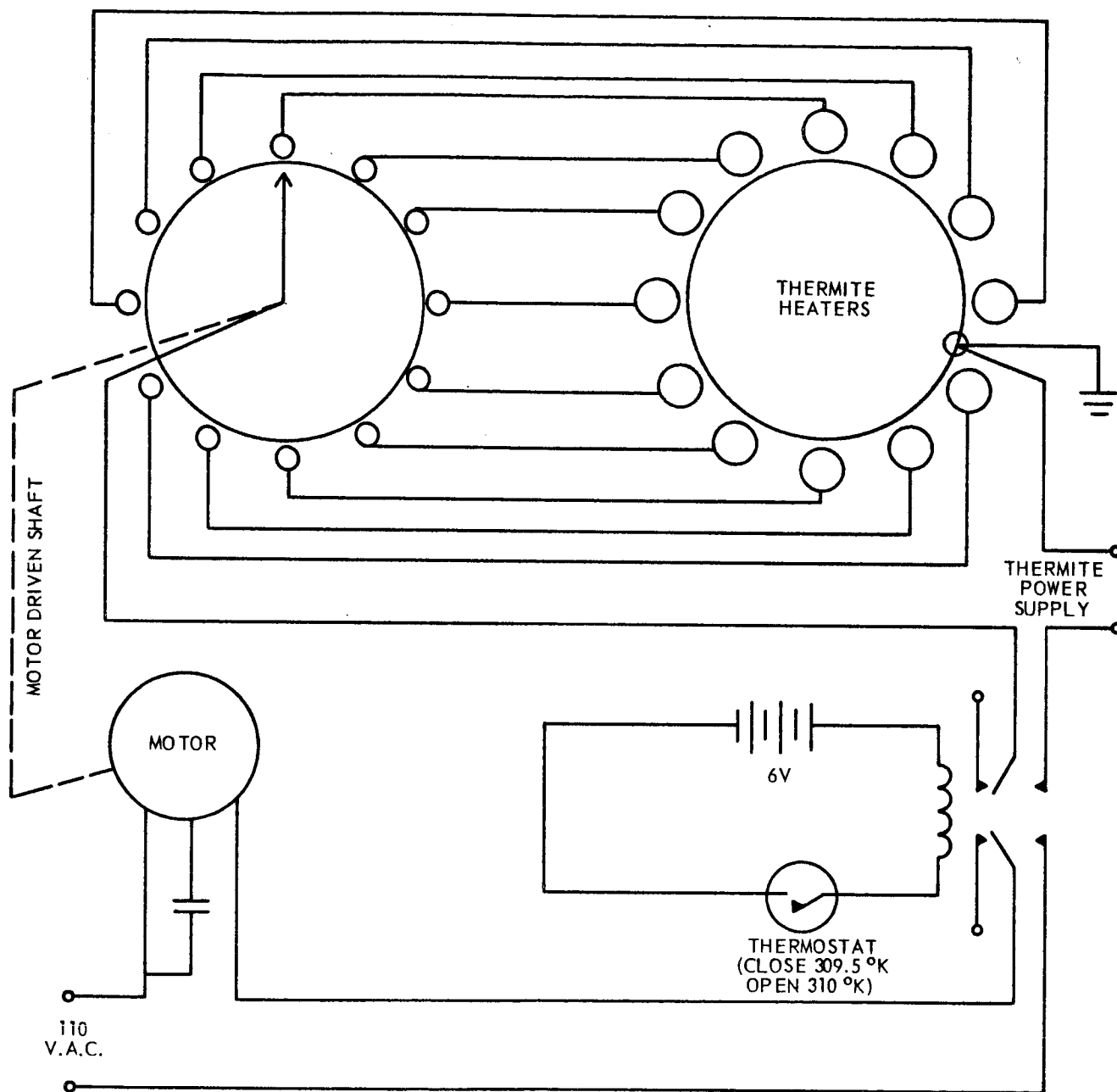
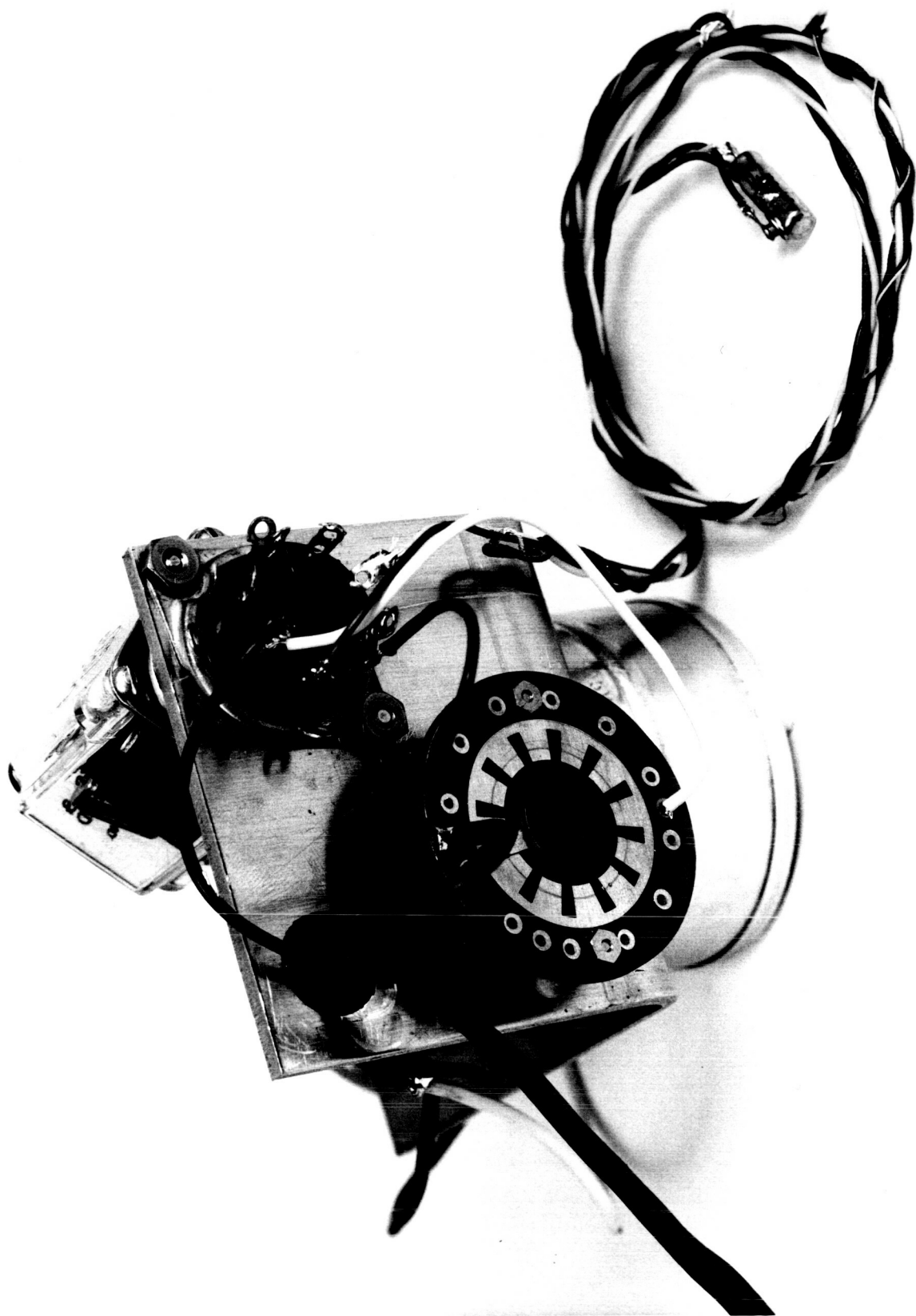


Figure 36. Schematic of FIRING Control Circuit for Oven



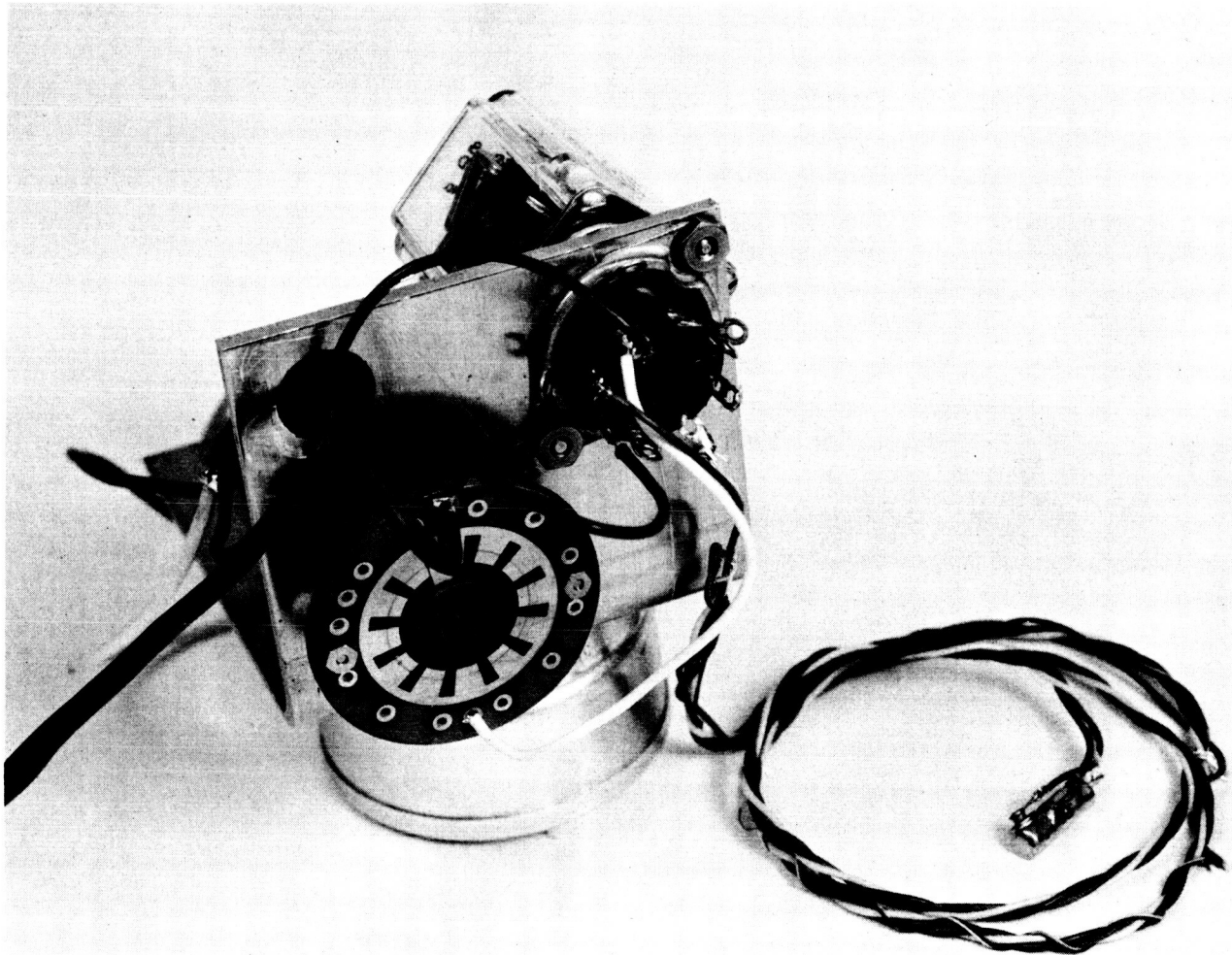
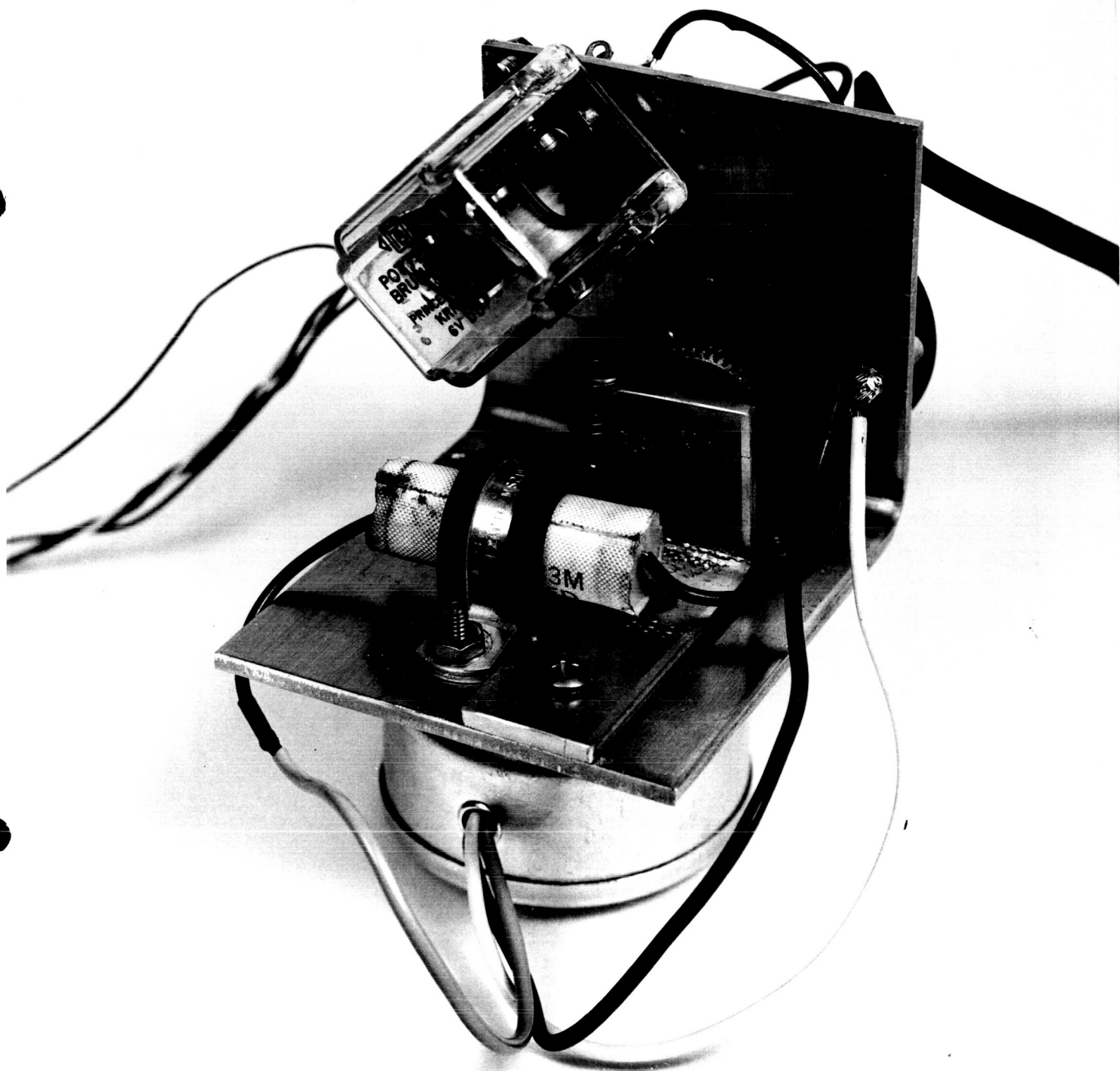


Figure 37. Photograph of Control Assembly



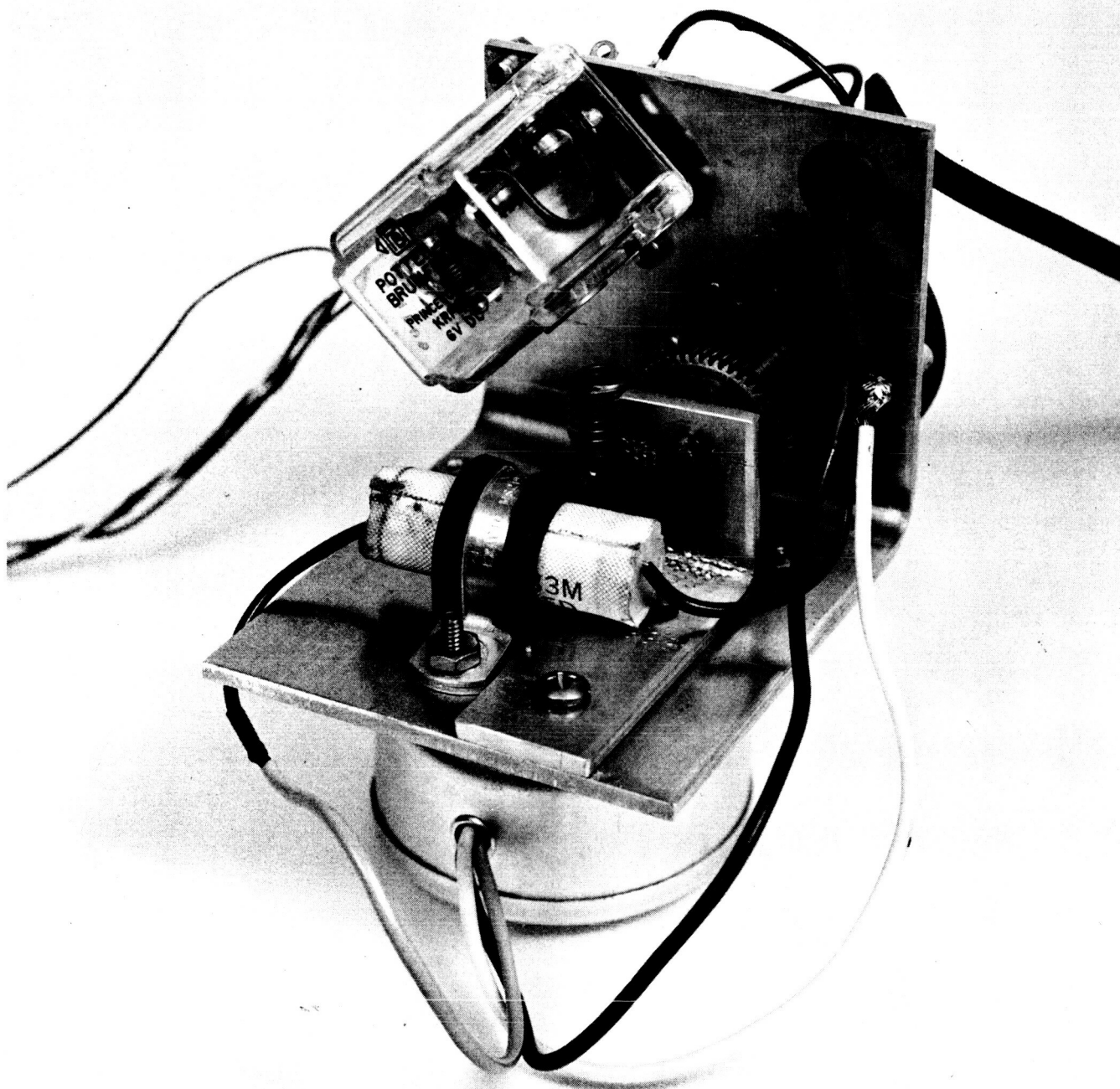


Figure 38. Photograph of Control Assembly

A small thermostat located next to the column in the oven controls the power to the motor and the subsequent firing of the charges. The thermostat is set to close and energize the circuit at 309.5°K and to open at 310°K. If the oven temperature is below 310°K, the thermostat will be closed and the wiper arm will move circularly. As it makes contact with the stationary contacts, the chemical charges will be fired. The wiper arm rotation stops as does the firing when the oven temperature reaches 310°K.

A motor is purposely geared to move at a very slow rate to enable the heat generated after each cartridge firing to be distributed throughout the oven. In this way an objectional overshoot is prevented.

This controller was built in conjunction with the chemical heating system to demonstrate the feasibility of the entire concept of chemical heating. No attempts were made at this time to minimize weight, size, and power. (See the design considerations in this connection in Volume III). In the breadboard unit, this function could logically be accomplished through the use of a small compact solid state system as described in Volume III rather than the large mechanical system demonstrated at this time.

4.3.4 Performance of the Laboratory Model

Two experimental runs have been made with the present chemical heating system in raising the temperature of the

simulated oven from 200°K to 310°K. The oven so heated was maintained at the higher temperature for at least an hour with the outside ambient at 200°K.

In figure 39 is shown the response data for the oven in one firing in which cartridges were fired over some 20 minutes in bringing the oven up to temperature. The oven was permitted to set in an ambient at 200°K until the temperature dropped to 300°K. The time taken for the heat leakage to lead to this temperature drop was some 80 minutes. At the end of this time an additional thermitic unit was fired; and the temperature rose to 315°K. At the end of 168 minutes when the temperature had once again dropped, a second additional cartridge was fired.

Some eight cartridges corresponding to an energy input of about 45,000 calories were fired in bringing the temperature of the oven from 200°K to 310°K. The extrapolation of these data show that 12 cartridges would be adequate for raising the oven temperature from 140°K to this level.

The heating characteristics shown by figure 39 correspond to an oven weight of 2.7 lbs. This weight includes dead weights in the oven wall that simulate the injector valve, the columns, and the detectors as well as the housing and cartridge heaters.

The fact that the oven can be raised to the sequenced temperature by chemical heating and then maintained at this

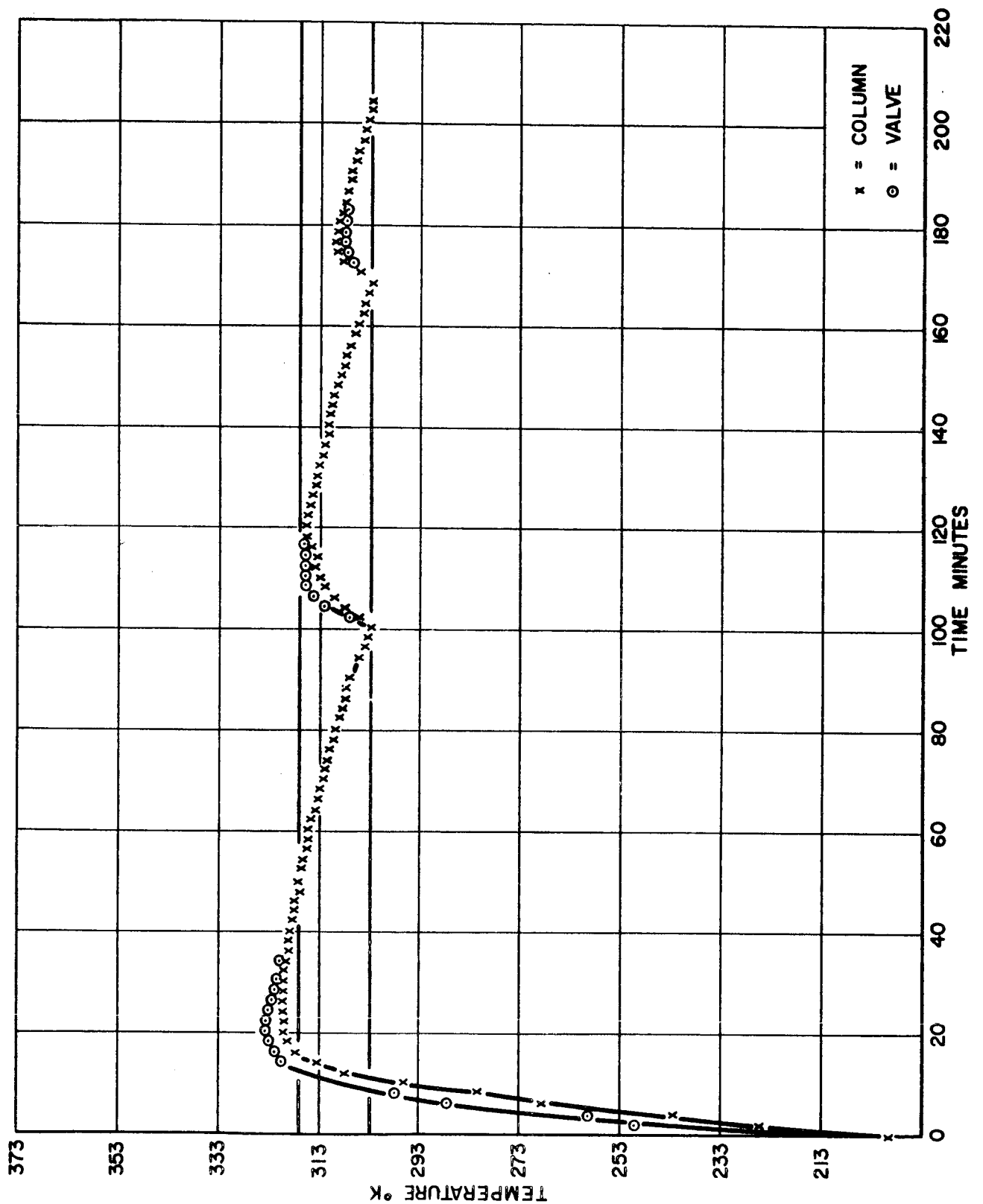


Figure 39. Temperature Characteristics of Simulated Oven Heated with Chemical Heaters

level by the same means without any direct electrical heating is encouraging. The salt which serves as a heat sink is performing perfectly in fulfilling its functions of preventing serious overshoot and in holding the oven at temperature. Even better oven heating characteristics may be realized by using a greater number of smaller chemical heaters than those used in this study.

4.4 Sampling and Injection Valve

The injection valve is one of the more critical components as far as the gas chromatographic package is concerned. As a consequence, major emphases has been given to the development of a reasonable, reliable valve that might be actuated quite simply.

Melpar's first consideration was a pneumatically actuated spool valve containing Teflon rings. In this design the carrier was initially permitted to pass directly through the valve and onto the column. At injection a solenoid switching valve switched the carrier stream from its normal flow position at one end of the spool (A) to the opposite end of the spool (B). As a result of this switching and the pressure developed at B the injector spool was shifted; and the sample was swept from the sample loop onto the gas chromatographic column. (For a sketch of this valve see figure 1 of the first monthly report). The spool is returned to the normal, non-sampling position

by switching the carrier flow back to the original flow condition. This valve affords a means of injecting the sample without wasting the carrier gas required for pneumatic actuation.

This valve alone in the laboratory works quite well at 80 lbs pressure without leaking. When incorporated with the column arrangement, it performed poorly. The pressure drop over the columns inhibited the helium venting of the low pressure side of the valve necessary for actuation to occur. As a consequence, a sufficient helium pressure differential was not realized across the valve, and the spool was not shifted.

It is felt that this particular design could be made to function; but the valve size required in realizing the desired pressure differential would be prohibitive. As a consequence, due consideration was given to the use of the slider injection valve, the design and development of which had been carried on concurrently with the work on the spool type valve.

The slider type sampling and injector valve has been found to perform quite satisfactorily in the laboratory model. This valve is actuated by squib firing. The squibs are nothing more than sealed units containing a charge which may be fired electrically to extend a metallic plunger.

In figures 40 and 41 are shown the final slider injector

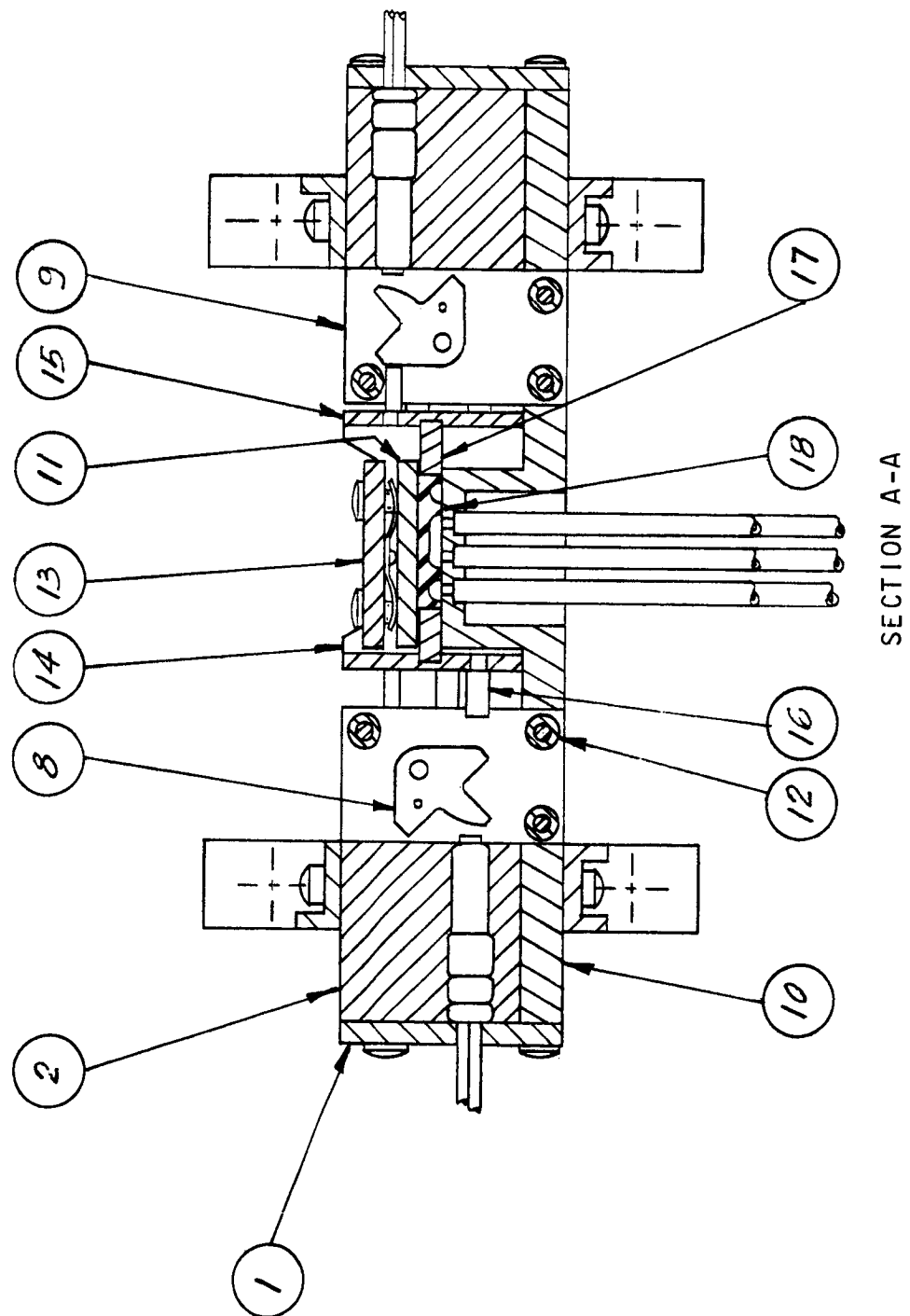


Figure 40. Slide Injection Valve (Side View)

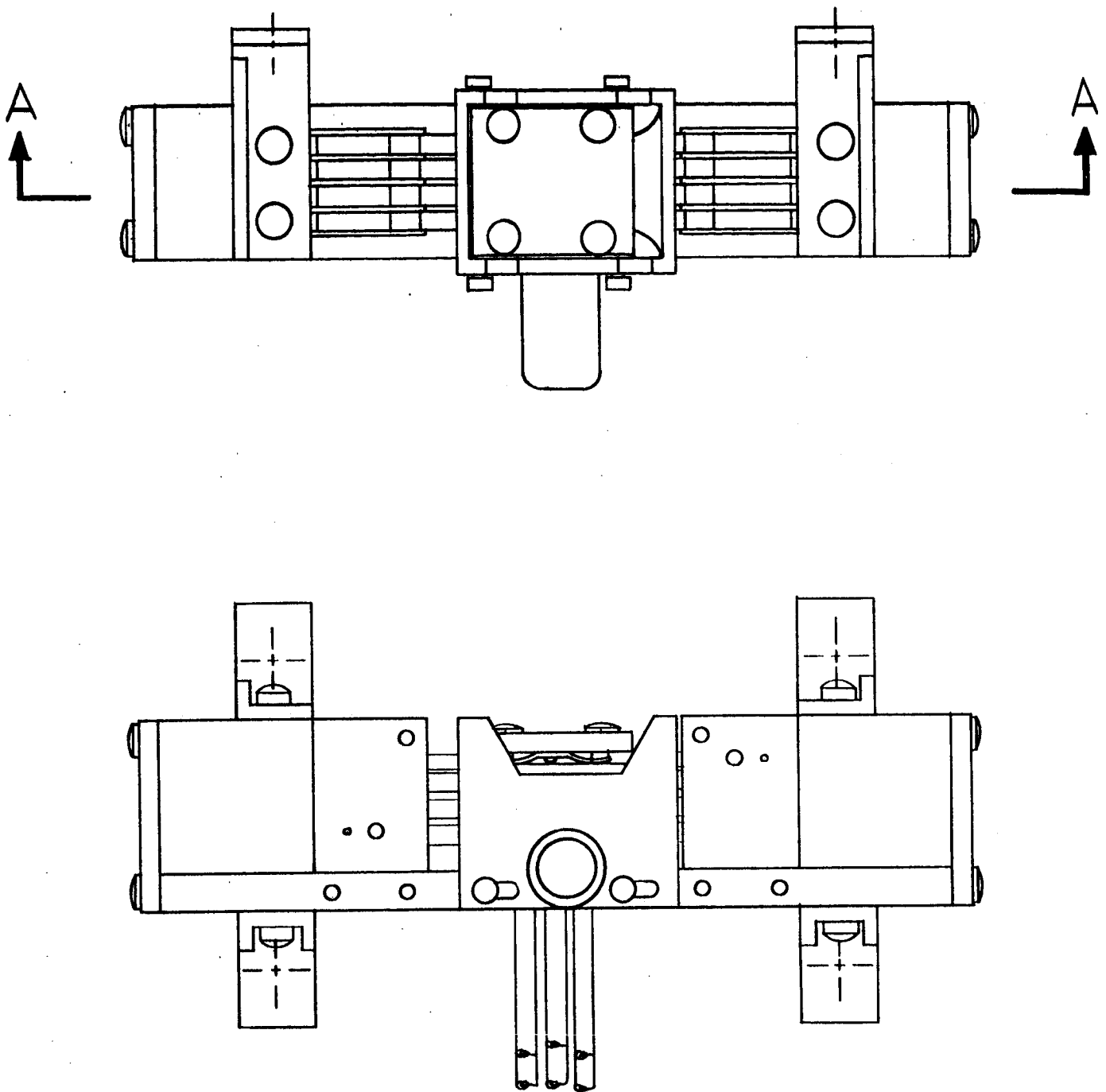


Figure 41. Slide Injection Valve (Top View, and Side View)

valve used for the lab model. The valve as shown in this figure consists of six ports in the flat-lapped stainless steel block, a Teflon slider valve suitable grooved and backed by a spring, and two end blocks containing four squib actuators at each end. Eight toggle links are mounted between the squibs and the slider plate. These links rotate 45° from position when the squib is fired, and the slider moves to the right. This link rotation allows passage of the cage on the return stroke. This linkage system is necessary since the squib plunger once fired cannot be retracted. Were the plunger permitted to come in direct contact with the valve when the squib was fired, the valve could not be returned to its initial position by squib firing from the opposite end.

The ports in the stainless steel block are connected by means of a brazed-in stainless steel tubing to the helium supply, the sample loop, the columns, and the inlet and exhaust ports of the Martian atmosphere simulator. Milled slots in the Teflon slider, alternately interconnect the ports for the charging of the sample loop or for injecting the sample from the loop onto the columns.

Drawings of the injector valve and of the injector valve components are given in figures A1, A1·D1, A1·D2, A1·D8 through A2·D19 in the appendix. These drawings are self-explanatory.

With this arrangement four sample injections are possible with the movement of the valve in two directions. In the post design considerations (Volume III) the use of two sample loops and the possible shifting of the slider in but one direction will be discussed in connection with the injector valve. If this proves to be feasible a total of only four squibs, two at each end, would be required for the injection of four samples.

Results of tests reported in the third month's technical letter report (Volume I) show that the injection valve can be operated with 80 psi helium pressure on the helium and column ports within the valve, and at a vacuum down to 50 microns of mercury on the inlet and exhaust ports. Under these conditions leak rates of 25 microns per minute were observed. This leak rate is acceptable since the valve performs well when incorporated with the columns and other gas chromatographic components.

The slider type valve for the laboratory model is certainly acceptable. It is necessary in the operation of the slider valve to insure that grit, dirt, or other particles are eliminated from the system. In some instances where particles were inadvertently introduced, the surfaces were abraded and excessive leaks were developed. This problem should not exist in the breadboard and prototype units.

4.5 Critical Orifice and Venturi Pump

Since the atmospheric pressure on Mars may be as low as 0.014 atmospheres, it is necessary to have incorporated into the system a restrictor on the column output if adequate control of the helium carrier gas through the system is to be realized. The use of a critical orifice in this connection appeared most promising. With the critical orifice the flow of the through it is independent of atmospheric pressure just as long as the ratio of atmospheric pressure to inlet pressure is equal to or less than 0.53. If this condition is satisfied, the gas flow is independent of atmospheric pressure; and it is determined by the diameter of the orifice. For a constant flow, the pressure at the orifice should remain constant.

The critical orifice desired for this application should be such as to provide a minimum of 15 psia on its high side for an atmospheric pressure as low as 0.014 atmospheres and as high as 0.150 atmospheres. Certainly the use of a critical orifice under these conditions is feasible since the 0.5 quotient limitation discussed above is applicable for the range of atmospheric pressures apt to be encountered. An orifice of approximately 50 mils enables a flow rate of 400 cc/minute to be maintained through it.

Melpar has incorporated with the critical orifice a Venturi throat that may be used to pump the Martian atmosphere

through the sample loop. This throat is tapped and connected to the sample loop outlet. The reduced pressure in the throat arising from the movement of the carrier gas through it serves as a basis for the pumping action. The Venturi pump would be most useful after impact where the normal movement of atmosphere through the sample loop could be practically insignificant. The critical orifice and the Venturi throat are shown in figure 2.

Several experimental units of the Venturi pump with restrictor have been designed and fabricated for testing. The optimum unit produced a flow ratio of 1 to 4 for helium gas to sample gas. That is, for a helium flow of 100/cc/min., a flow of 400 cc of sample or atmospheric gas was experienced.

In figure A2 in the appendix the pump nozzle which effectively acts as the restrictor or critical orifice is shown. This brass nozzle fits down into the pump body shown in figure A3. The connection to the sample loop as indicated is made just prior to the Venturi throat.

4.6 Reference Gas Injection

The reference gas injector fabricated for this program consists of a simple metal Tee which contains a glass ampule placed between glass fiber filters and a gas squib actuator which is used to rupture the ampule. This component has been tested and operated satisfactorily.

This Tee could be incorporated into the sample loop.

The seal on it would be broken just as the injector valve was switched for sample injection. The size of the ampule in the 1/4 in. Tee would be such as not to inhibit the normal flow of sample around it. The Tee could be just as easily incorporated into the helium line prior to the injector valve.

The unit as constructed works quite well in the laboratory. It has not been incorporated into the system as yet.

A design drawing for this Tee is shown as Figure A4 in the Appendix.

4.7 Transit Sealing

In order to protect the columns against the absorption of foreign substances within the earth's atmosphere and at blast off as well as to avoid changing their state of activation in the vacuum of space, in-transit sealing must be effected. It is proposed that the injector valve be hermetically sealed and that transit seals be used at (1) the atmospheric inlet (2) between the helium reservoir and the regulator valve, and (3) at the outlet Venturi which is at the end of the columns. The columns would be sealed under helium.

The transit seal device consists of a block which contains a diaphragm and a squib actuator. This diaphragm, which for the preliminary considerations has been made of glass is hermetically sealed in place. It will be a metallic seal in the breadboard. The squib actuators would

rupture the seals when the unit was activated. They would be fired simultaneously from the programmer. Squib actuators used for all seals would be identical.

In figure 42 is shown a two-way valve which is squib actuated. This valve was designed for switching the helium to the pneumatical valve previously considered. This valve has not been used as such mainly because the particular pneumatic spool valve as discussed above was abandoned. However, the squibs used for breaking seals and for moving the slider in the injector valve are represented by either side of this design. Detailed drawings on the squib mechanism are given in the Appendix as figures A5 and as figure A5.D1 through figure A5.D 10.

4.8 Carrier Gas Reservoir and Controls

For the laboratory model of the gas chromatographic unit a tank of commercial helium will be used for the demonstration. A standard pressure regulating valve will also be used. In the projected design considerations a titanium sphere designed to hold the carrier will be covered as will a miniaturized pressure regulating valve.

The carrier gas control system originally envisioned and described in the first monthly letter report has been considerably simplified. The need of a control valve for the injector valve has been obviated by the use of squib actuation.

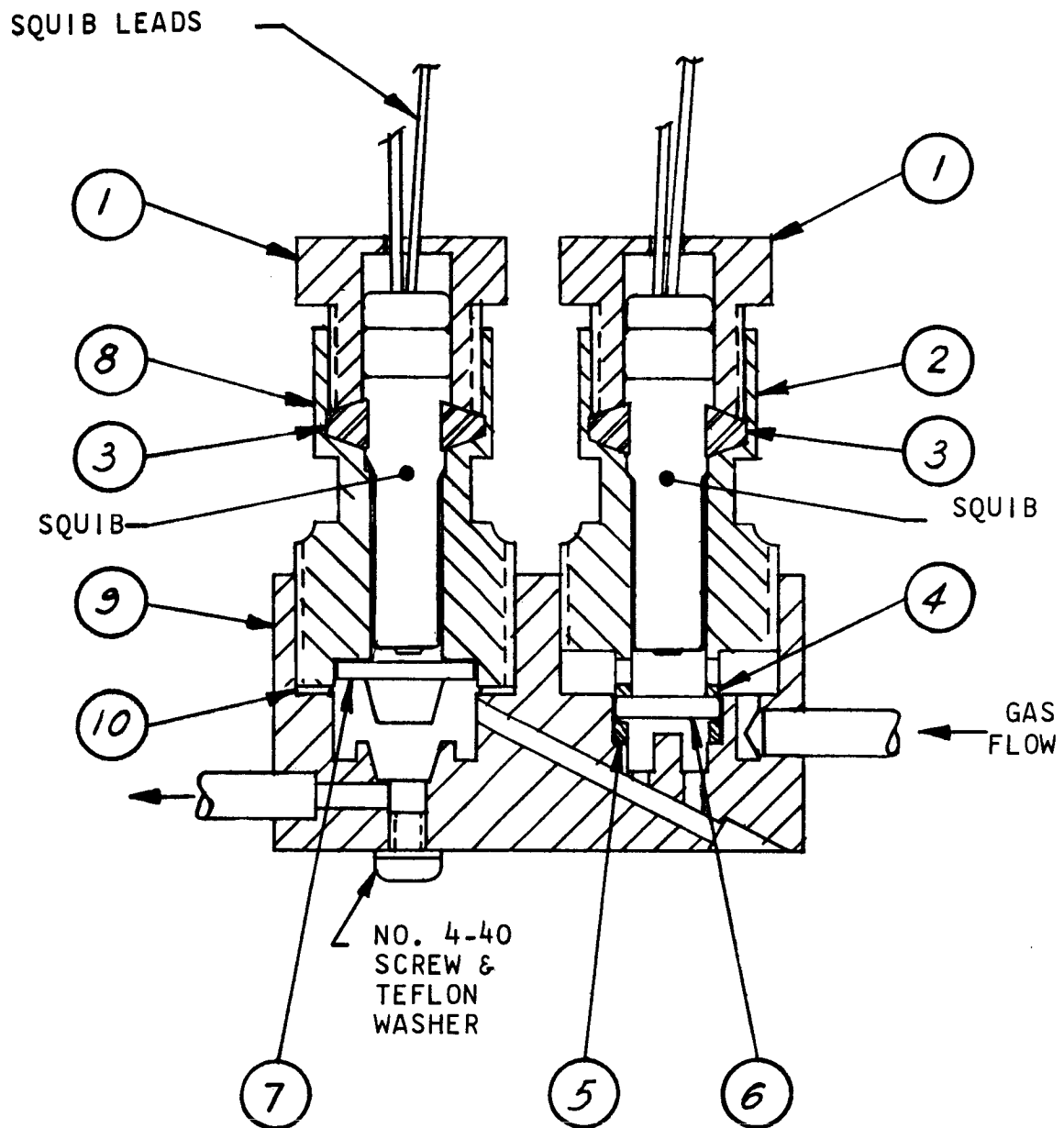


Figure 42. Squib-Actuated, Two-Way Valve

In figure 2 was shown the general schematic arrangement of the system with special emphasis being given to the placement of squib actuators, to be used in conjunction with the sample injector and the in-transit seals, and the Venturi-orifice arrangement at the end of the last column. This latter arrangement incorporates a restricting orifice for limiting the flow of carrier gas through the system in the very sparse Martian atmosphere and a Venturi throat for pumping atmospheric sample through the sample loop.

4.9 Packaging for Demonstration

To simplify and perhaps clarify the demonstration of the gas chromatographic unit fabricated by Melpar a mock-up board has been constructed and the various components mounted on it (figures 3 and 4). No attempts in making this mock-up were made to actually compact the various components. It was necessary to have ready access to the columns, detectors, injector valve, etc. in the integration and evaluation of the various and sundry components.

The drawing of the mock-up board is shown in figure 43. In figures A6 and A7 of the appendix the design drawings for the electronic case are shown.

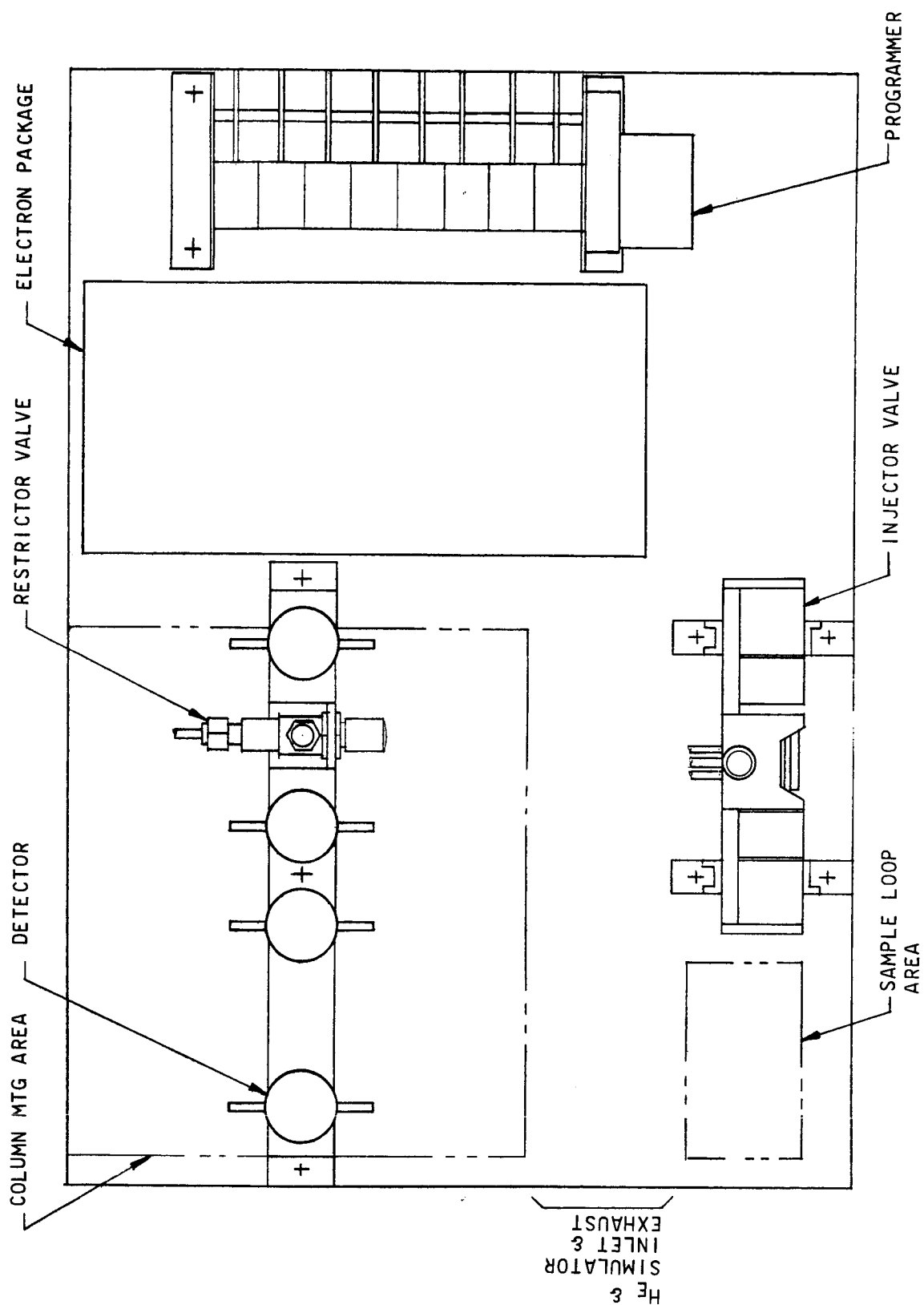


Figure 43. Mock-up Board

4.10 Electronic Components

4.10.1 Introduction

The electronic requirements of the Mars Gas Chromatograph primarily involve the acceptance of current from a high impedance gas detector cell and conversion of this current to a zero to five volt analog of gas concentration. Secondary requirements are the supply and regulation of power, the sequencing and timing of all command functions such as the ignition of heaters and the injection of gas samples. Another electronic requirement is the recognition of output data, its quantizing, coding and transmission. The last mentioned requirements were not studied on an experimental basis as part of this program. However, they have been considered theoretically and will be discussed in Volume III of this final report.

The requirements that were studied experimentally in the laboratory are discussed in detail in the following pages, together with experimental results. The final design employs all solid state electronic components. This provides the basis for a system possessing exceptionally high reliability.

4.10.2 Electrometer Amplifier

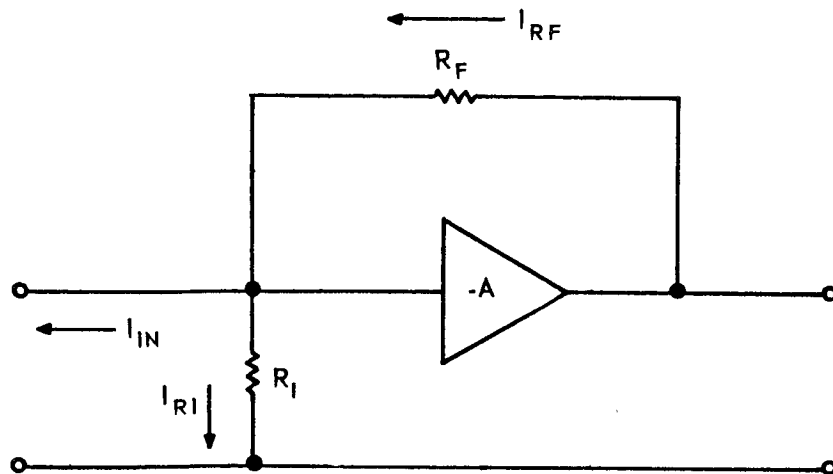
An important consideration in selection and design of any operational amplifier is that nearly all the signal current entering the summing point pass through the feedback resistor. This can be interpreted as implying that the feedback

resistance divided by amplifier gain must be much less than the amplifier input impedance in the pass band. A commercially available packaged amplifier known as the Philbrick P-2 was tried for this application. Its minimum advertized gain is 2×10^4 . Its input impedance is about 7.5×10^7 ohms and it is capable of delivering an output voltage in the range of ± 10 volts.

In the operational amplifier connection, as shown in figure 44, the gain of the amplifier can be employed to advantage to cause most of the detector current to flow through the feedback resistor, even with a relatively low input impedance amplifier. It is quite simple to show that for an operational amplifier with an input resistance of R_I , a feedback resistor R_F and a gain of $-A$ that the ratio of current I_{RF} through the feedback resistor to that through the input resistance I_{RI} is

$$\frac{I_{RF}}{I_{RI}} = \frac{(1 + A) R_I}{R_F} .$$

In the case employed for the electrometer design for the subject system, $R_F = 10^9$ ohm, $R_I = 7.5 \times 10^7$ ohm, $A = 2 \times 10^4$. Hence, it is seen that the ratio of current flow in the feedback resistor to that in the input resistance of the amplifier is 1500 and it becomes quite obvious that only a very small fraction of the detector current, i.e. .067%, is lost to the input impedance of the amplifier.



$$\frac{I_{RF}}{I_{RI}} = \frac{(1+A) R_I}{R_F}$$

Figure 44. Simplified Operational Amplifier Connection

From this consideration it is apparent that variations in amplifier input impedance due to leakage will produce relatively small variations and hence error in the amount of detector current flowing through the feedback resistor. Since the amplifier output voltage is determined by the product of current flow through the feedback resistor and the value of the feedback resistor's value, it too is equally independent of variations in input impedance. For the extremely low input currents from very high impedance sources, the operational amplifier connection is thus seen to possess many desirable attributes for stable operation in an unattended situation. For this reason, we have selected this method as the basis of design for the Mars Gas Chromatograph Electrometer.

4.10.2.1 Direct-Coupled, High-Input Impedance Amplifier:

One obvious way to achieve high input impedance is to drive all other terminals of input stage except the input terminal in such direction as to follow the input voltage itself. The motivation for doing this is apparent from an equivalent circuit shown in figure 45. The current appearing in the input of the equivalent circuit is $I_{in} = \sum E_i/Z_i$ independent of V_{in} , where all E_i are constants. This is precisely the condition of high impedance. The techniques employed here to approach this ideal is the use of a high gain feedback amplifier to drive the collector of the input emitter follower.

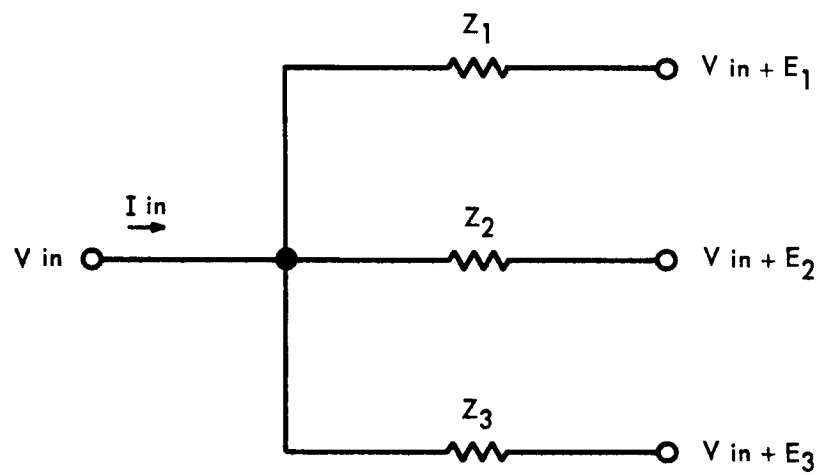


Figure 45. Infinite Impedance Input Equivalent Circuit

The actual circuit employed is shown in figure 46. To understand the operation of the circuit, consider first the input stage as a simple emitter follower and the second stage as a simple common emitter stage employing a resistor in its emitter to control its gain. The third stage is a common emitter stage having its emitter connected to positive supply. The collector of the third stage is in phase with the input having suffered two inversions. Its voltage is fed back to the emitter of the second stage. This reduces the changes of signal voltage appearing across the emitter-base junction of the second stage so that the gain of the second and third stages combined is nearly unity. The collector of the first stage is also driven by the output voltage through a Zener diode. If the transistors have voltage gain A_1 , A_2 , A_3 respectively, the output voltage is

$$E_o = \frac{E_i A_1}{1 + \frac{1}{A_2 A_3}}$$

The input impedance is in the order of 300 megohms in experimental circuits constructed for this project. The main drawback to using this type of circuit seems to be high base current in the input transistor. In the experimental circuits this was measured at about 8×10^{-8} amperes. It is felt that it may be unreasonable to expect to keep this constant to one part in 10^6 in order to measure perturbations of input

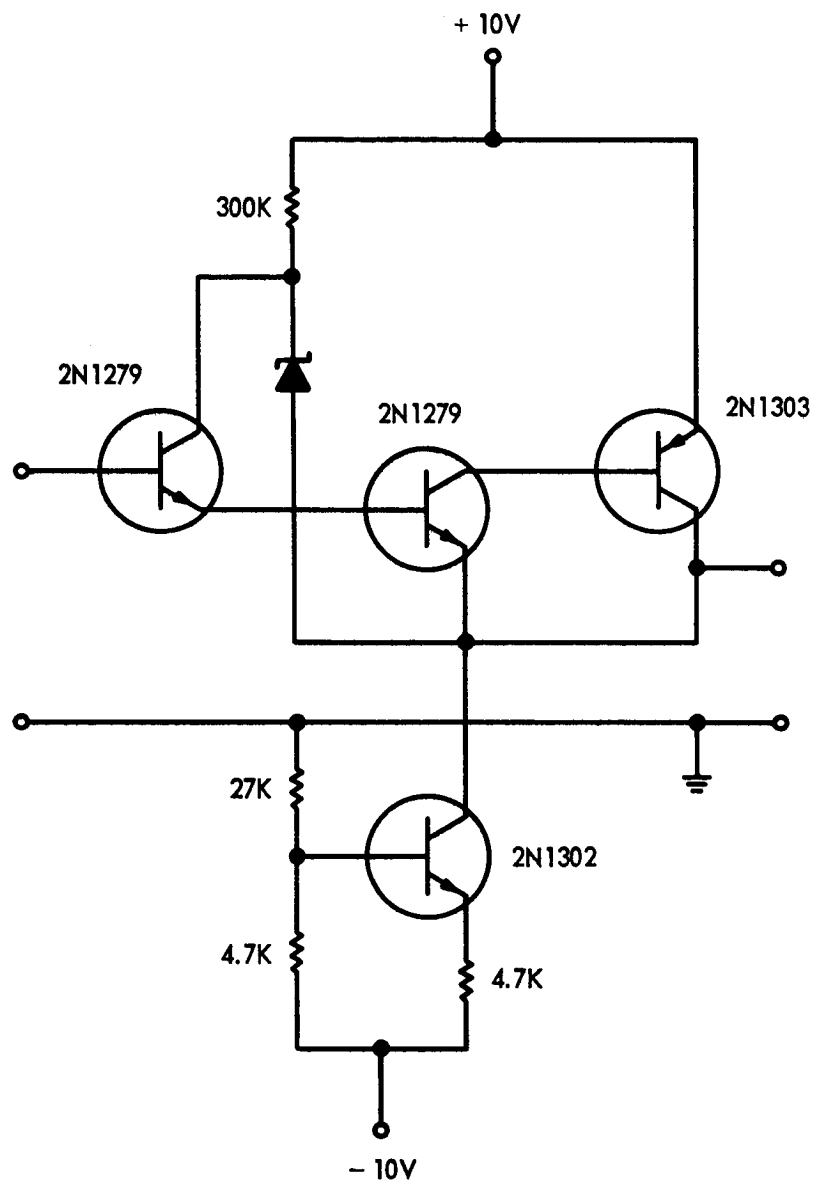


Figure 46. High Input Impedance D.C. Amplifier

current in the order of 10^{-12} amperes. Other techniques such as those described in the following paragraphs may be required to offset this drawback in a very high input impedance solid state amplifier.

4.10.2.2 Impedance Multiplication by Sampling: It is possible to significantly raise the apparent impedance presented by an amplifier by the process of sampling the input signal for a very short time interval compared to the period of sampling. The situation leading to the effect is illustrated in figure 47. Here, the effect of sampling switch S1 is synthesized for its influence at the input terminals by imagining that for the open condition it is switched to the open condition impedance R_o and for the short circuit condition it is switched to the closed circuit impedance R_c . It is further assumed that the switch remains closed for an interval τ and is open for the interval $(T-\tau)$ where T is the period of sampling. This is exhibited in figure 48 as is also the resulting impedance condition as a function of time looking into the input terminal of the switch. It is obvious that for an applied dc voltage E_s , during the period τ the power absorbed by the load is E_o^2/R_c and during the period $(T-\tau)$ it is E_o^2/R_o . Hence, during the period the energy absorbed by the load is,

$$\text{Energy} = E_o^2 \frac{\tau}{R_c} + \frac{T-\tau}{R_o}$$

S-1

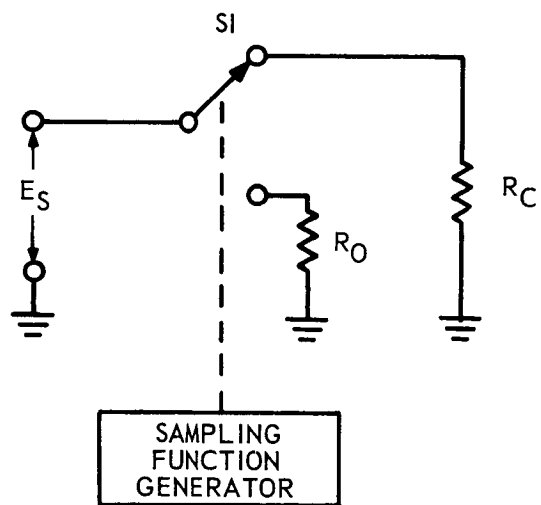


Figure 47. Equivalent of Input Signal Sampling Amplifier

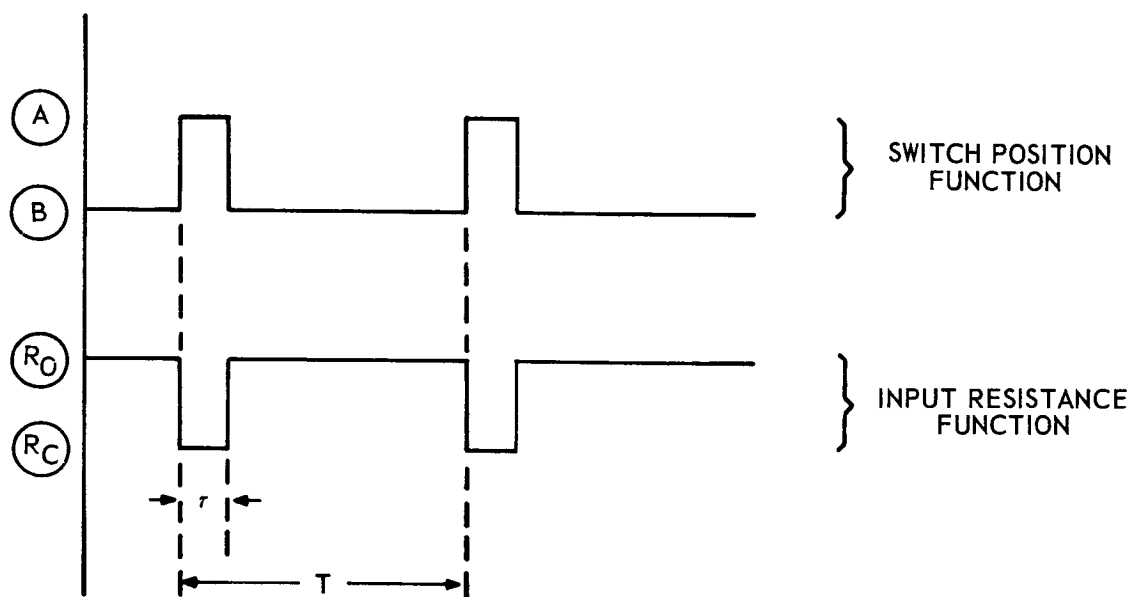


Figure 48. Input Impedance Multiplication By Sampling

However, as far as the load is concerned this energy can be considered as being expended in an apparent constant impedance R_I which is chosen in value such that it consumes the same energy as that given in equation S-1 above. Equating the energy consumed by the artificial load to that given in equation S-1,

$$E_o^2/R_I = E_o^2 \tau/R_c + (T-\tau)/R_o \quad S-2$$

Hence, the apparent input impedance presented at the input terminals to the sampling switch is

$$R_I = \frac{R_c \frac{1}{\tau}}{1 + \frac{R_c}{R_o}} \left(\frac{T}{\tau} - 1 \right)$$

Note that if R_o becomes infinite, then the above expression reduces simply to $R_c (T/\tau)$. From this it is apparent that the influence of the sampling is to multiply the impedance of the load by a factor equal to the duty cycle of the sampling.

The principle outlined above could provide the high input impedance dc amplifier required for the electrometer portion of the gas chromatograph instrumentation. Using this method, a high impedance input amplifier is coupled to the load by means of a solid state sampling network using possibly the configuration illustrated in figure 49. The coupling network as shown consists of a set of silicon diodes arranged in a balanced bridge circuit. Under the excitation of a short

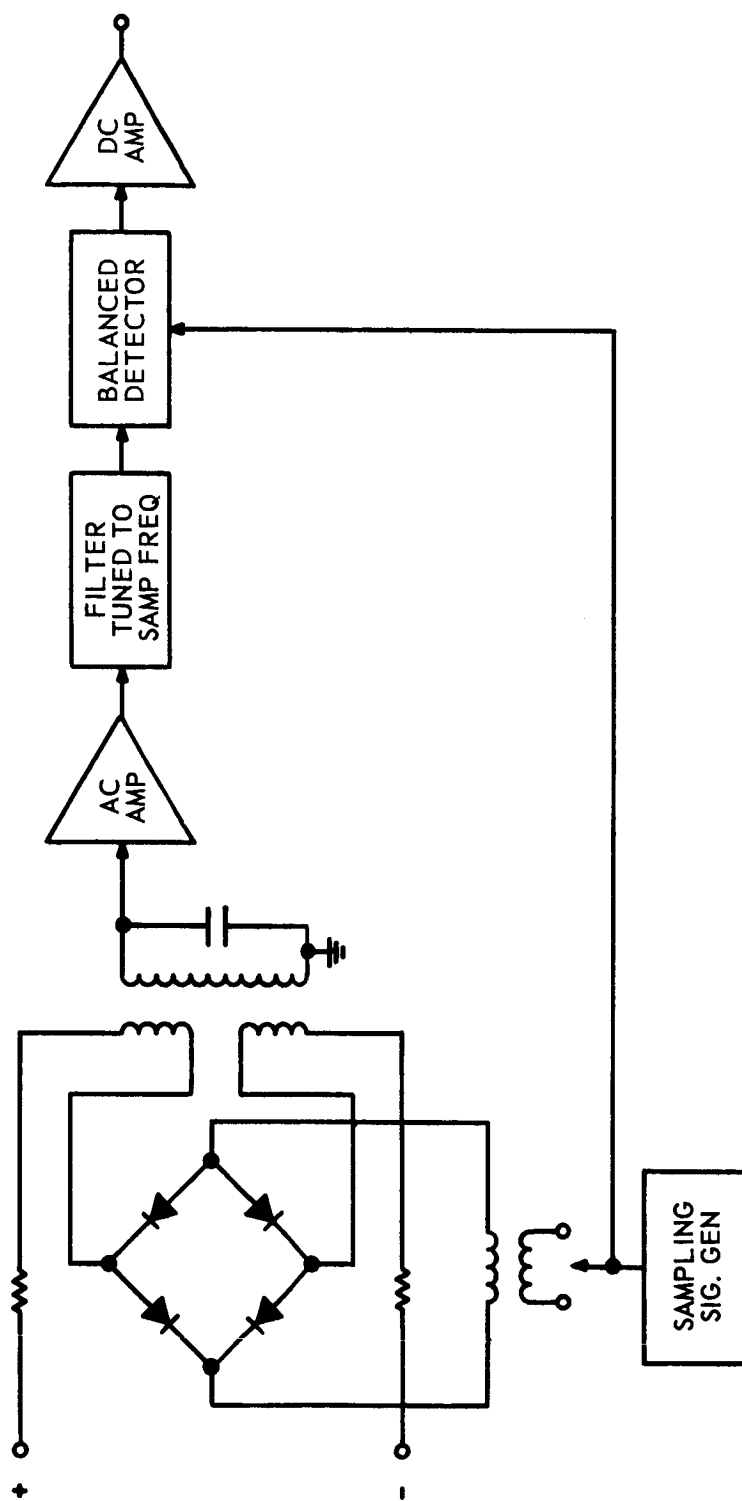


Figure 49. Functional Block Diagram of Sampling D.C. Amplifier

duty cycle switching signal the diodes behave in the manner described in the previous paragraph to connect the signal input to the high impedance amplifier for a very short interval once each sampling period. As further illustrated in figure 49, the high impedance input stage is followed by an ac amplifier tuned to the sampling frequency. This amplifier should be able to provide an overall gain for the configuration of at least 10,000. The output signal is derived from a synchronous balanced demodulator which converts the signal to dc and preserves polarity discrimination.

4.10.2.3 Resulting Design Considerations: Because subsequent modifications in the gas detector cells increased the signal current to 10^{-8} amperes full scale, it was possible, and in fact necessary, to reduce the feedback resistance to 10^9 ohms. As previously shown, the ratio of current in the input resistance of the P-2 operational amplifier to that in the feedback resistor is only 0.067% for this case. Hence, the P-2 operational amplifier is quite acceptable electrically under these conditions and has been used in the demonstration model. For requirements of outer space and the low pass band needed for gas chromatographic applications a modified version of P-2 amplifier possessing all silicon transistor construction, lighter weight construction, reduced physical size, and simplified circuit design is recommended and is well within the state of the art. A schematic diagram of

the present P-2 operational amplifier is shown in figure 50.

4.10.3 Zero Correcting Electrometer Amplifier

4.10.3.1 Servo Type Zeroing Circuits: The gas detector cells used in this gas chromatograph conduct a finite amount of electric current in the presence of carrier gas only. This current that flows in the absence of any sample gas is the baseline current. The customary laboratory technique is to compensate for this baseline current by the use of a buckout box. A buckout network consists in essence of a potentiometer bridged across a battery with a high resistance connected to its wiper as shown in figure 51. The potentiometer is adjusted so that the current flow through the high resistance compensates for the baseline current. The magnitude of the baseline current depends on carrier gas flow rate, pressure, composition and other variables. In the laboratory as the baseline current changes, the potentiometer is simply readjusted to compensate.

It would be unreasonable to expect the baseline currents of the Mars Gas Chromatograph detectors to remain sufficiently stable to permit their buckout currents to be preset before launch. One obvious solution is a servo type automatic zeroing device to adjust the potentiometer as shown in figure 52. Of course the resolver would have to be braked during the actual chromatographic analysis run if it is not to destroy the information. This consequence would be avoided if the

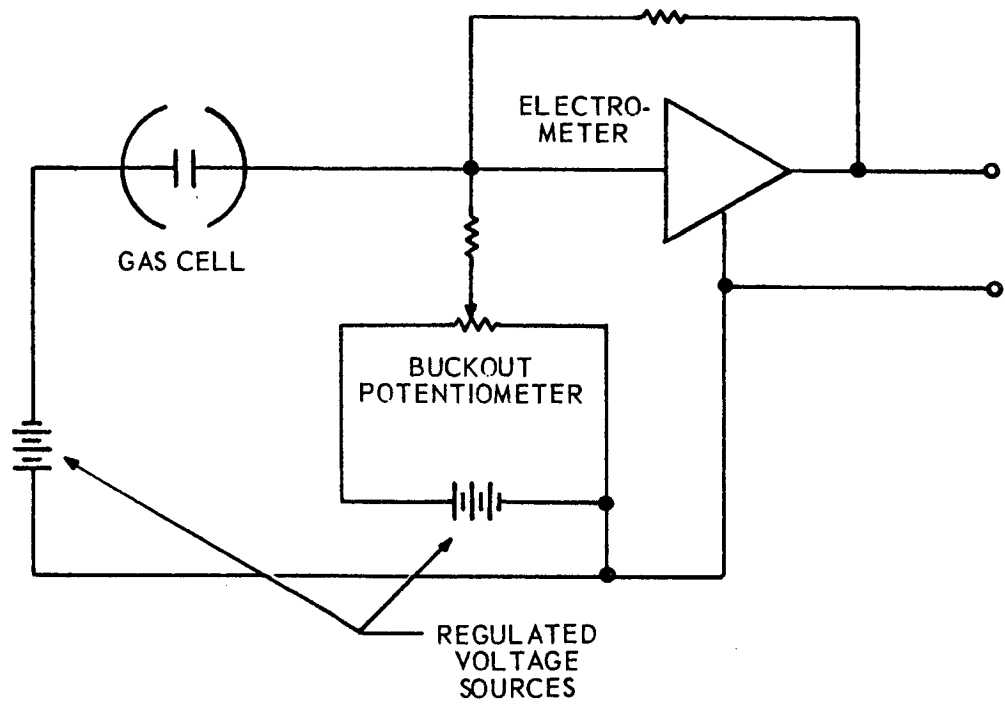


Figure 51. Customary Laboratory Buckout Network

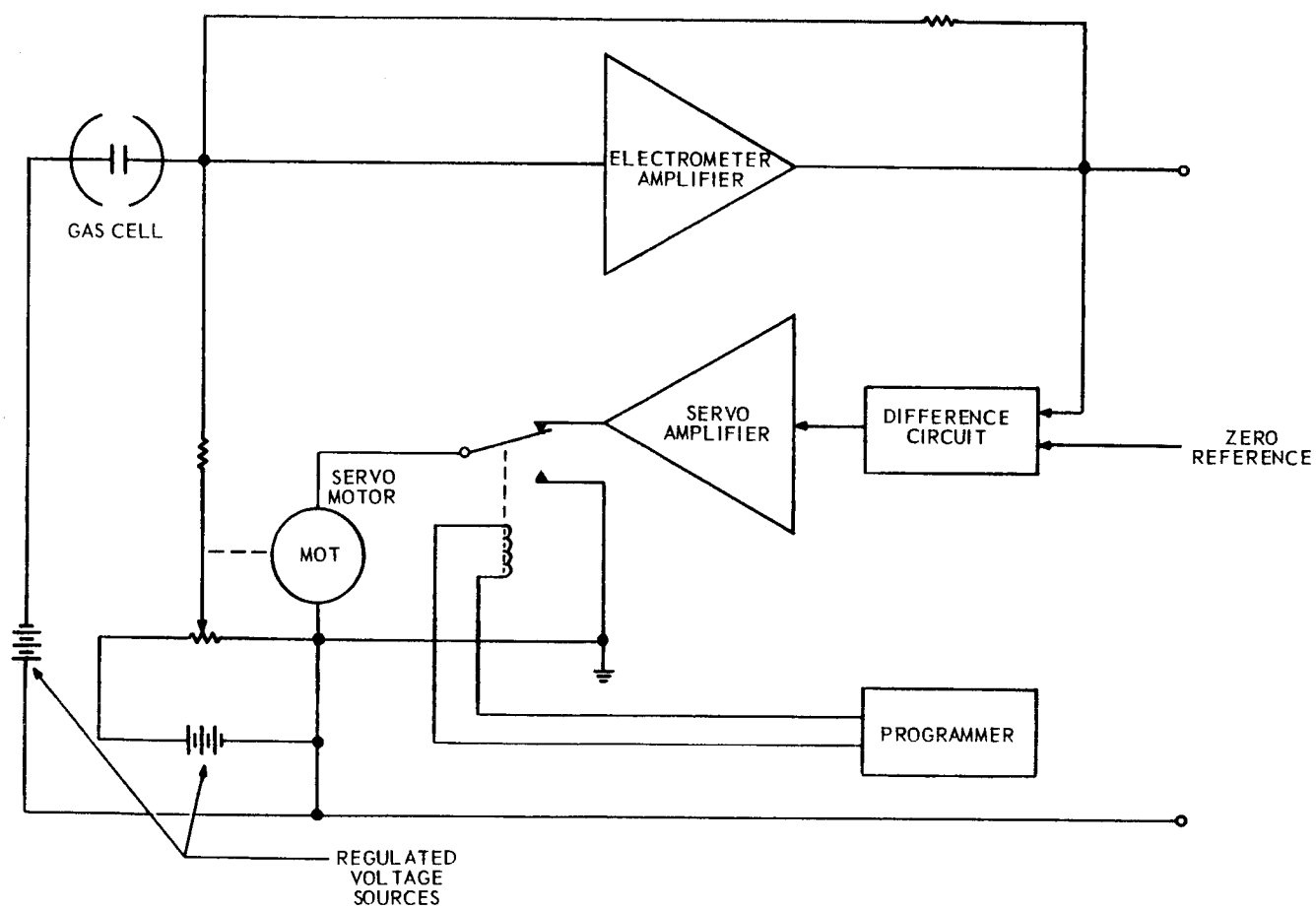


Figure 52. Servo-Type Automatic Zeroing System

correction rate of the resolver were very slow. In any case, a servo system would require electro-mechanical devices with their associated reliability problems and friction related offsets.

An alternate approach avoiding the electro-mechanical components lies in the use of an electronic amplifier to produce the buckout current directly. This would have to be switched to a memory mode to prevent the destruction of information unless its response were very slow. A possible configuration is shown in figure 53. In this configuration the charge stored on capacitor C would be automatically adjusted during the time immediately preceding an chromatographic analysis run to produce a buckout current precisely equal and opposite to the detector base line current. This result is created by the action of the differential amplifier and d.c. feedback amplifier which forces the electrometer output voltage to equal that of the zero reference. Then during the run the input to the charge correction circuit would be broken by a switch activated from the programmer and the zero correction would then be held unmodified during the analysis. The principal difficulty anticipated in this design would lie in the rather large value of capacity that would be required to hold the charge to within 0.1% or better during the analysis interval.

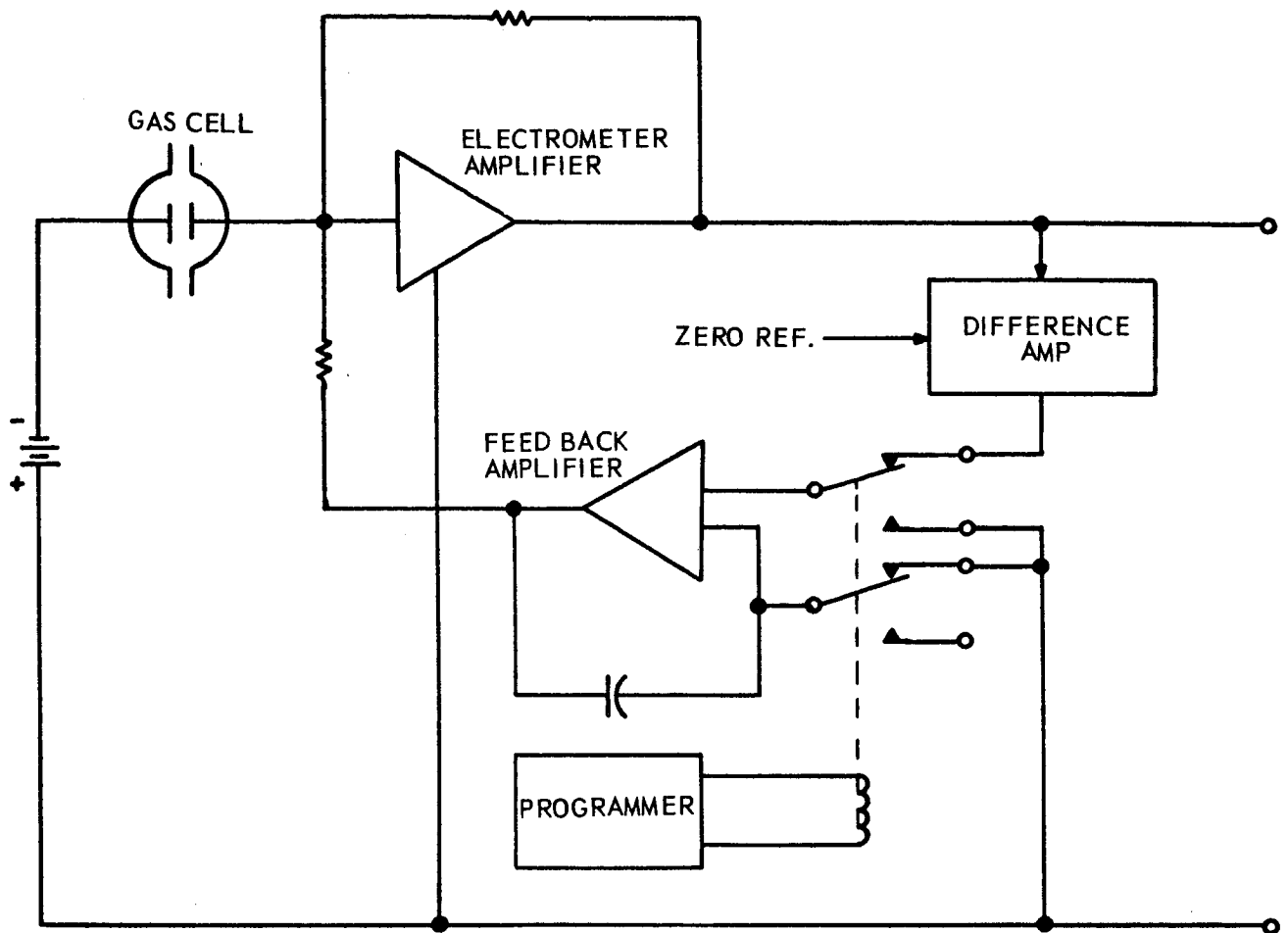


Figure 53. Switched Electronic Automatic Zeroing System

4.10.3.2 Zero Correction by Transfer Response: It is possible, by use of an appropriate linear feedback network placed in the feedback loop of the operational amplifier, to achieve zero correction by greatly suppressing the low frequency variations in the baseline current while permitting full amplifier response to the higher rate variations that constitute the desired chromatographic response function. Using this method, it has been possible to devise an all solid state electrometer amplifier capable of operating at detector base line current levels of 3×10^{-8} amperes, possessing sufficient dynamic range and frequency response to transmit signals that represent perturbations as small as one-thousandth of this baseline current, and capable of correcting the amplifier zero for long-term shifts in baseline current to within 0.1% of the magnitude of the shift. (The cross section detectors used have baseline currents near 3×10^{-8} amperes.) The circuitry automatically zeros a prescribed baseline current; and it corrects for any deviations from the prescribed value to within 0.1% of the deviation.

A functional block diagram of the self-zeroing electrometer circuit is shown in figure 54. In this diagram the detector is represented as a source of internal impedance R_D drawing a baseline current I_D . For baseline buckout, a reference source of voltage E_R is supplied to the current

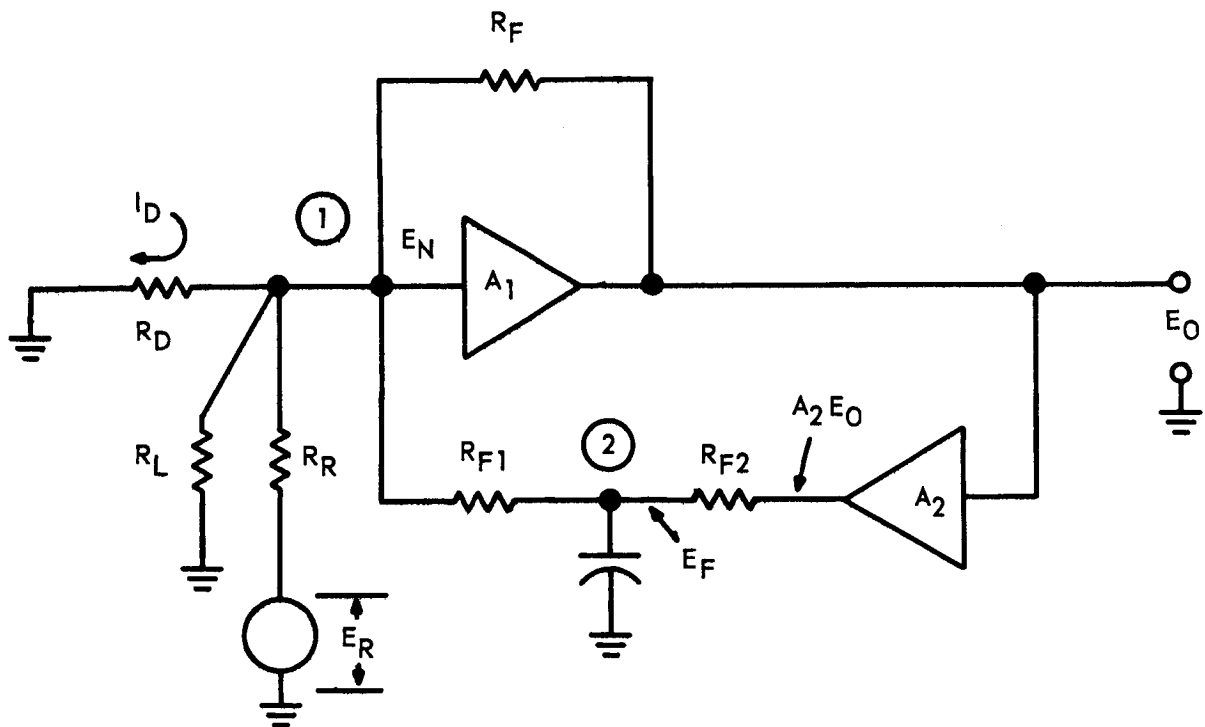


Figure 54. Functional Block Diagram of Self-zeroing Electrometer Amplifier

node 1 through the resistor R_R . Also, leakage at the input is represented as resistor R_L which appears between ground and the current node 1. The chopper amplifier is represented by A_1 , and a feedback resistor R_F is connected from the amplifier output to the current node 1. The self zeroing action is realized by incorporating the feedback network consisting of resistors R_{F1} and R_{F2} , dc amplifier A_2 and capacitor C_F . This latter network acts to permit the application of high negative feedback for very long period variations such as are associated with long term drift in baseline current; and, hence, greatly suppresses them. For short term variations, such as those associated with the desired chromatography responses, this strong negative feedback does not occur and hence full response is achieved.

The operation of the amplifier is easily explained in terms of its frequency response characteristic. This response is derived as follows. The node equations are first written for the nodes 1, 2 and 3 as shown in figure 54. These are then solved simultaneously to give the result

$$E_o = \frac{R_F (I_o - I_R)}{1 + \frac{R_F}{R} \frac{A_2}{2} 1 + \frac{i\omega R_{F1}}{2} C_F}$$

where

$$R_{F1} = R_{F2}, A_1 \gg R_F/R_T, R_T^{-1} = R_F^{-1} + R_D^{-1} + R_L^{-1} + R_R^{-1} R_{F1}^{-1},$$

$\omega = 2\pi f$, and f is the frequency of the variation. The frequency

response is simply the absolute value of the ratio of signal output to signal input for sinusoidal variations in I_D of frequency ω . Hence, the frequency response function is

$$\frac{\delta E_o}{R_F \delta I_D} = 1 + \frac{K_F (2+K_F)^{-1/2}}{1+(\omega\tau_F)^2}$$

where the parameters K_F and τ_F are defined as

$$K_F = R_F/R_{F1} \cdot A_2/2$$

$$\tau_F = \frac{R_{F1} C_F}{2}$$

The plot of the above response function is shown in figure 55 for the situation $K_F = 1000$ and $\tau_F = 1000$ seconds. This plot illustrates that, for the parameter values selected, fluctuations of 10 second duration and shorter are amplified fully to the value of $\delta I_D R_F$, whereas fluctuations of long period such as 10,000 seconds are suppressed by a factor of K_F^{-1} relative to the above amplification level for short period fluctuations.

4.10.4 Logarithmic Circuit

To encode and recover the anticipated three decades of significant data current with desired resolution (1% of reading), it will be expedient to have the signal in a non-linear form. Specifically, the information must be generated in a nonlinear form or it must be linear and converted to a nonlinear form. An example of the former might be the use

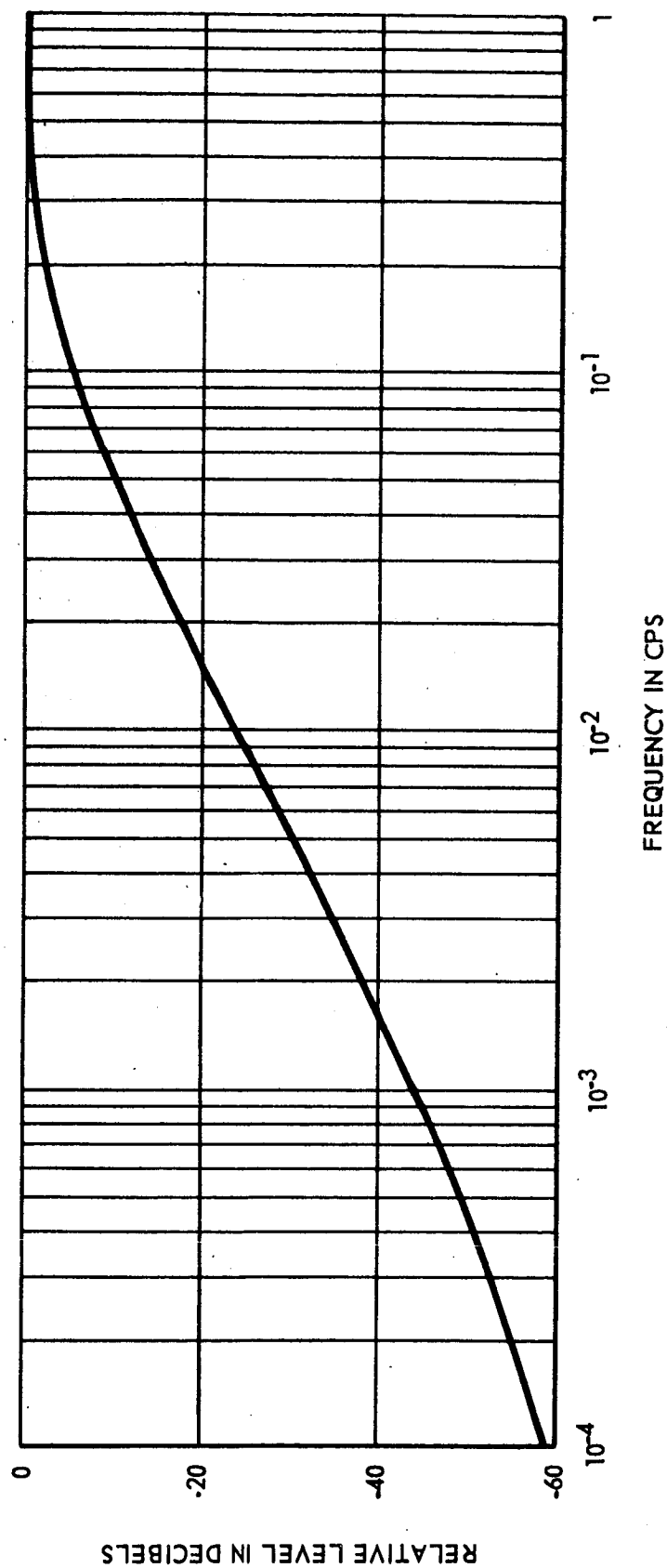


Figure 55. Frequency Response of Electrometer Amplifier

of nonlinear detectors. Ideally, they might be logarithmic. If that is not feasible, one would consider three basic methods of modifying the signal: (1) the strictly passive device, (2) the active nonlinear device, and (3) the nonlinear digital encoder.

(1) The passive nonlinear device is a network of resistors and varistors connected to yield an output approximately logarithmically related to input voltage or current. Its main advantages are simplicity, size and reliability. Its drawbacks are that it depends strongly on the nonlinear characteristic of its components and these may be limited in useful range and subject to variation with temperature and age.

(2) The active nonlinear device contrives to minimize the deviations from true logarithmic response by the use of feedback. Its calibration is, therefore, somewhat more repeatable. The disadvantage is in the loss of reliability associated with the use of active components.

(3) Conversion to logarithmic form can also be achieved directly in the analog to digital conversion portion of a binary digital encoder by employing a logarithmic matrix for generation of the encoding voltage reference. Since the binary digital method of data transmission is to be ultimately employed for transmission of the data to the earth, it may be most expeditious to simply reserve the logarithmic

conversion as part of the encoding operation. The principal disadvantage incurred here lies in the fact that a wide dynamic range of 60 db must be supplied in the communications link between the chromatograph sonde and the orbiting parent satellite to accomodate the significant information of the chromatograph output. Log conversion in the chromatograph sonde avoids the requirement of this wide dynamic range and aids in the preservation of the significant information content in a noisy environment.

For use in the gas chromatograph, where space is a premium, it will be acceptable to limit the approach to one which will lend itself to small packaging, even though this entails a sacrifice, to some degree, of the logarithmic characteristic of the amplifier.

As shown in figure 56, logarithmic amplification is obtained by using the nonlinear forward conducting characteristic of a diode as a feedback element in a DC Operational Amplifier. The resistor network is simply a voltage divider, designed to match the amplifier output to that portion of the diode's Voltage-Current curve which is most nearly logarithmic. It was found that a closer approximation to a logarithmic curve could be obtained by cascading several 1N270 diodes in the feedback loop. The single diode, CR7, is used as a convenient device to assure the monopolarity of the feedback voltage.

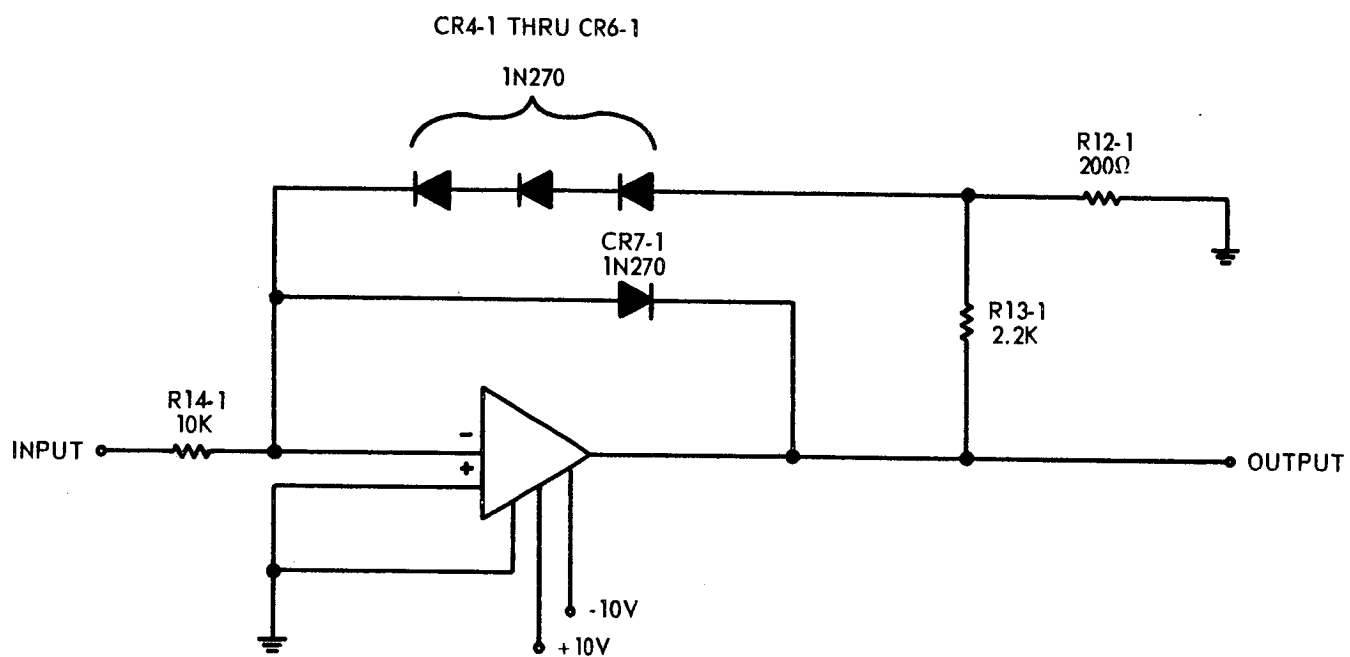


Figure 56. Block Diagram of the Logarithmic Amplifier

The near logarithmic modification of a triangular function, as accomplished by this circuitry, is shown in figure 57. This type of waveform was obtained from the Hewlett Packard Model 202A Low Frequency Function Generator, where a triangular wave of .01 cps can be obtained.

Figure 58 is a transcription of figure 57 where the full width of the oscilloscope graticule is taken as 10. Measurements could be made with dividers down to 0.1 centimeter on the oscillograph, thus permitting the use of two cycle log paper for plotting the curve.

Tests were run using an actual detected gas sample (figure 59, upper trace), and the logarithmic compression of this signal as seen in the lower trace of figure 59 is very much in evidence.

4.10.5 Power Supplies

For expediency, it was decided to use a very simple, direct coupled, low voltage regulator (figure 60) on the laboratory model. Its output voltages are controlled directly by the zener diodes of the regulator circuit. Output impedance was found to be about 85 ohms, positive to common, and 76 ohms, negative to common. These values vary somewhat with supply voltage but have been demonstrated to be sufficiently low for the electronic load. A more sophisticated electronic package, which would derive its power from a common 28 vdc battery, would require a much more refined power supply,

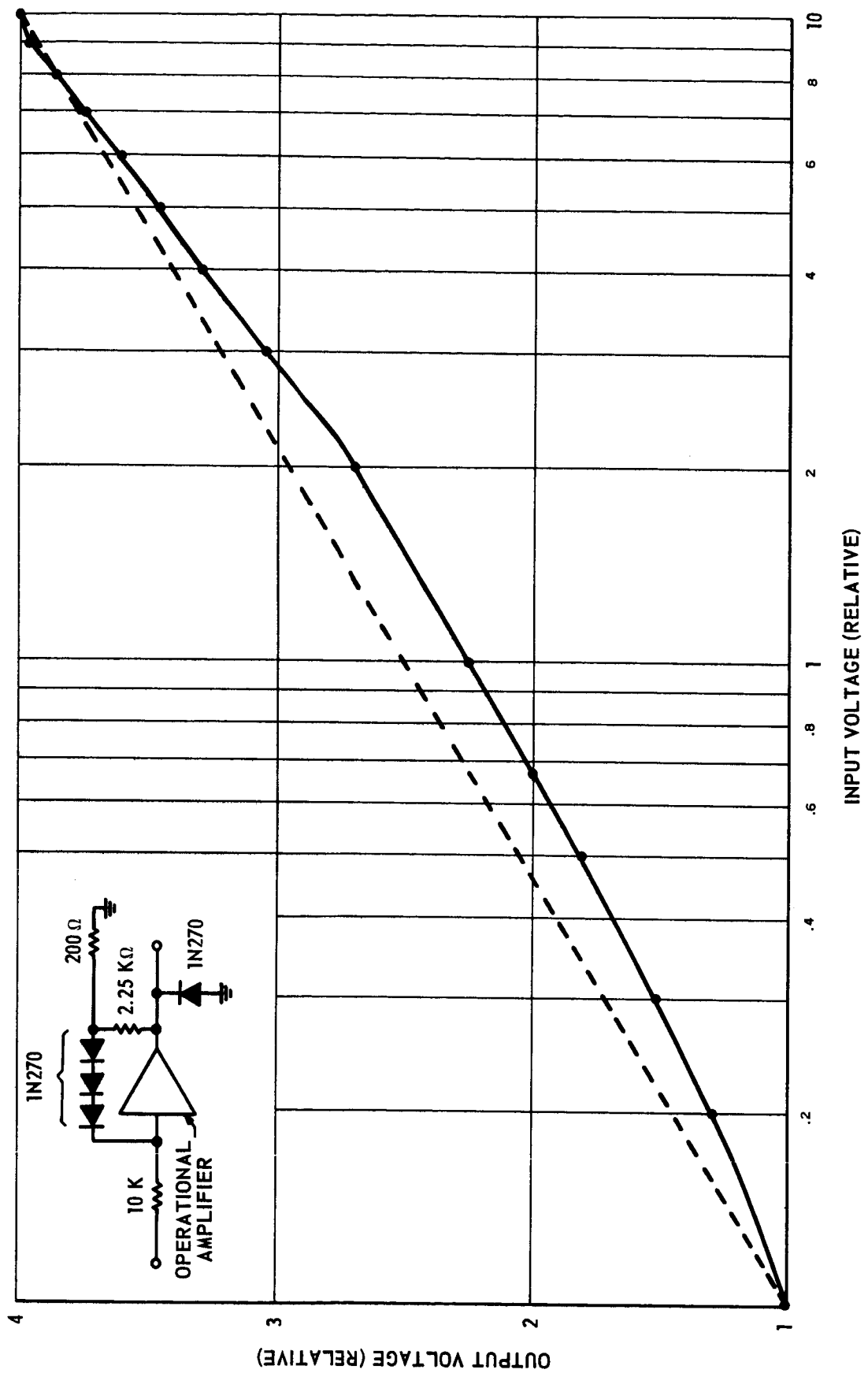


Figure 57. Response of Logarithmic Amplifier to a Triangular Waveform

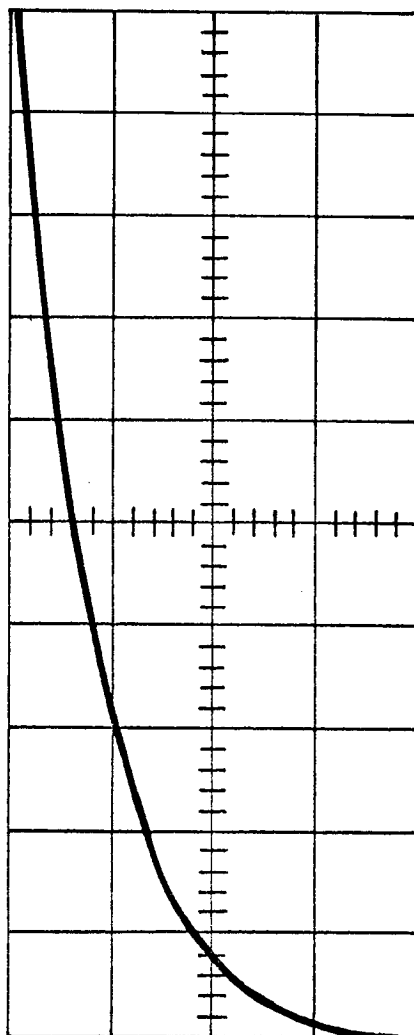
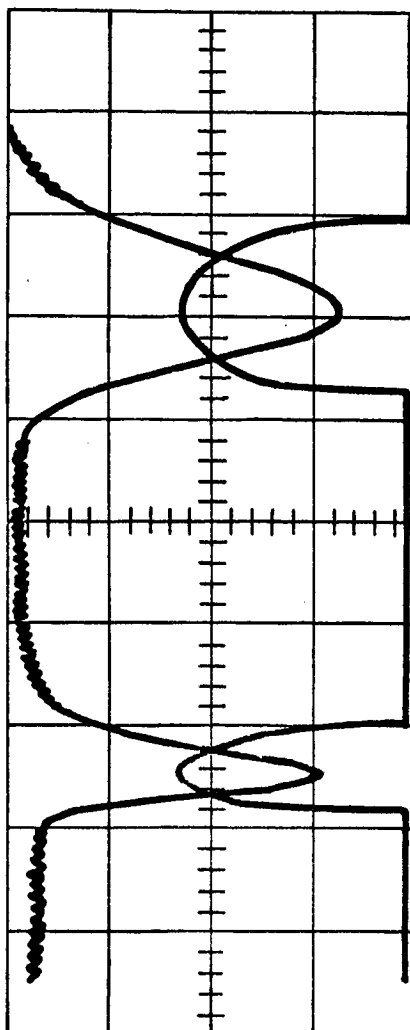


Figure 58. Response Function of Logarithmic Amplifier



一、
 二、
 三、
 四、
 五、

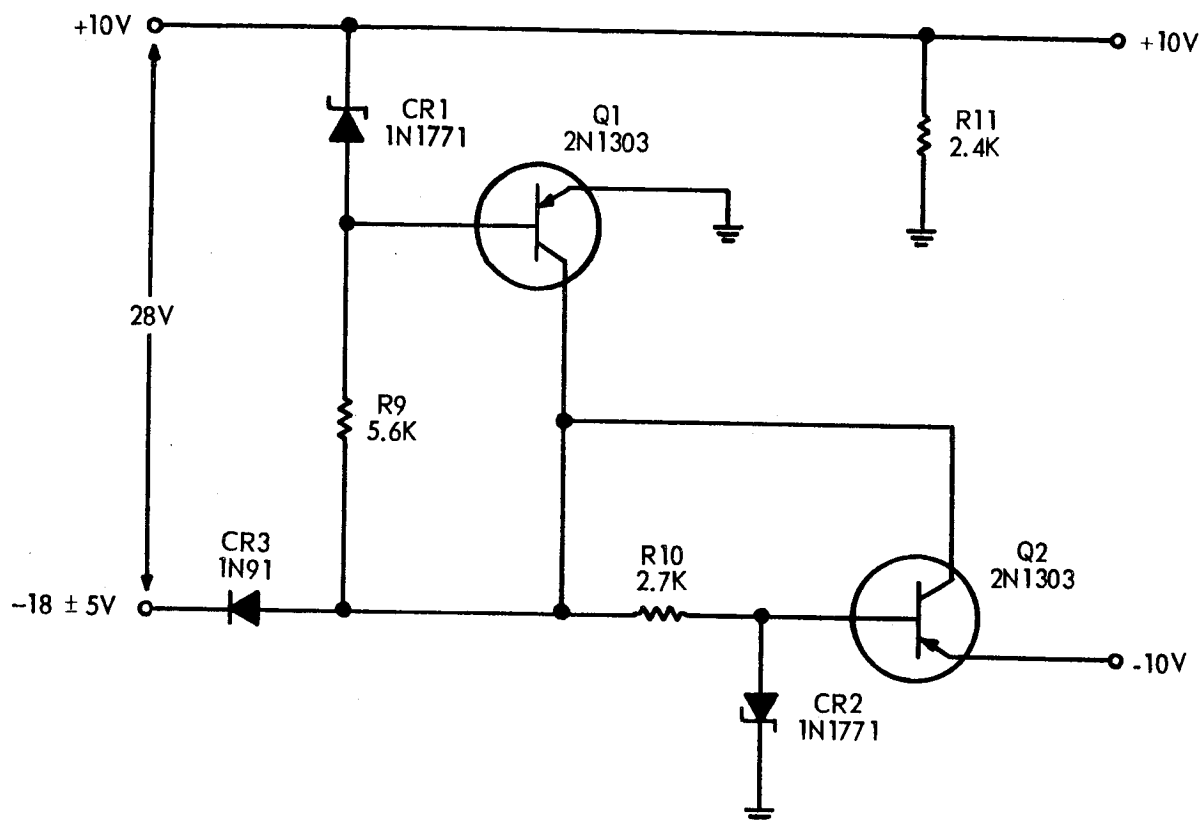


Figure 60. Low-Voltage Power Supply

consisting, typically, of an oscillator, a rectifier, and a regulator such as the one shown in figure 61.

Initial investigations of detector cells prompted the purchase of a dc - dc converter. This item, operating off 28 vdc, provides a floating 1000 vdc output to a maximum load of 2 ma. From no load to full load the output is regulated to better than 1%, while, with an input change of $\pm 10\%$, the output regulates to within 0.3%. Maximum ripple is less than 1%.

The gas detector cells are presently being operated from 45 vdc batteries. Future cells will require only 10 vdc which will be obtained from the low voltage regulator.

4.10.6 General Physical Description of the Electronics Package

The electronics laboratory package (figure 4) consists of a chassis approximately $5\frac{1}{2}$ " high, by $4\frac{1}{2}$ " wide, by $8\frac{1}{2}$ " long with all connectors, switches, and potentiometer adjustments on the front panel. The components on the left hand side, facing the front panel, are associated with the amplifier located in the front section of the chassis while the right hand components are associated with the rear amplifier. In exception to this are the two connectors located at the bottom corners, the left one being the power connector and the other a spare, and the two inboard miniature coaxial connectors which have been included as spares. The dash one

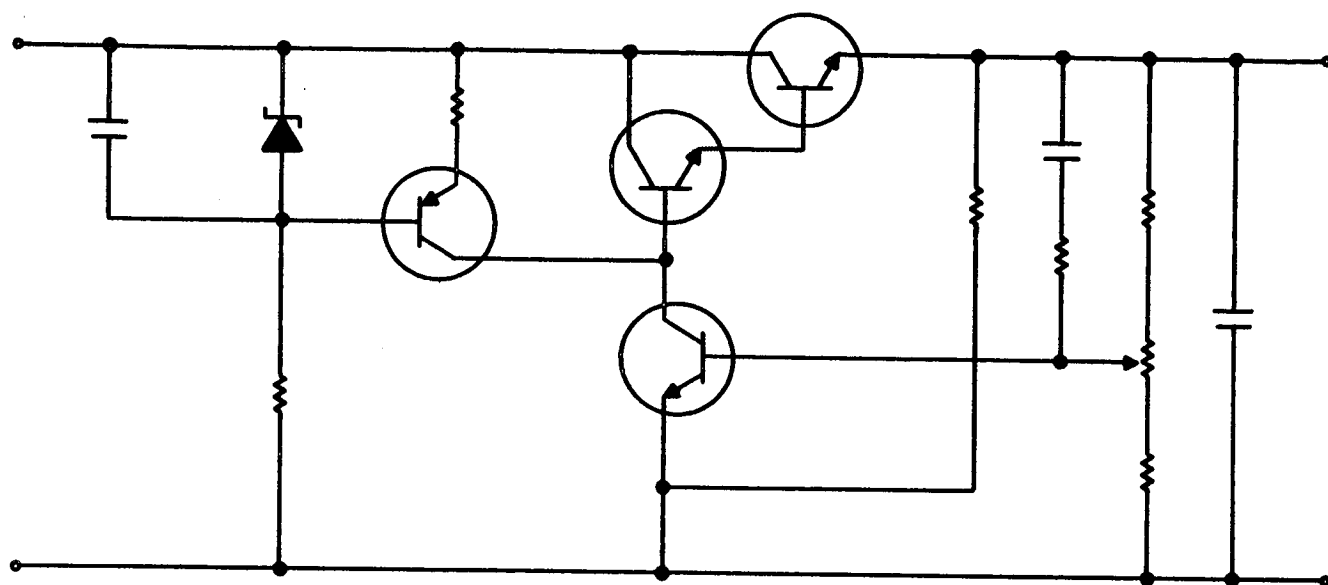


Figure 61. Typical Series Voltage Regulator

(-1) suffixes shown in the schematic diagram are used to distinguish between the two amplifiers and do not refer to a specific amplifier.

The electrometer amplifiers are mounted on the ends of the chassis while their associated feedback amplifiers, on plugboards, go into adjacent sockets. The low-voltage regulator is mounted on the second plugboard from the front end, while the third plugboard provides the voltage connections for the two buckout current potentiometers, R5-1 and R5-2 as shown in figure 61. Although not required for shielding, a cover has been included to close the two sides as well as the top.

4.10.7 Operation

The laboratory electronic package contains two solid-state electrometer amplifiers of the self-zeroing design each operating with 2 detector cells. Figure 62 is a functional block diagram of one of these electrometer units.

With the gas detectors connected to the amplifier as shown in figure 62, and all voltages applied, the amplifier output is ready to be zeroed. Both switches are initially in the "down" or "normal operating" position. Disconnect capacitor C2 from the circuit by putting three-position switch S2 in its center position. By monitoring the electrometer amplifier output with a voltage indicating device, such as a voltmeter or a recorder, one can zero the amplifier

R4402

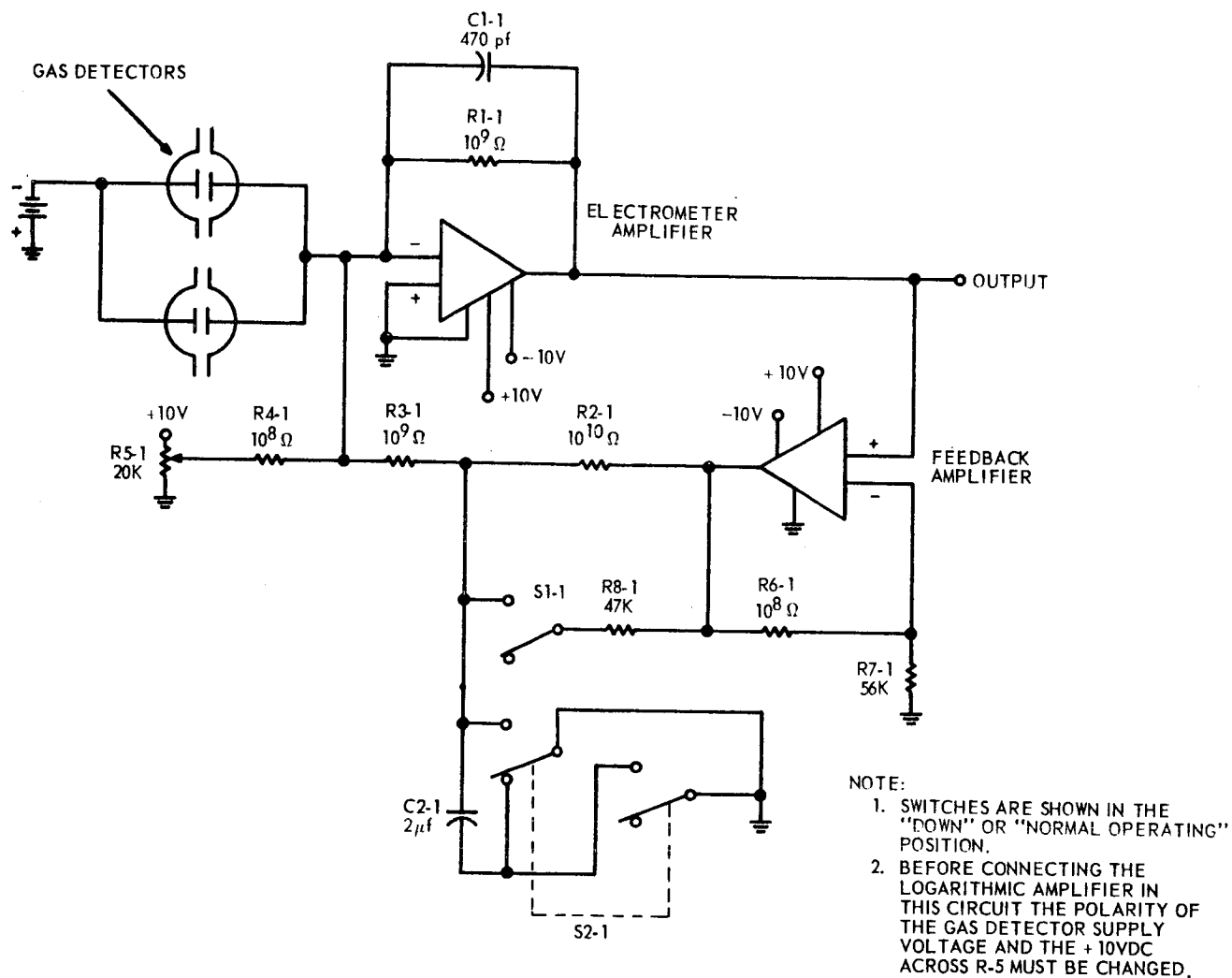


Figure 62. Functional Block Diagram of Gas Chromatograph Amplifier

by adjusting R5 on the front panel. After zeroing, the shunt resistor R8 is connected by switching S1 to the upward position and the filter capacitor C2 by switching S2 to the downward position. (The voltage indicator may pin severely when these switches are thrown so that appropriate precautions should be taken to not damage the instrument.) In a matter of seconds C2 should be charged as indicated by the amplifier output approaching zero again and the shunt resistor is then removed by switching S1 to the downward position.

The two buckout potentiometers, R5-1 and R5-2 are connected to the +10 vdc through a separate plugboard (third plugboard from front end). This facilitates changing the buckout current polarity and permits one to greatly increase the buckout current resolution for zeroing purposes by connecting a voltage dropping resistor in series with the resistive element of the appropriate potentiometer. This latter capability is particularly desirable when the two gas detectors are used back to back or in a current bucking condition and the additional buckout current is derived from a potential of less than 0.5 vdc.

The Program will include the zeroing of the electrometer by closing S1, shunting R2 with 47 kilohms. In actual practice this shunt needs to be in place for some ten or fifteen seconds. If it is wished to reduce this even further,

it is a simple matter to reduce the value of R8. Care must be taken, of course, not to let its value become so small as to permit a current surge into C2 that would damage the output stage of the feedback amplifier.

The final design of the electrometer has been adjusted to operate with a nominal base line current of 2×10^{-8} amperes. For this operation, the feedback resistor value of 10^9 ohms has been selected. This provides an optimum match of the dynamic range of the P-2 operational amplifier to the detector current characteristics. An earlier estimate for the base line current of 10^{-9} amperes required that some consideration be given to an operational amplifier design with at least 3 to 5 times greater input impedance than the P-2 would provide to keep the error due to input leakage less than 0.1%, a level considered to be desirable for this application. Hence, several design configurations were theoretically and experimentally treated for high input impedance circuits using solid state components. The results of these considerations are also presented in the following, even though they now appear unnecessary to realizing acceptable performance of the electrometer.

4.10.8 Programming

For the laboratory model, an electromechanical programmer is employed to control the system. Actually, it is felt that this electromechanical programmer is suitable only

for laboratory demonstration and is not recommended for use in the actual Mars Chromatographic System. For the actual system, an all solid state programmer employing solid state binary counting techniques in combination with "and" and "or" gates is recommended. Such techniques will provide a flexible, reliable design of light weight. Consideration of the design aspects of this solid state programmer is made in Volume III of the report.

5. SUMMARY

Melpar, in fulfilling the terms of this contract, has constructed a laboratory model of a gas chromatographic instrument for the analysis of some 12 components that may be present within the Martian atmosphere. A complete analyses for these components may be carried out in some five minutes. Provisions have been made for doing four complete determinations in a completely automated unit.

Compounds that may be resolved with this instrument are NH_3^* , CO_2^* , H_2O^* , H_2^* , N_2^* , O_2^* , A^* , CH_4^* , CO^* , N_2O , C_2H_6 , and Kr. Cross section ionization detectors are used as sensors. All compounds with the exception of ammonia may be sensed at the level of 10 ppm within the Martian atmosphere. Detection at the high concentration levels specified by JPL is also possible. With the present liquid column ammonia is strongly adsorbed at low concentrations, and as a consequence detection sensitivity is poor.

With this system all compounds of prime interest (the starred compounds) may be detected and quantitatively measured; and most of the compounds of secondary interest may be determined. Compounds of secondary interest not detected with this system are NO , NO_2 , H_2S , Ne, and He. The two oxides of nitrogen are irreversibly adsorbed by the columns. (The detection of N_2O which is possible with this system, however, could be indicative of their presence). H_2S may be resolved

with the liquid column if the present analysis time of some 5 minutes is approximately doubled. Neon which is not resolved by the columns from hydrogen with this system or any known system near 300°K will not be sensed at concentrations near 1%. As a consequence it should present no interference with the hydrogen determination. Helium is used as the carrier gas.

The series arrangement of four major columns is most effective for this application. Columns used include a quadrole-silicone oil liquid column; a silica gel column; a molecular sieve column; and a charcoal column. Two delay columns have also been incorporated into the system. The injection of a reference gas with the first atmospheric sample will be used for standardizing the system after prolonged flight. Four very stable and highly reliable cross-section ionization detectors are used in the series configuration. The detectors are paired in sequence, and their outputs of each pair is fed to separate electrometer.

Several significant facets of this program from a research and development point of view are as follows:

1. A slider injection valve which seals tightly, has negligible dead volume, and which can be operated with extremely low power has been fabricated. The slider is actuated by squib firing.

2. A large number of different columns have been evaluated. The most notable column innovations in the series

configuration are the use of a charcoal column to irreversibly adsorb oxygen in effecting the argon-oxygen differentiation and the use of a short molecular sieve column to separate N_2O and CO_2 .

3. A large number of ionization detectors were evaluated. These included the helium ionization, electron capture, and cross-section ionization detectors. The microcross section detector was chosen for this application because of its high reliability, good sensitivity, and extremely wide dynamic range.

4. An electronic buck-out system automatically compensates for the background current in the detectors. This system together with the amplifiers and power supplies developed by Melpar are compact and require very little power.

5. Provisions have been made for heating with chemical heaters the oven package containing the injector valve, the columns, and detectors. Melpar has raised the temperature of the oven from $200^{\circ}K$ to $310^{\circ}K$ through the sequence firing of chemical cartridges; and the oven is maintained near this temperature without heat input for approximately one hour. A salt heat sink has been effectively used for preventing temperature overshoot in the sequence firing and for maintaining oven temperature.


6. A Venturi at the exit of the last column for the pumping of atmospheric sample through the sample loop has been

designed and tested. A restrictor which is an integral part of the Venturi controls the carrier flow through the system at a given level even when the atmospheric pressure varies quite markedly.

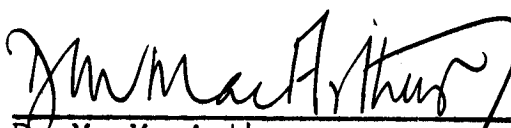
There are some minor problems with the laboratory model which should be solved during the next phase. These include (1) a more accurate method for calibrating the detectors, (2) the insertion of a second loop in the injector valve in preventing variations in carrier flow with switching, (3) an improvement in the resolution of ethane and nitrous oxide, and so on. These problems in no way have detracted from the feasibility experiments carried out with the laboratory model.


Melpar's gas chromatographic unit is a highly reliable unit that adequately does the job required. The unit as such does not greatly exceed the weight, power, and volume requirements for the prototype unit. No insurmountable problems are envisioned in miniaturizing this system to conform with the rigid specifications of the breadboard instrument.

Prepared by:


J. H. Chaudet
Head, Physical
Instrumentation Section

Approved by:


D. M. MacArthur
Head, Chemical and Life
Sciences Department


P. E. Ritt
Vice President-Research

APPENDIX

Laboratory Model
Design Drawings

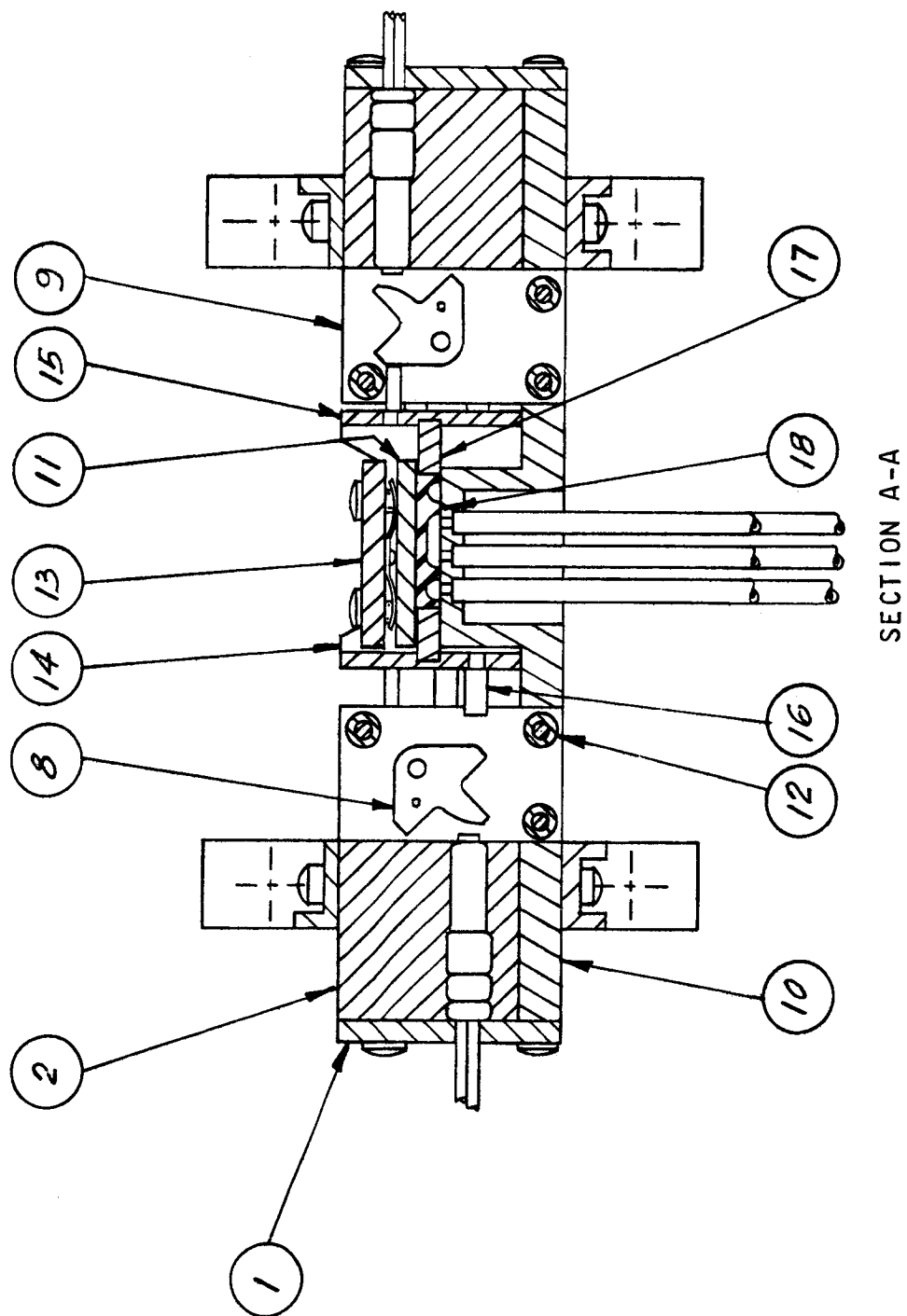
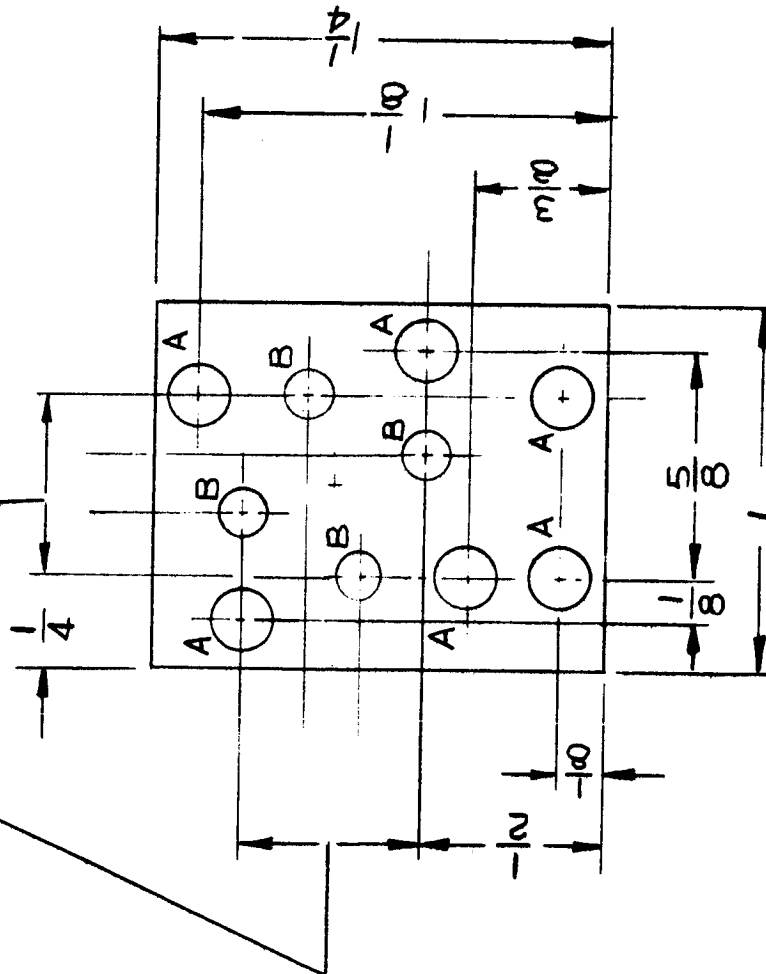


Figure A 1. Injector Valve

A HOLES = $.161 \pm .005$ DIA
 B HOLES = $.125 \pm .005$ DIA

3 EQUAL SPACES @ $.166 = .498$
 TOL NONCUM



TOL $\pm \frac{1}{64}$

MATERIAL: $\frac{1}{8}$ THK ALALY
 6061 TG
 FIN: IRIDITE/ALODINE

Figure A 1.D1. Squib Retaining Plate

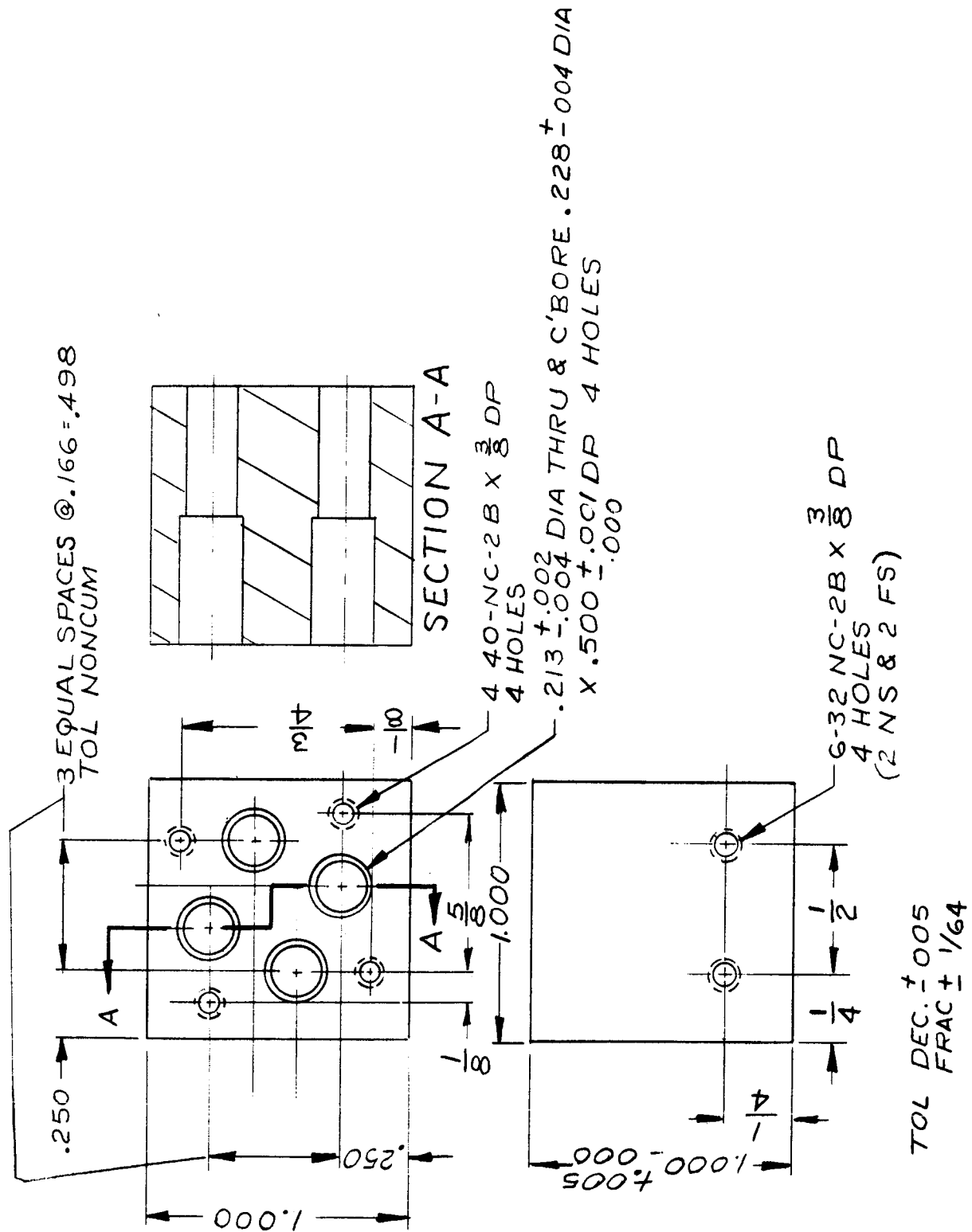


Figure A 1.D2. Squib Retaining Block

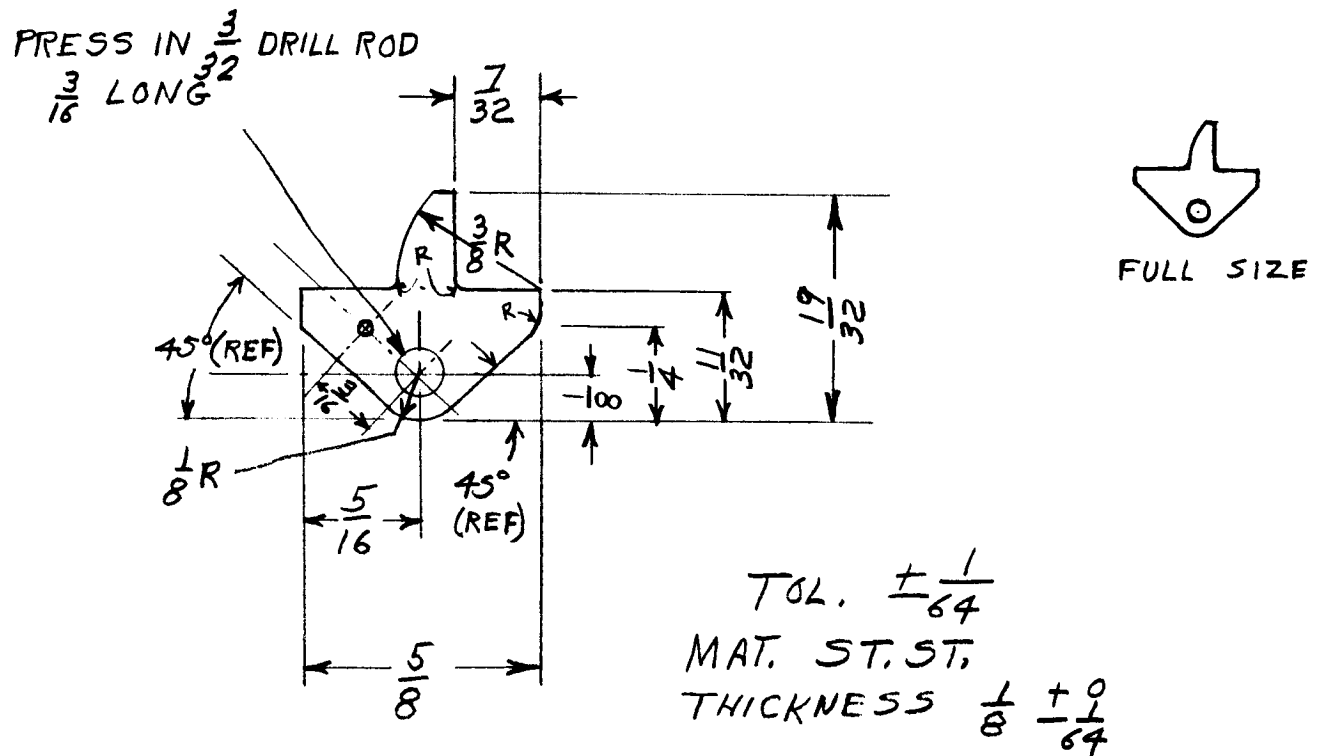
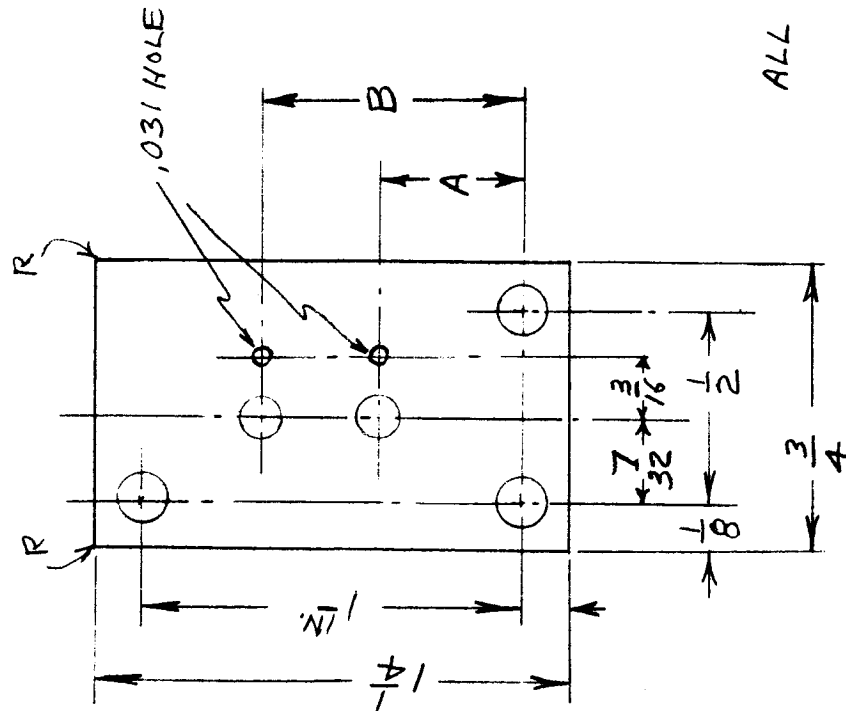


Figure A 1.D8. Squib Housing No. 2 Rocker Arm

PT No.	A	B
3	.853	.561
4	.687	.561
5	.687	.395
6	.853	OMIT
7	.395	OMIT

TOL. $\pm \frac{1}{64}$

MAT. AL ALLOY (6061-T6)
.031 THICK



ALL HOLES .093^{DIA} EXCEPT AS NOTED

Figure A 1.D9. Plate

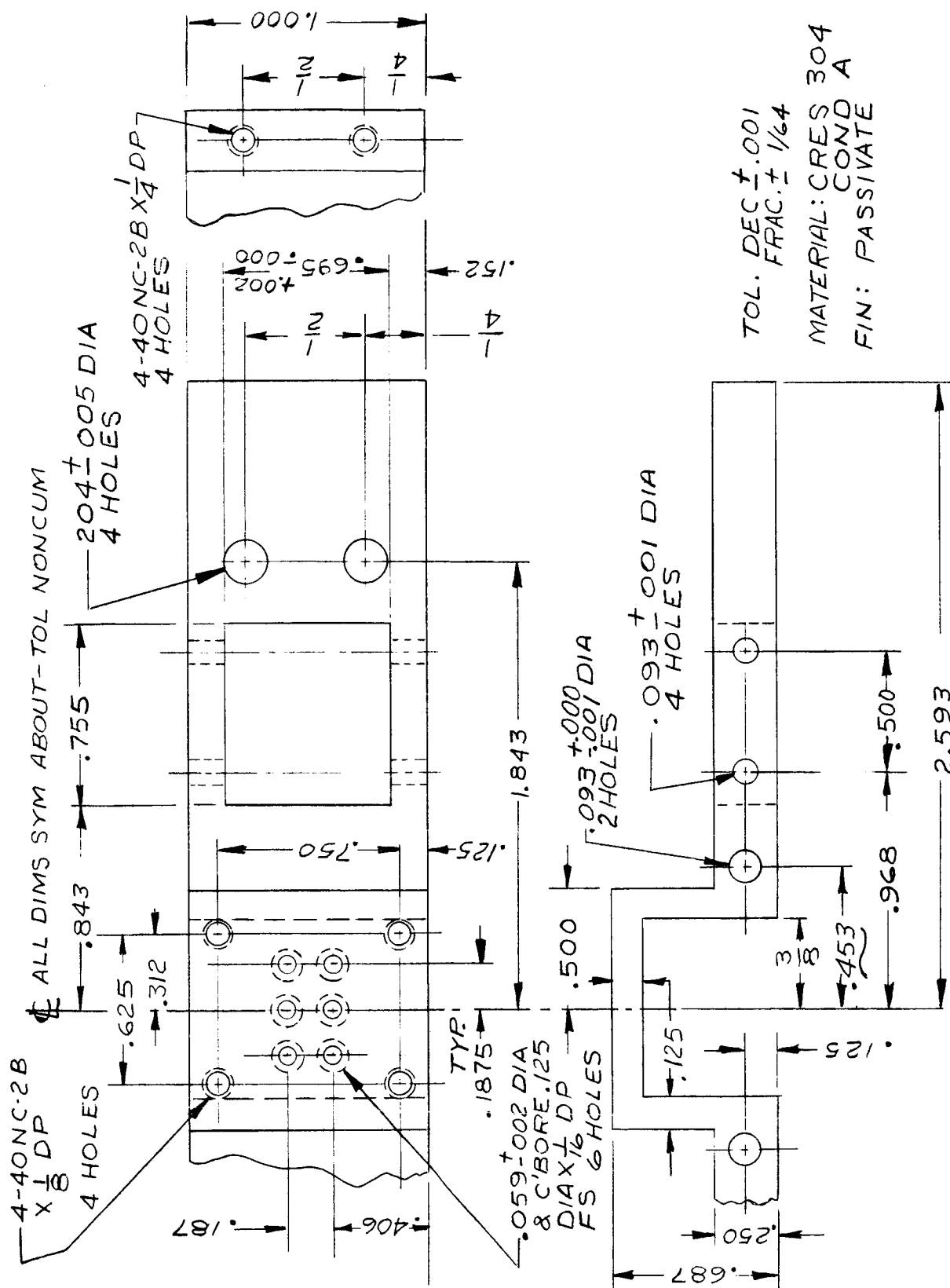
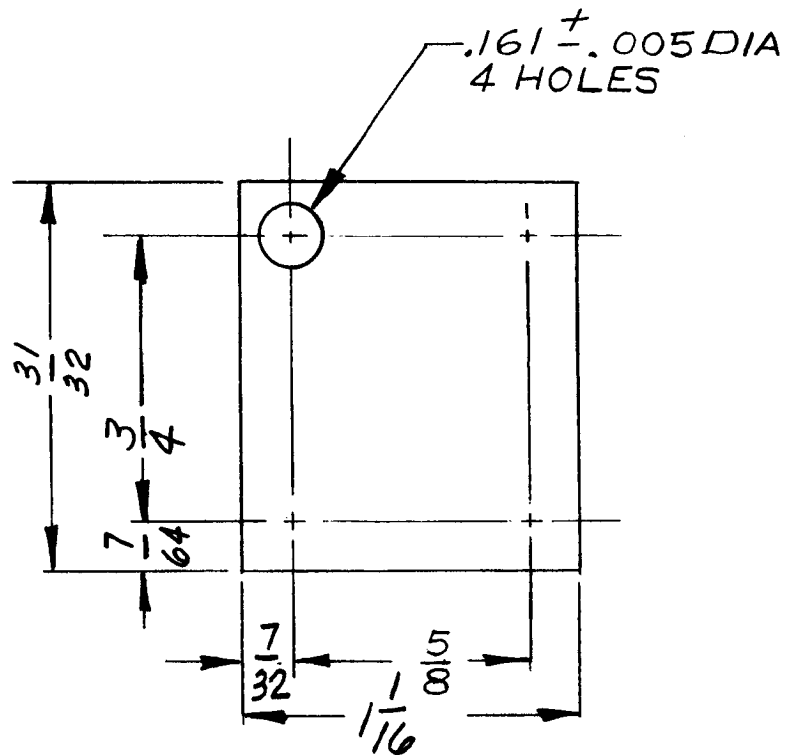


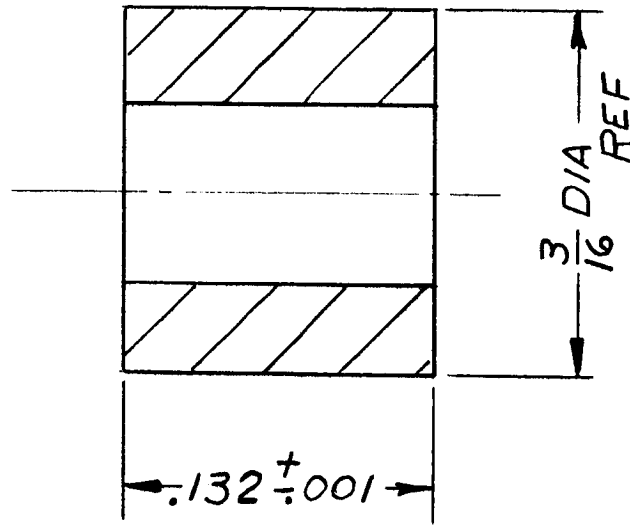
Figure A1.D10. Base Plate



TOL $\pm \frac{1}{64}$

MATERIAL: CRES 304 COND A $\frac{1}{8}$ THK
FIN: PASSIVATE

Figure A 1.D11. Pressure Plate



MATERIAL: $\frac{3}{16}$ ODX.047 WALL AL ALY 6061 T6
FIN: IRIDITE/ALODINE

Figure A 1.D12. Plate Spacer

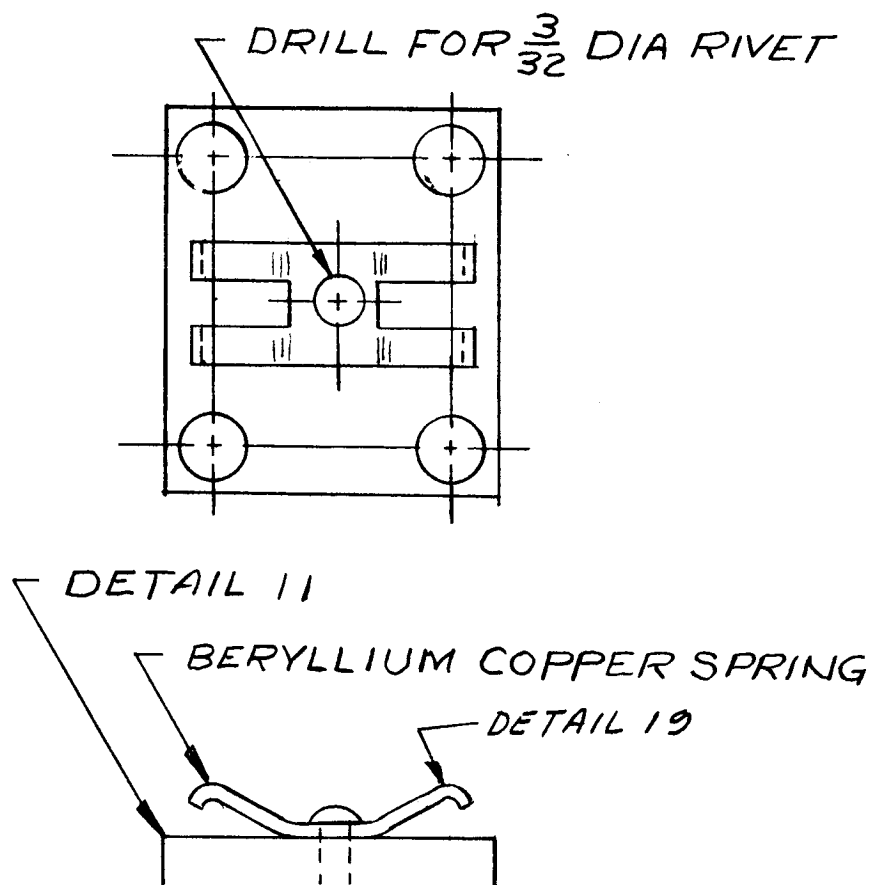
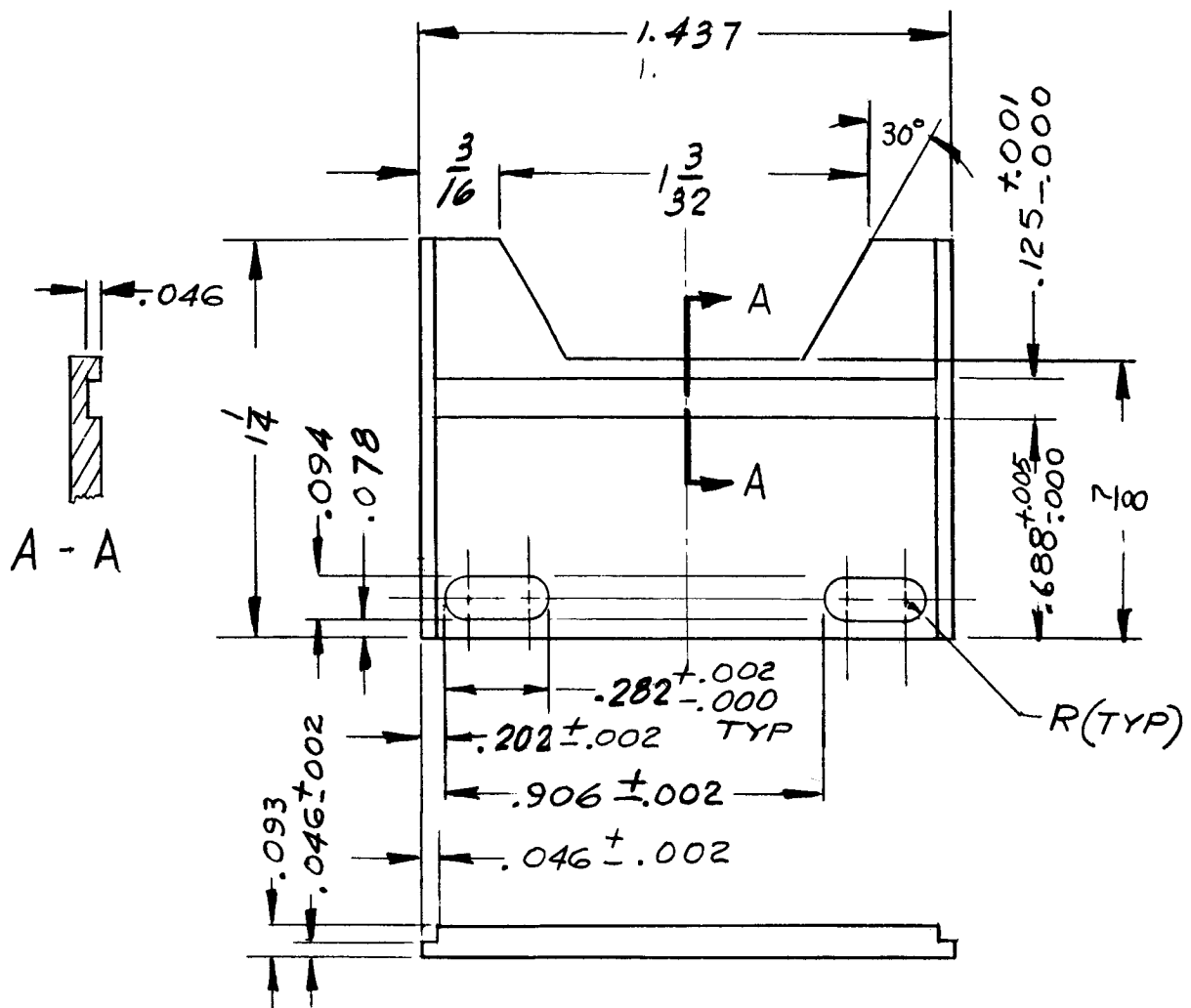


Figure A 1.D13. Pressure Spring Plate



TOL: DEC. $^{+}$
 FRACT. $\pm \frac{1}{64}$

MATERIAL - CRES 304 COND A
 FIN - PASSIVATE

USED ON R350158

Figure A 1.D14. Side Plate, Selector Valve

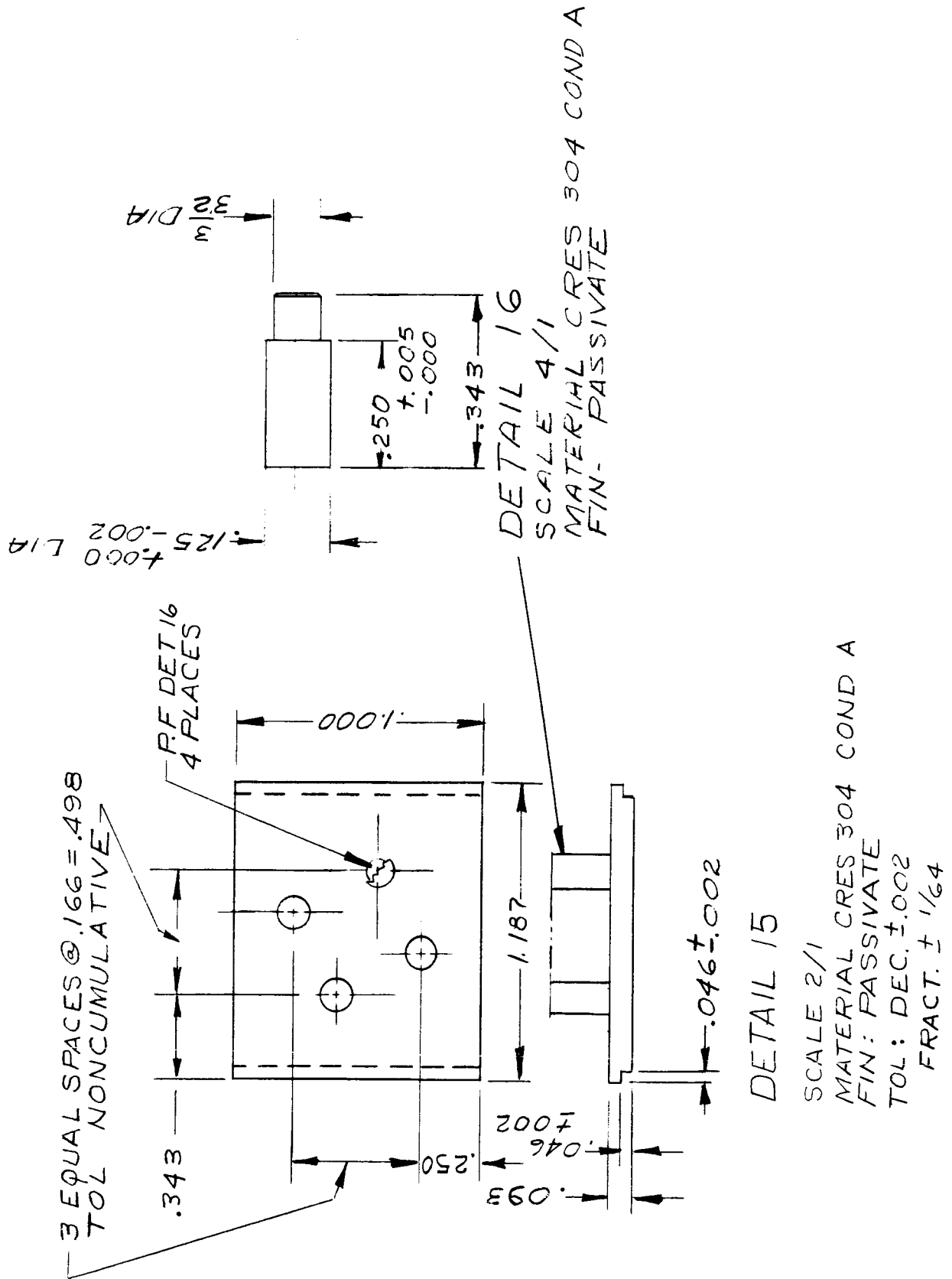


Figure 1.D15 and 16. Cage End Plate and Pin

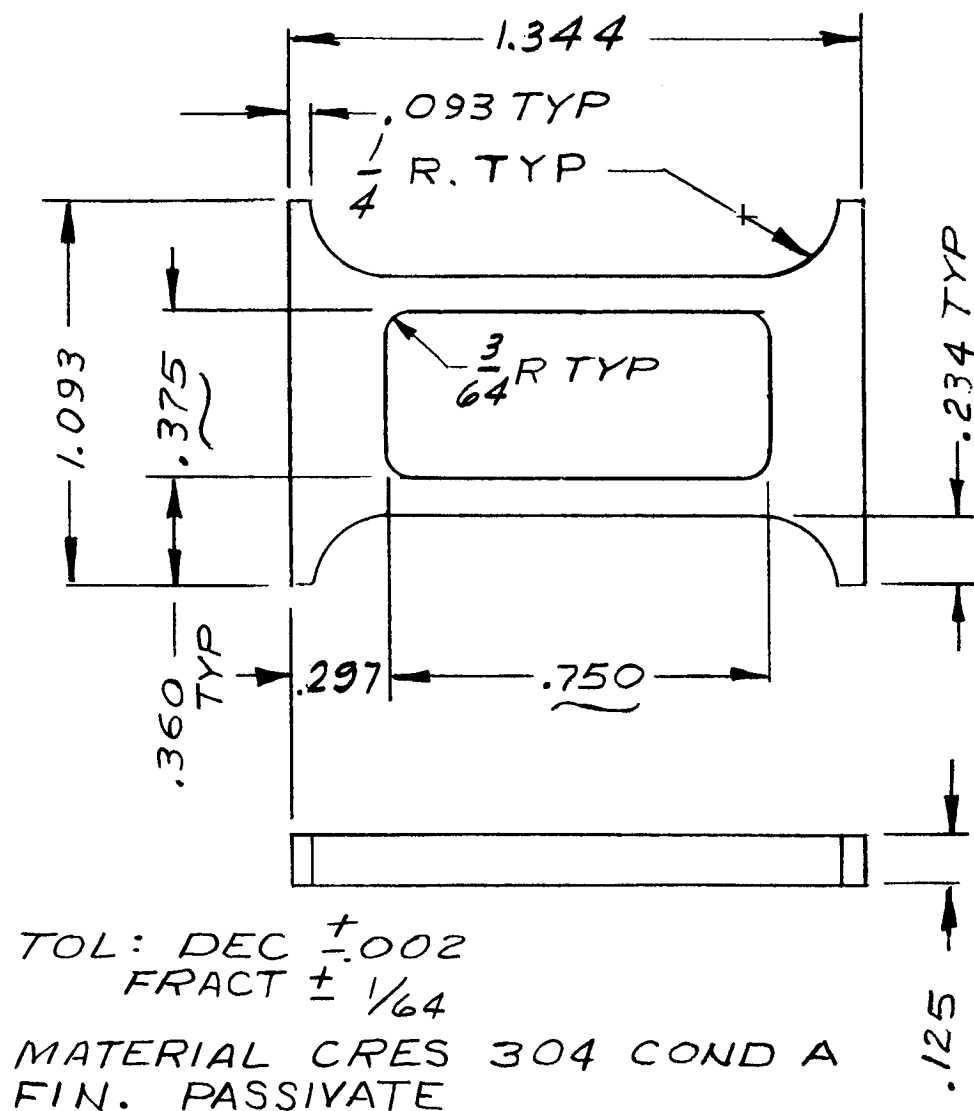


Figure A 1.D17. Retaining Plate

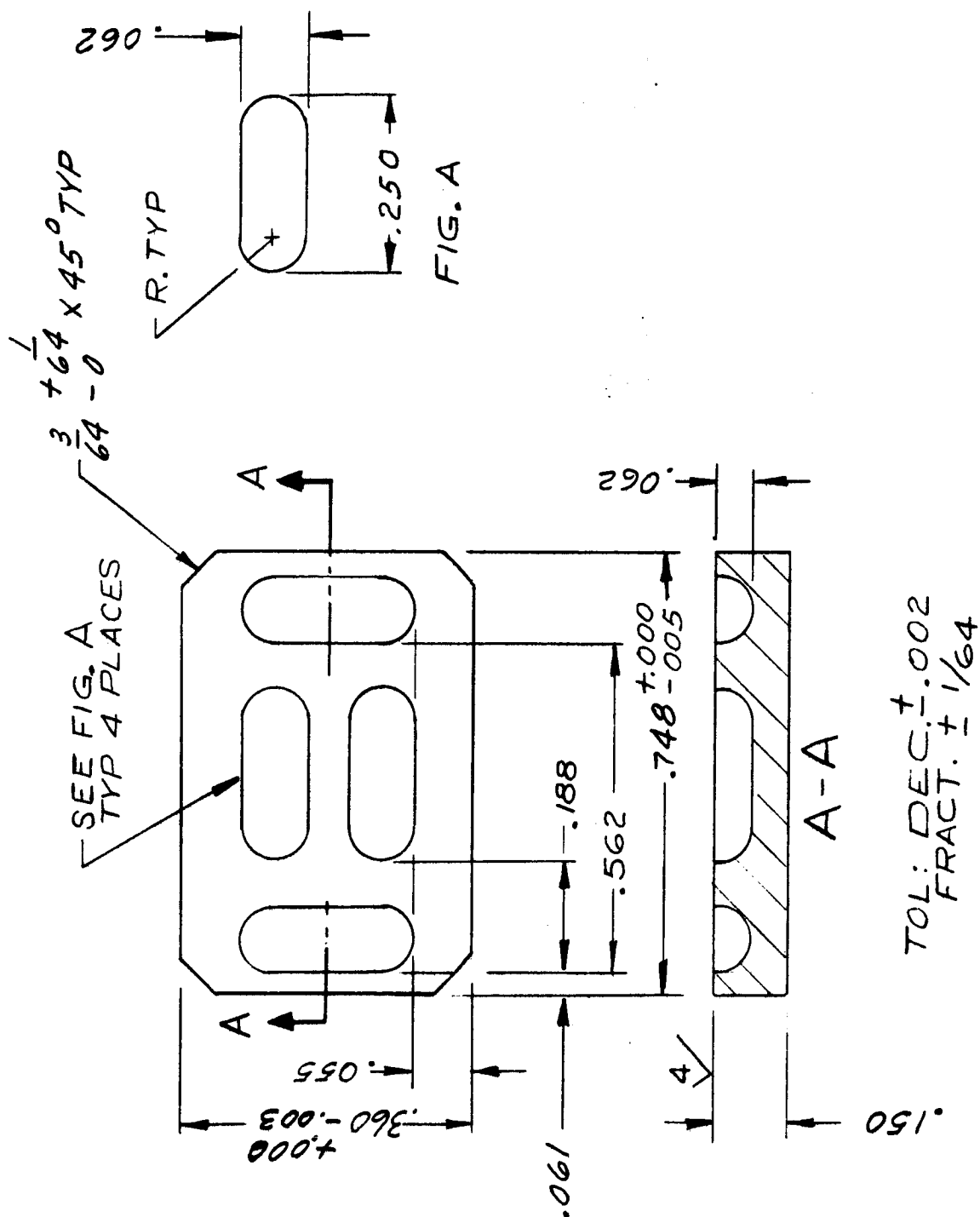


Figure A 1.D18. Selector Valve

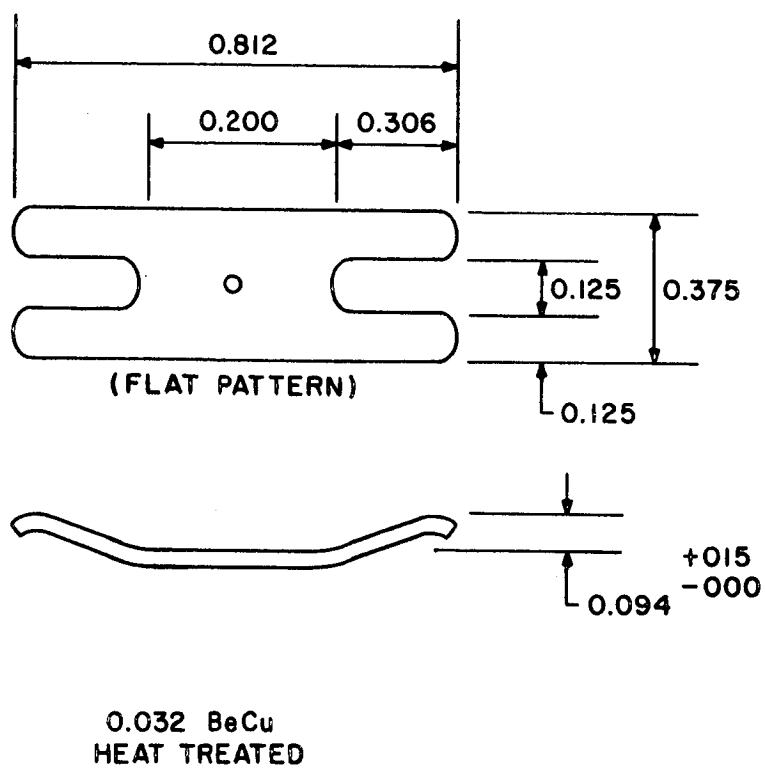


Figure A 1.D19 Spring

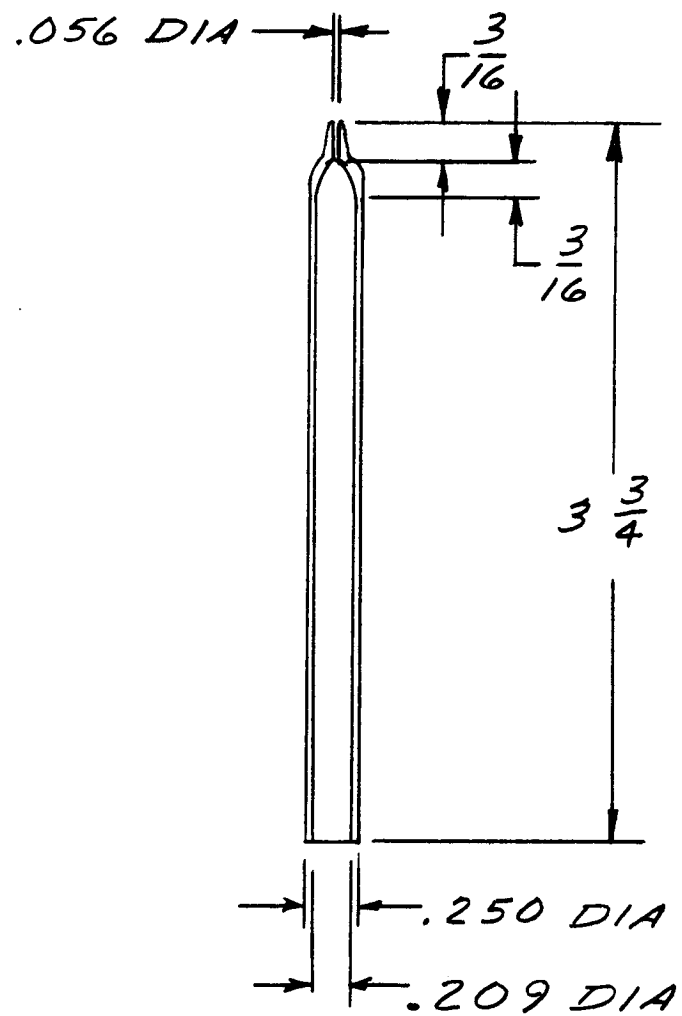


Figure A 2. Pump Nozzle Restrictor

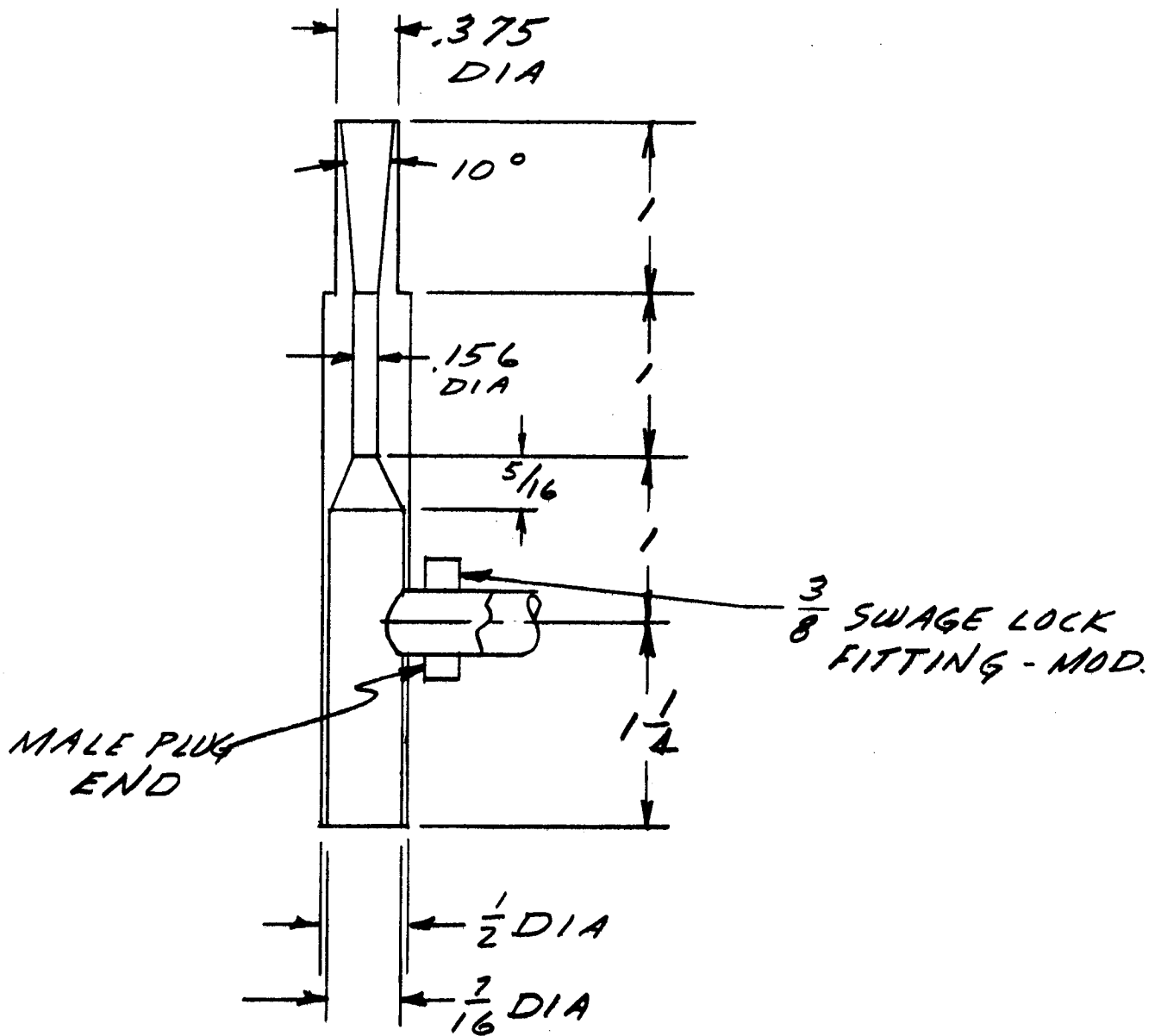


Figure A 3. Pump Body

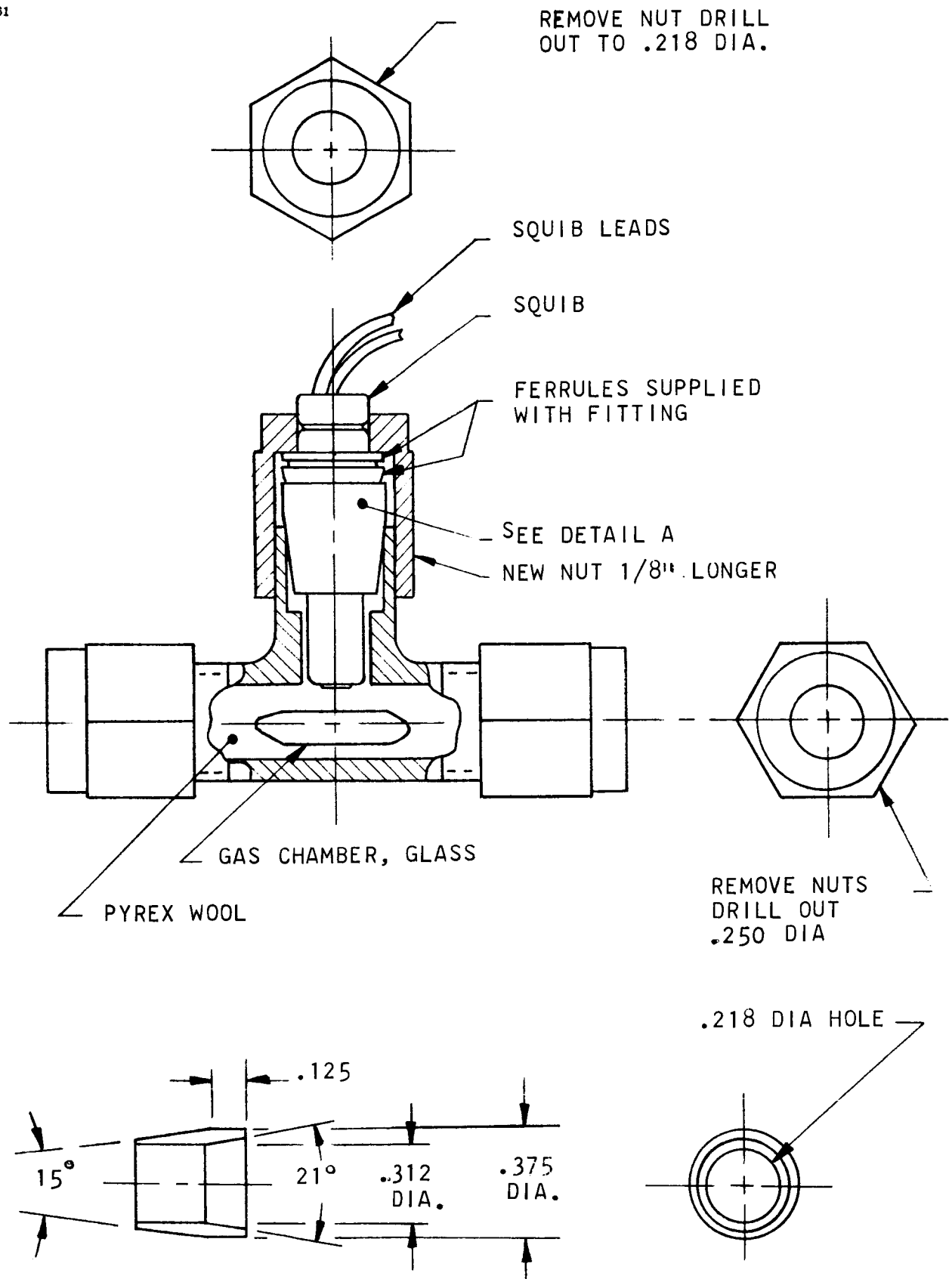


Figure A 4. Reference Gas Chamber

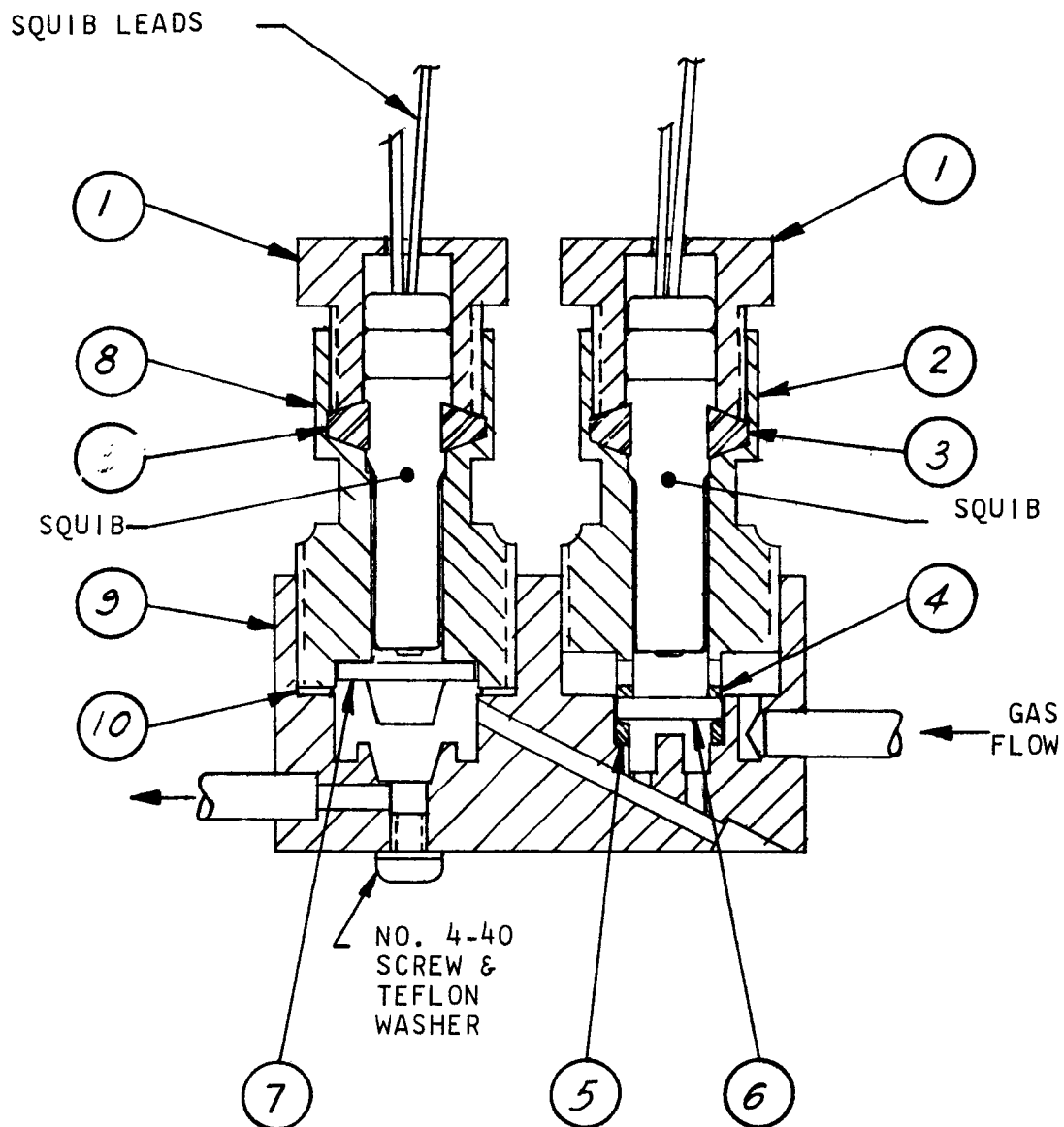
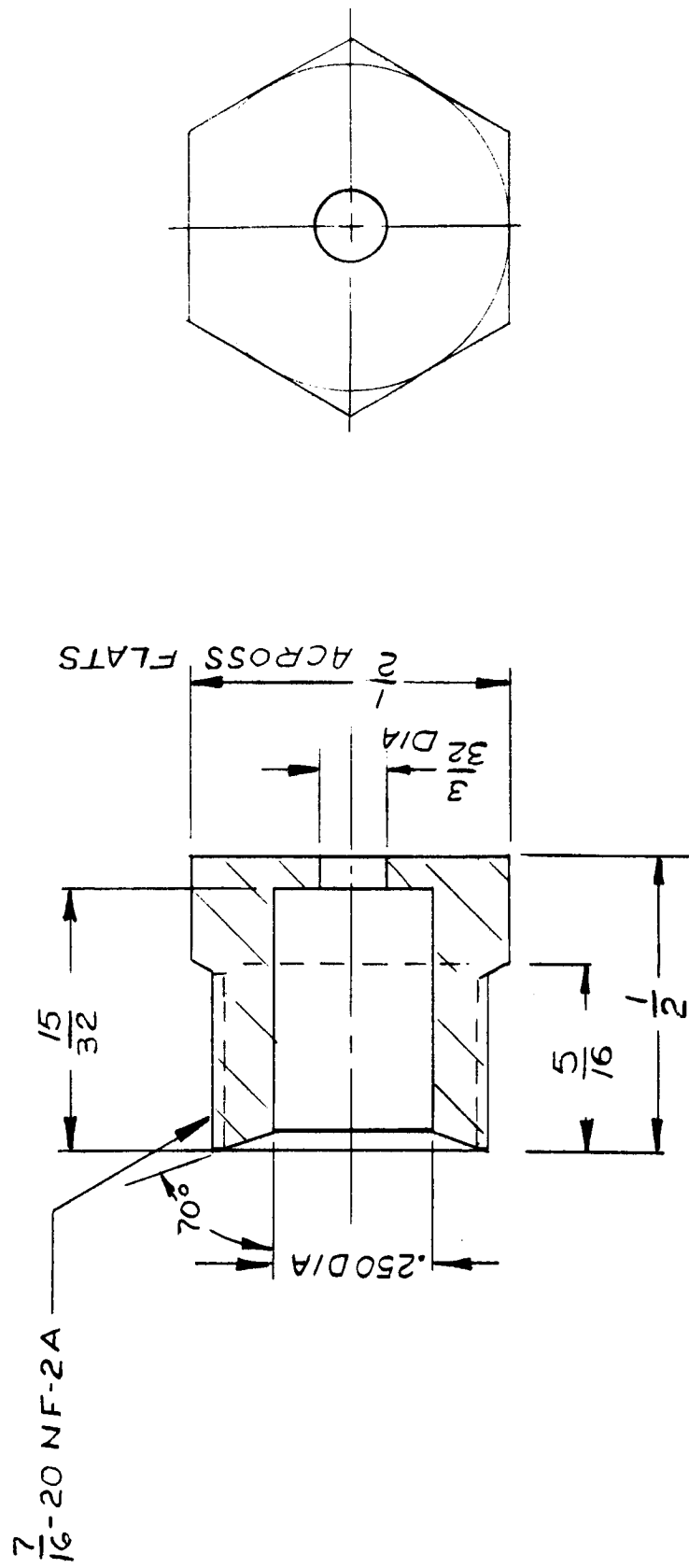


Figure A 5. Squib-Actuated, Two-Way Valve



TOL: DEC: $\pm .002$
 FRACT: $\pm 1/64$

MATERIAL: CRES 304 COND A
 FINISH: PASSIVATE

Figure A 5.D1. Squib Retained

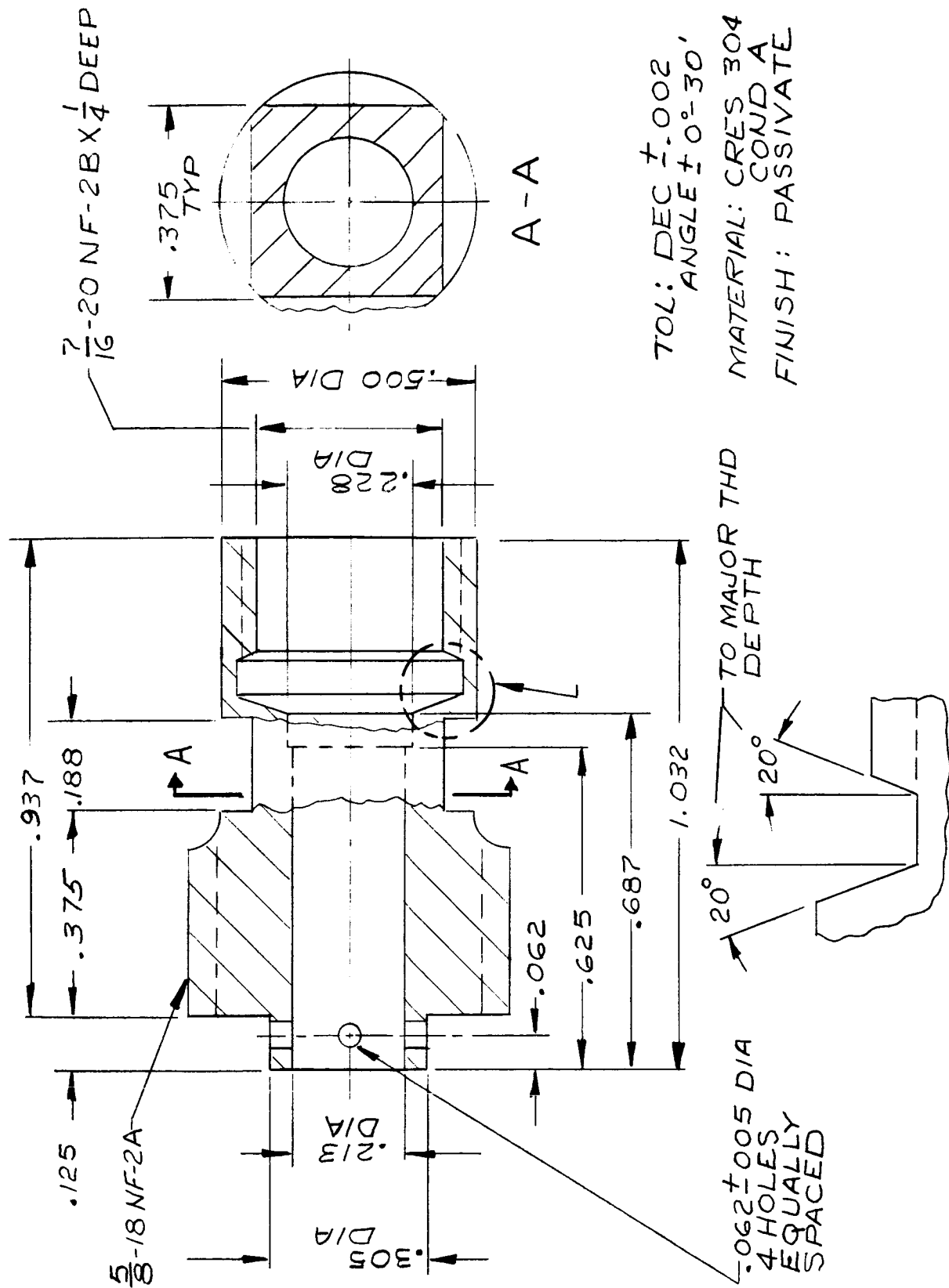


Figure A 5.D2. Squib Housing No. 1

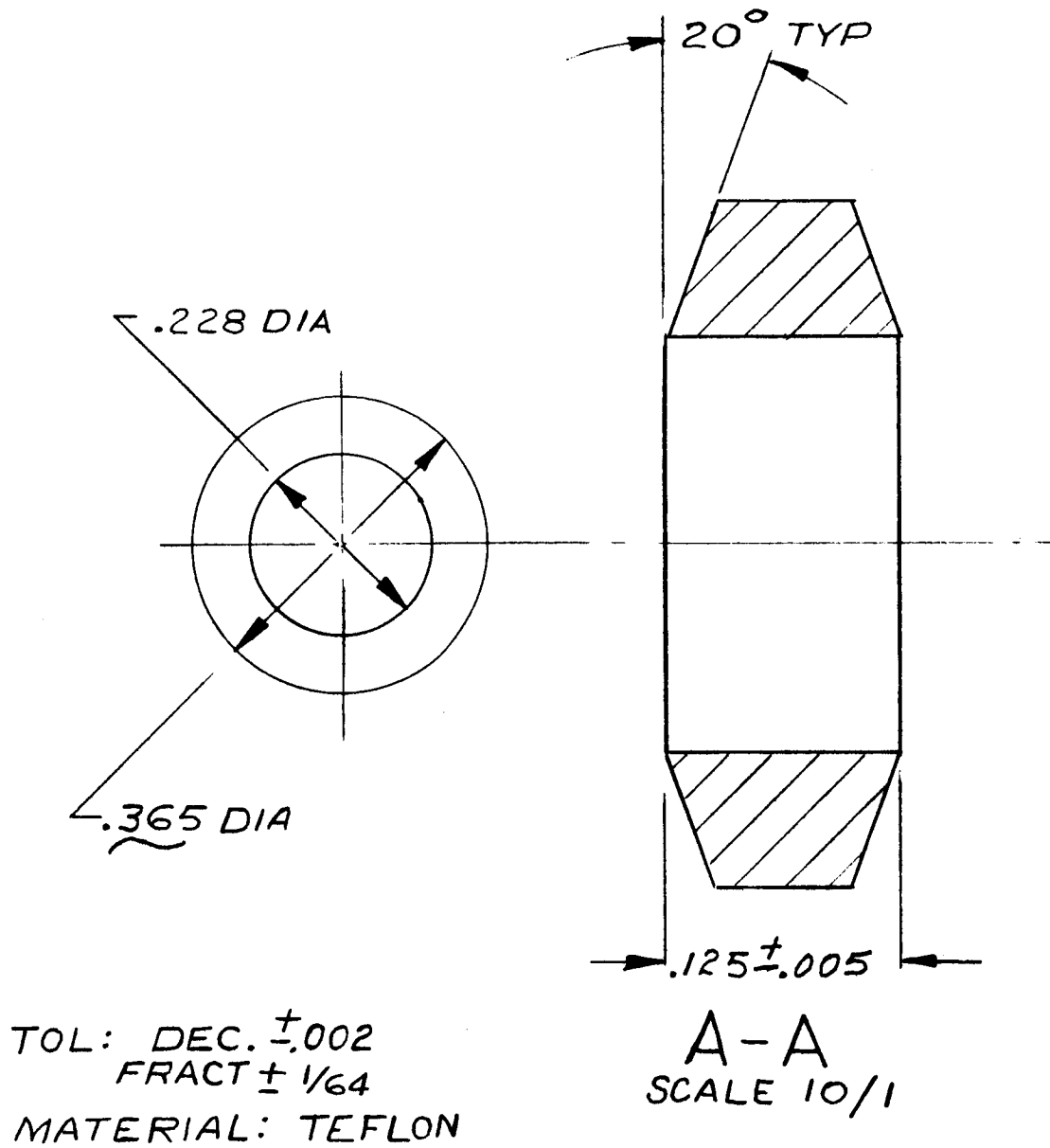


Figure A 5.D3. Squib Seal

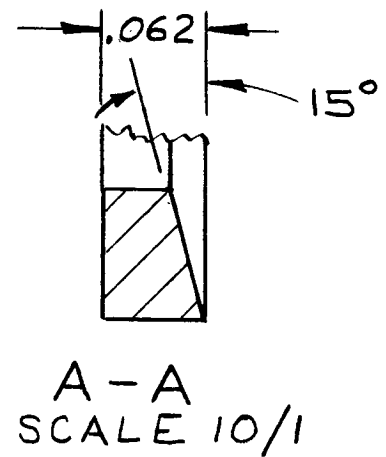
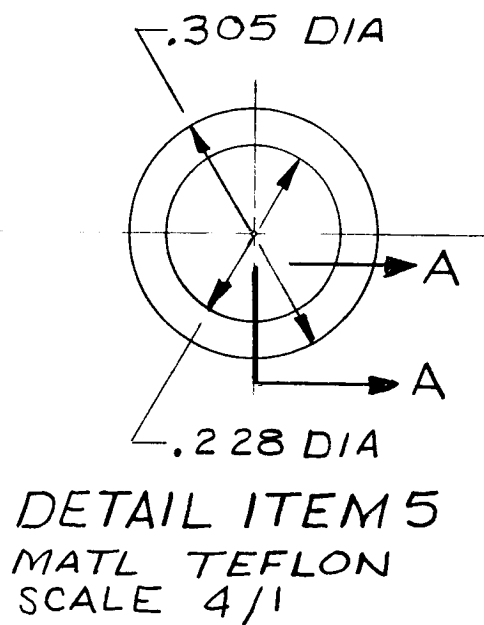
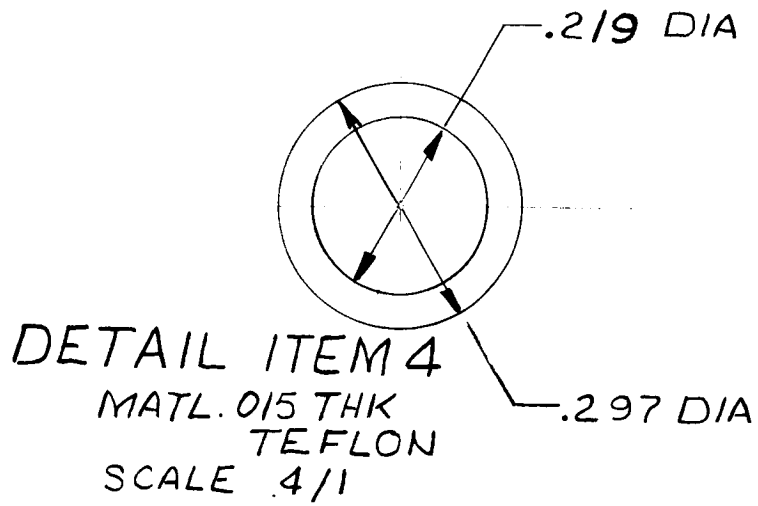
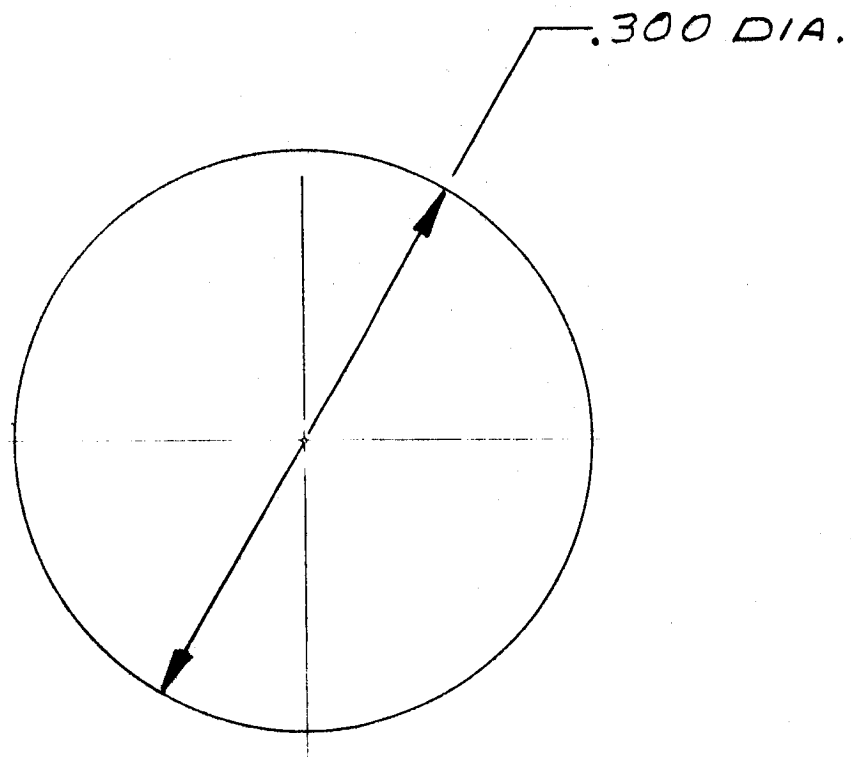
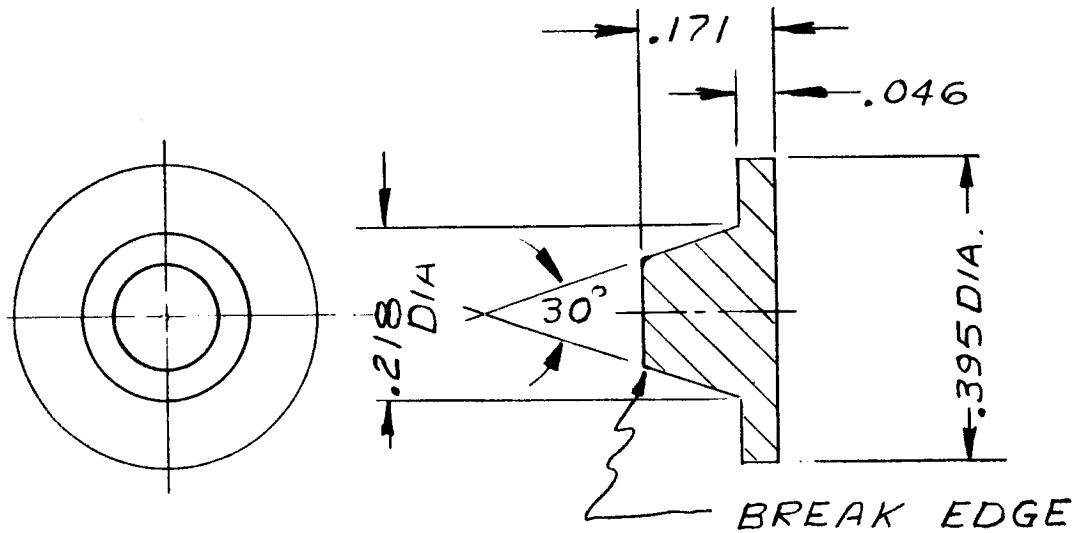


Figure A 5.D4 and D5. Spacers



TOL: DEC $\pm .005$
 $-.010$
MATERIAL 1/16 THK GLASS

Figure A 5.D6. Glass Diaphragm



TOL: DEC. $\pm .002$
ANGLES $\pm \frac{1^\circ}{2}$

MATERIAL: CRES 304 CONDA
FINISH: PASSIVATE

Figure A 5.D7. Plunger

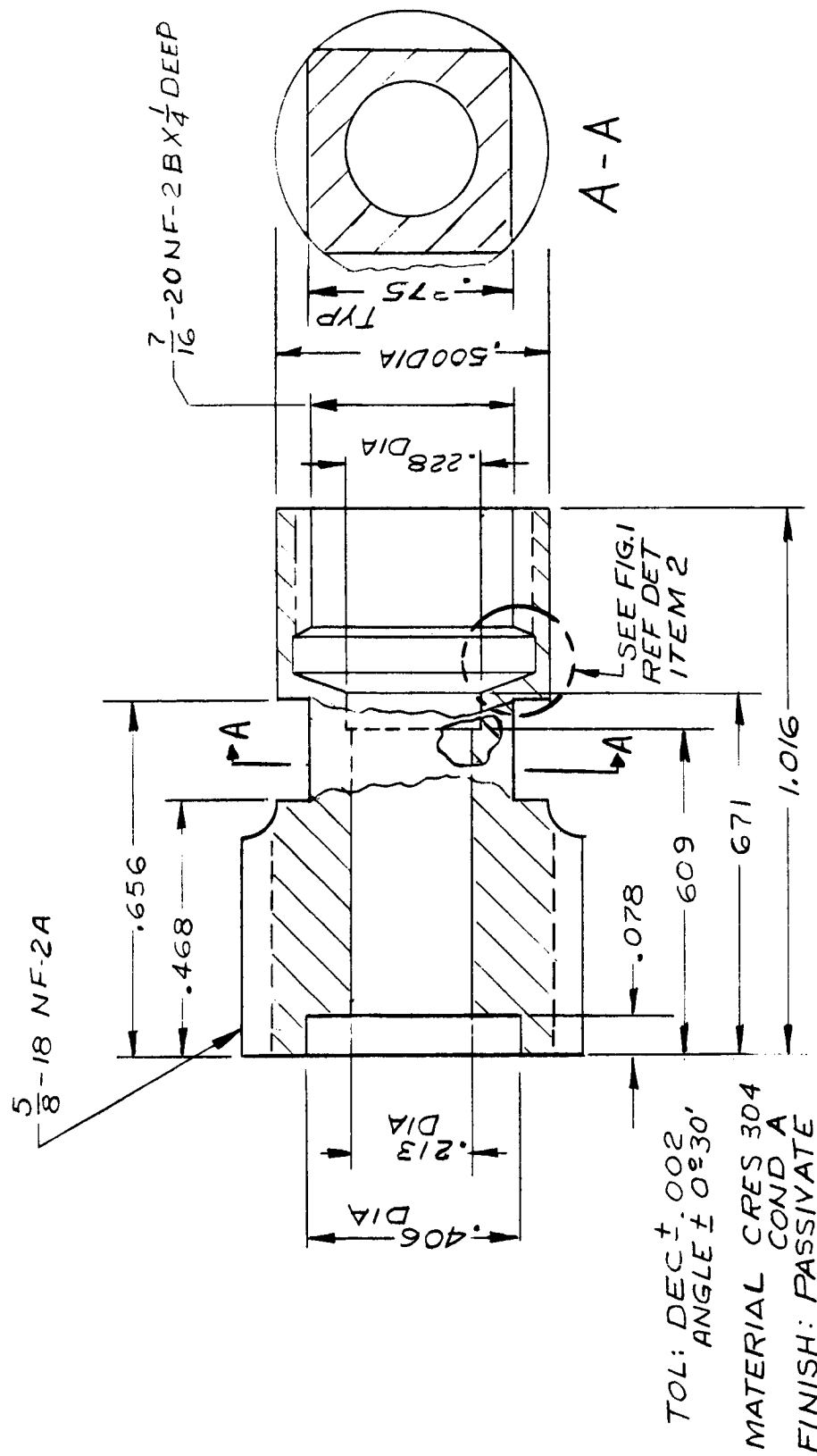


Figure A 5.D8. Squib Housing No. 2

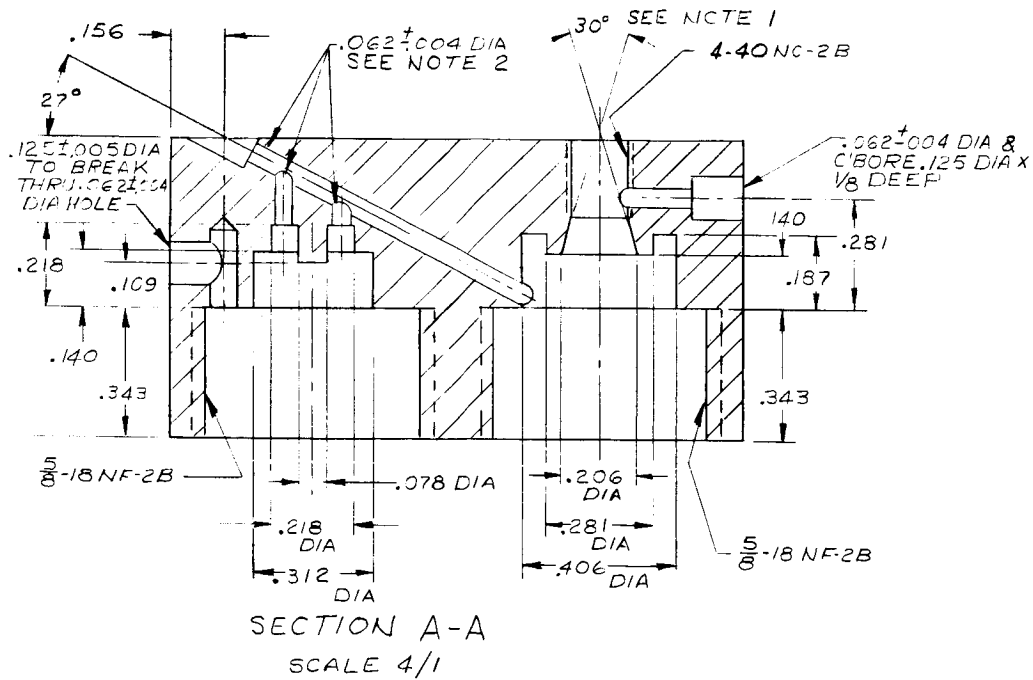
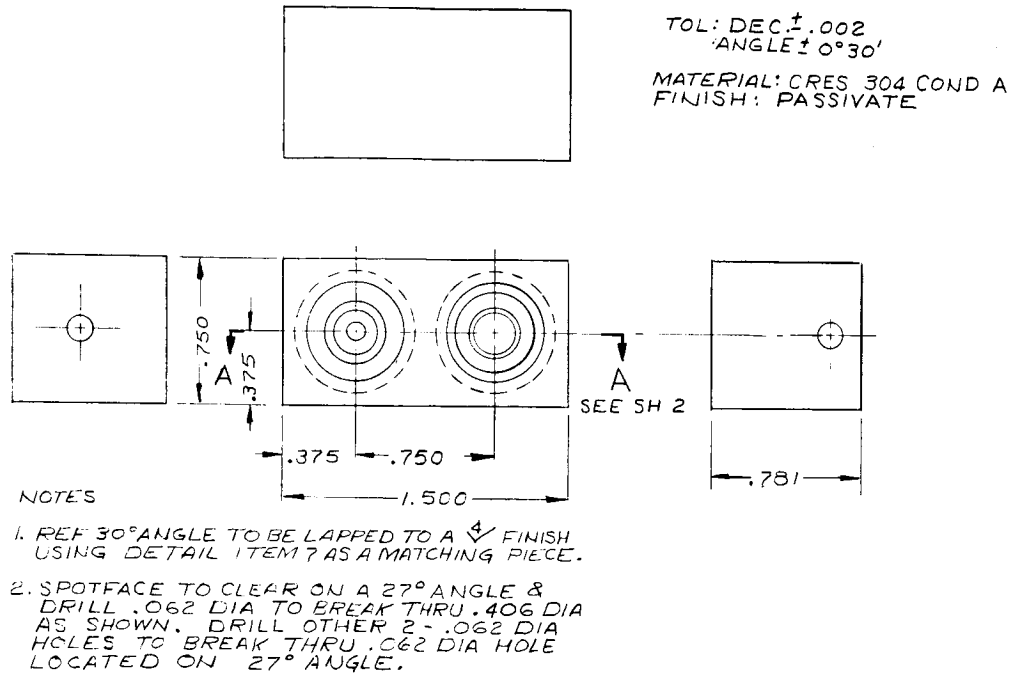
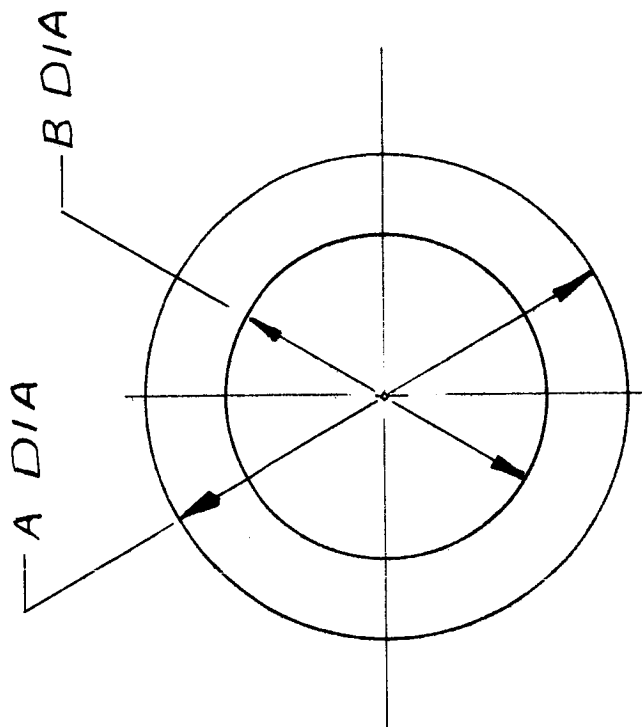


Figure A 5.D9. Squib Housing No. 3

DETAIL ITEM NO	A DIA	B DIA
10	.562	.406
11	.375	.203



TOL: DEC. \pm .005
MATERIAL: TEFLON

Figure A 5.D10. Seal

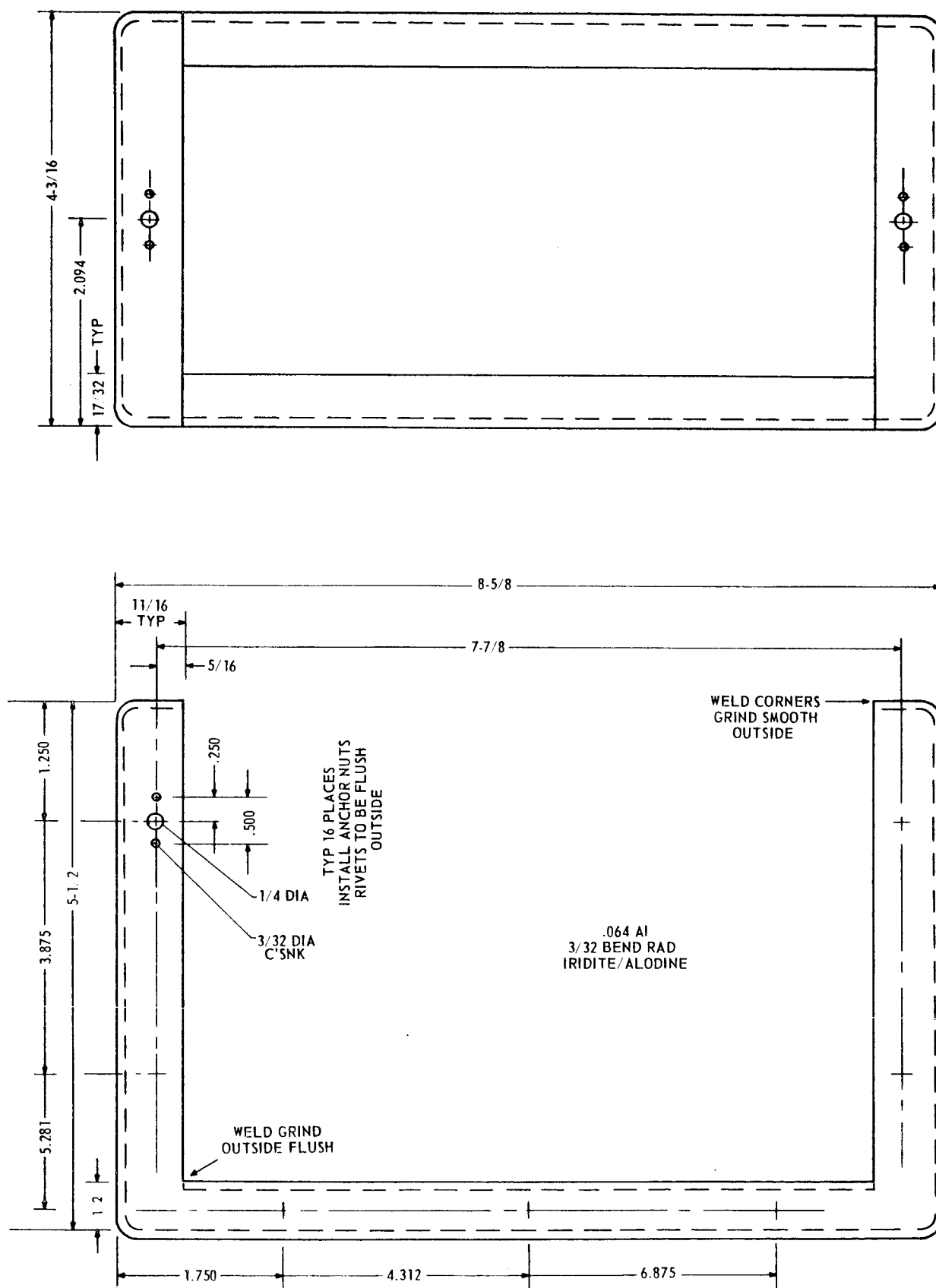


Figure A 6. Electronic Chassis

.064 AL
3/32 BEND RAD
IRIDITE/ALODINE

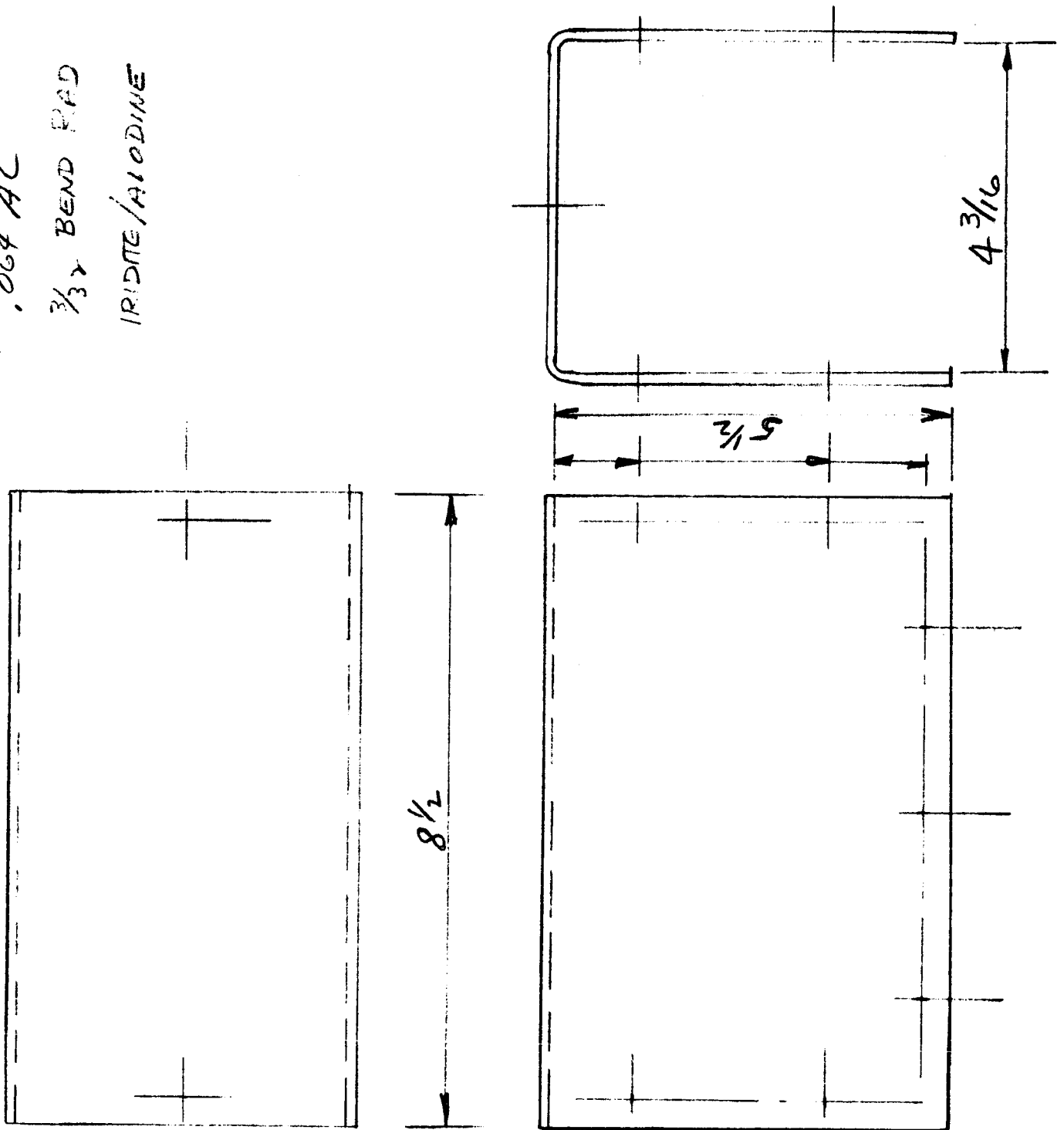


Figure A 7. Cover for Electronic Chassis

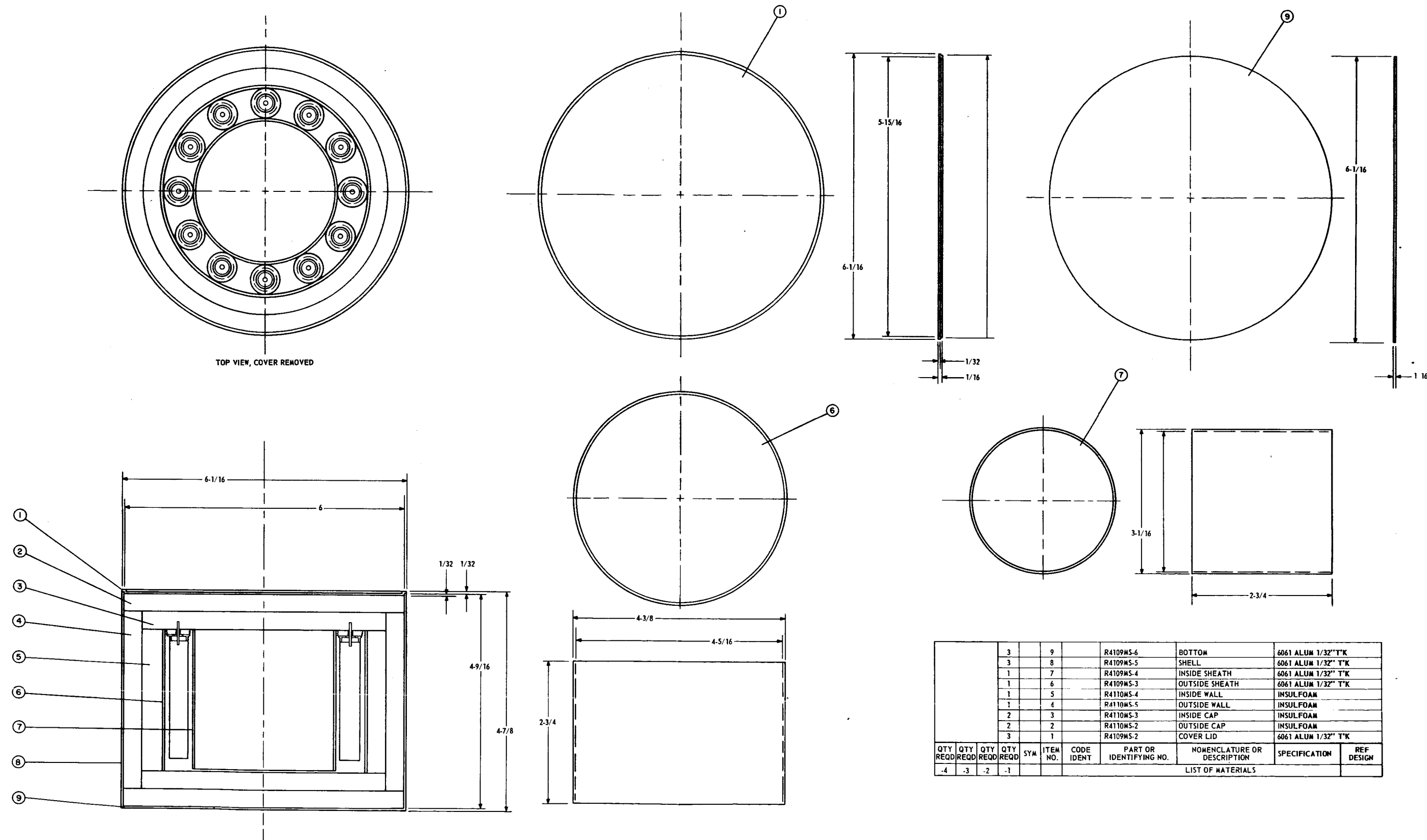


Figure A 8. Design Drawing for Gas Chromatography Oven

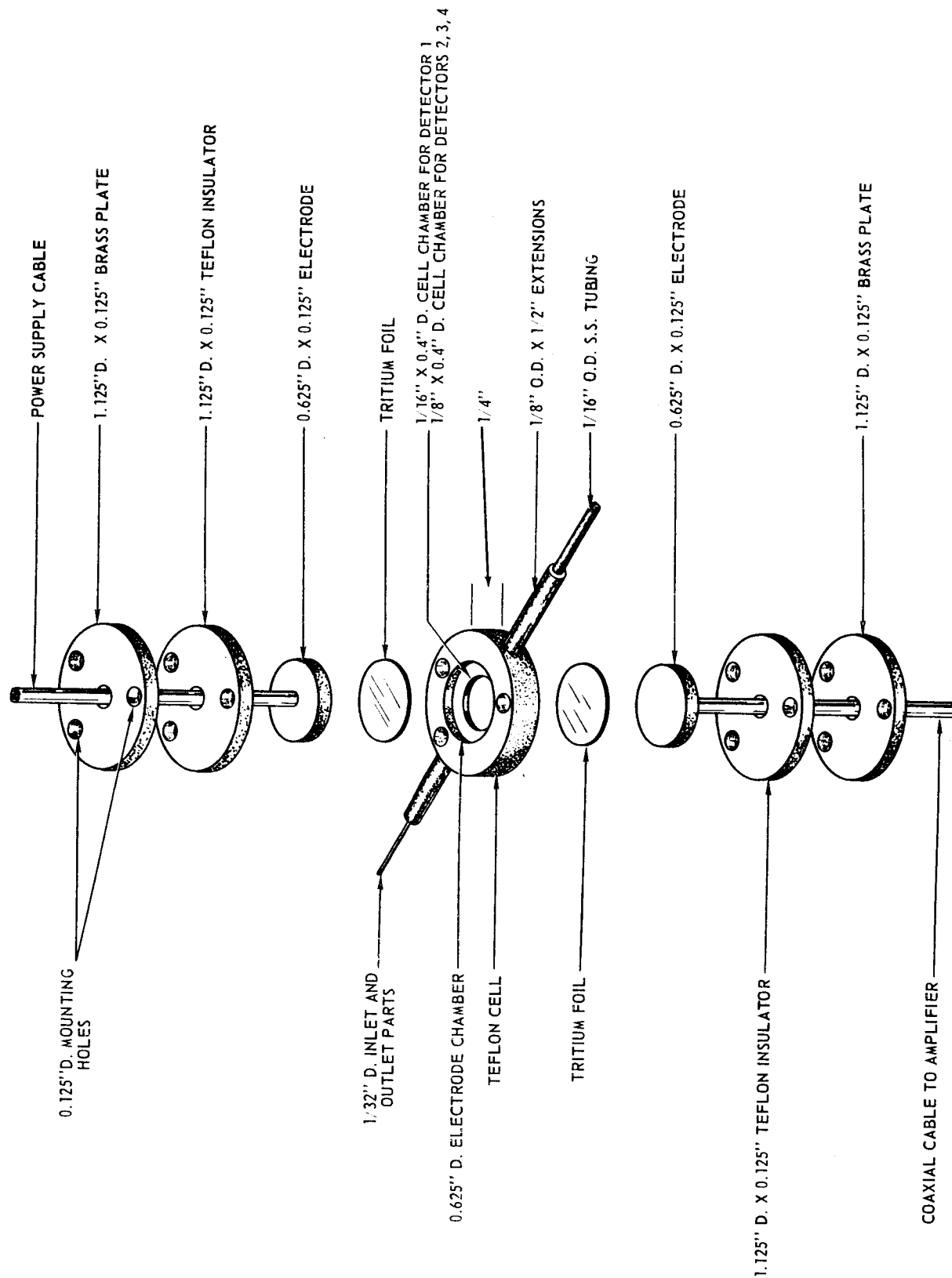


Figure A 9. Design Drawing for Cross Section Ionization Detector